In presenting the dissertation as a partial fulfillment of
the requirements for an advanced degree from the Georgia
Institute of Technology, I agree that the Library of the
Institute shall make it available for inspection and
circulation in accordance with its regulations governing
materials of this type. I agree that permission to copy
from, or to publish from, this dissertation may be granted
by the professor under whose direction it was written, or,
in his absence, by the Dean of the Graduate Division when
such copying or publication is solely for scholarly purposes
and does not involve potential financial gain. It is under-
stood that any copying from, or publication of, this dis-
sertation which involves potential financial gain will not
be allowed without written permission.

3/17/65
b

TRANSIENT FILM BOILING ON

A HORIZONTAL CYLINDRICAL SURFACE



A THESIS

Presented to

The Faculty of the Graduate Division

by

Donald Ross Pitts



In Partial Fulfillment

of the Requirements for the Degree

Doctor of Philosophy in the

School of Mechanical Engineering



Georgia Institute of Technology

August, 1967

TRANSIENT FILM BOILING ON

A HORIZONTAL CYLINDRICAL SURFACE

Approved:

_____
Chairman

_____

Date Approved by Chairman: 30 Aug. 1967

## ACKNOWLEDGMENTS

The author is indebted to many people for the opportunities which have enabled him to undertake this task, especially to those who have aided and assisted him at their personal expense. Foremost among those to whom sincere gratitude and appreciation is expressed is Dr. Thomas W. Jackson. His enthusiasm, friendship, and tireless efforts served as a source of constant encouragement throughout the research, which could not have been undertaken without his advice.

Appreciation is also expressed to the thesis reading committee members, Dr. N. W. Snyder and Dr. J. E. Sunderland, who maintained an active interest throughout the research. A special note of thanks is due to Dr. Frank Nottingham who made invaluable suggestions concerning electronic circuitry and furnished several major components for the system. Indebtedness is expressed to Mr. Howard H. Yen, graduate assistant, for his cheerful participation in collection and reduction of experimental data, and for proofreading portions of this thesis.

The author wishes to express his appreciation to the Lockheed Aircraft Company which provided part-time employment during part of the research and assisted him financially throughout the lengthy course of study leading to it, and to the National Science Foundation for support during the latter part of the research (Grant GK 1416).

A genuine sense of indebtedness is expressed toward the author's parents, who instilled the desire for educational achievement throughout his formative years. The author is incapable of expressing the depth

of his appreciation for the encouragement, patience, and understanding of his wife, Bettie, and for the sacrifices that both she and our children made during the years of post-graduate study.

Lastly, a deep sense of gratitude is expressed toward God for the many undeserved physical, mental, and financial blessings which the author has enjoyed throughout life.

# TABLE OF CONTENTS

v

TABLE OF CONTENTS (Continued)

LIST OF TABLES

LIST OF FIGURES

SUMMARY

Transient film boiling of distilled water at, or very close to, saturation conditions from small diameter, horizontal, electrically heated platinum wires has been investigated. An approximate step change in wire temperature was accomplished by rapid discharge of energy from an electrical capacitor into the heating element. The resulting wire temperature rise occurred in the order of 50 microseconds and was measured by means of prior thermometric calibration of a Wheatstone bridge, element wire, and oscilloscope system. The transient film growth was recorded by means of high speed motion pictures.

Wire sizes used in this study were ten mils and twelve and one-half mils. A total of twelve experiments were conducted covering a range in excess temperature from 1019 to 1529 degrees Fahrenheit. The resulting vapor growth could be described as approximately cylindrical for an excess temperature greater than 1000 degrees Fahrenheit, but could not be so described for lower temperatures. The transient cylindrical growth usually lasted for approximately ten milliseconds, after which the onset of large bubble formation at nodes along the length of the wire, typical of steady state conditions, was evident.

The motion picture data were reduced to yield vapor growth rate information. This involved about 250 diameter measurements for each film, or a total of more than 3000 measurements. Volume median diameters were computed from these data, and are presented as a function of time for each experiment.

Evidence of vigorous nucleate boiling was noted during the first fraction of a millisecond during each test. That this phenomenon was not peculiar to platinum surfaces, due, perhaps, to a catalytic action, was demonstrated by the use of a high purity gold wire heater element.

An analysis to predict vapor growth rate for saturated pool transient film boiling from a horizontal cylindrical surface is presented. This analysis presumes that the primary mode of heat transfer is by conduction through the film to the vapor-liquid interface. Thus the energy equation is reduced to the transient conduction equation in cylindrical coordinates, and a closed form solution for small intervals of the time was found. The solution utilizes the customary law of the phase change front that the location of the interface is proportional to the square root of the time. This is modified slightly to account for the initial wire radius. The solution to the energy equation is found to be the function $E_i(-\frac{r^2}{4\alpha t})$, and the resulting transcendental equation for the constant of proportionality in the assumed law of the phase change front can be readily solved by slide rule and tables of the exponential integral. The analytical solution thus obtained correlates the experimental data of this investigation quite well.

Heat flux rates were calculated from the measured vapor formation data, and when time averaged for a nine millisecond interval, range from 50,000 to 90,000 Btu/hr-ft$^2$ for the 10 mil size wire with corresponding excess temperatures from 1043 to 1529 degrees Fahrenheit.

NOMENCLATURE

| Symbol | | Units |
|---|---|---|
| A | wire surface area | $in^2$ |
| a | total hemispherical absorptance | dimensionless |
| B | oscilloscope drift | mm |
| b | phase change growth proportionality parameter defined by Equation (4.38) | $in/sec^{0.5}$ |
| C | capacitance | farads |
| $C_1, C_2$ | constants used in solution of energy equation | dimensionless |
| $C_p$ | specific heat at constant pressure | Btu/lb °F |
| D | diameter | in |
| $d_1$ | actual wire diameter | in |
| $d_2$ | projected wire diameter | in |
| $d_3$ | projected vapor cylinder diameter | in |
| $d_4$ | vapor-liquid interfacial definition error | in |
| $E_i$ | exponential integral function defined by Equation (4.21) | dimensionless |
| E | Wheatstone bridge applied potential | millivolt |
| e | Wheatstone bridge unbalance | millivolt |
| F | body force in momentum equation | lb |
| G | oscilloscope gain | millivolt/cm |
| H | potentiometer error | millivolt |
| $h_{fg}$ | heat of vaporization | Btu/lb |
| I | Wheatstone bridge current | milliampere |
| k | thermal conductivity | Btu/sec in °F |

| Symbol | | Units |
|---|---|---|
| L | vapor cylinder total length | in |
| $\ell$ | length | in, cm |
| M | mass | lb |
| m | variable of measurement in error analysis | - |
| n | integer | dimensionless |
| P | thermocouple error | $^\circ$F |
| p | static pressure | psi |
| Q | capacitor charge | joule |
| $\mathring{q}$ | heat flux | Btu/sec in$^2$ |
| R | vapor-liquid interfacial radius, electrical resistance | in ohm |
| $\mathring{R}$ | vapor-liquid interfacial velocity | in/sec |
| r | radius | in |
| S | oscilloscope reading error | mm |
| T | temperature | $^\circ$F |
| t | time, general | second |
| V | electrical potential vapor cylinder volume | volts in$^3$ |
| v | velocity | in/sec |
| x | general mathematical variable | dimensionless |
| y | dummy variable of integration, Equation (4.20) | dimensionless |

Greek
Letter
Symbols

| | | |
|---|---|---|
| $\alpha$ | thermal diffusivity | in$^2$/sec, cm$^2$/sec |
| $\beta_1,\beta_2,\beta_3$ $\beta_4,\beta_5$ | constants used in solution of energy equation | dimensionless |

| Greek Letter Symbols | | Units |
|---|---|---|
| $\varepsilon$ | thermal emissivity | dimensionless |
| $\zeta$ | parameter defined by Equation (4.30) | dimensionless |
| $\eta$ | parameter defined by Equation (4.03) | dimensionless |
| $\theta$ | non-dimensional temperature gradient defined by Equation (4.13) | dimensionless |
| $\lambda$ | second coefficient of dynamic viscosity | lb/in sec |
| $\mu$ | coefficient of dynamic viscosity | lb/in sec |
| $\rho$ | density | $lb/in^3$ |
| $\sigma$ | Stefan-Boltzmann constant | $Btu/in^2\ sec\ {}^{\circ}R^4$ |
| $\tau$ | specific time | second |
| $\emptyset$ | angular coordinate | radian |
| $\psi$ | arbitrary mathematical function used in Equation (C.1) | – |

## Subscripts

| | |
|---|---|
| i | incremental unit |
| $\ell$ | refers to liquid phase |
| m | mean, mass |
| o | initial condition |
| p | most probable |
| r | radial |
| sat | refers to saturation condition |
| v | refers to vapor phase |
| w | wall (wire) |
| z | length coordinate |
| $\emptyset$ | angular coordinate |

CHAPTER I

INTRODUCTION

There is a current interest at the Georgia Institute of Technology in the possibility of metering small volume, periodic fluid flows by means of boiling heat transfer. Specifically, this interest is concerned with fuel injection systems for internal combustion engines. The present investigation was undertaken largely as a direct result of this interest. Also, there is a more widespread interest in transient boiling behavior because the control and response of some thermal systems, notably nuclear reactors, depend to a large extent upon this phenomenon. Indeed, the safe operation of such systems can be assured only if the designer has adequate knowledge of rate of vapor formation throughout the boiling range which could result due to large, rapid temperature excursions. In addition to these applications, transient film boiling is frequently encountered in metal quenching operations. A better knowledge of the phenomenon would be useful in predicting the transient temperatures of the metal, and thus could lead to improved treatment procedures.

## Historical Background

Prior to discussing the specific problem investigated, a brief review of boiling phenomena will be presented. Modern investigations into this mode of heat transfer began in 1934, when Nukiyama (1) aroused academic curiosity because of his then unusual findings relative to heat transfer during boiling of water from a submerged resistance wire. This

marked the beginning of intensive efforts by many researchers throughout the world to understand and explain the various phenomena associated with boiling heat transfer. This activity has continued unabated to the present date; indeed the present author's literature survey revealed 134 technical publications concerned with boiling heat transfer during the past seven years.

The simplest form of boiling is encountered when a heated surface is exposed to a liquid at or near saturation conditions with no external agitation or forced convective currents. This is generally referred to as pool boiling. It is perhaps the most frequently encountered form of boiling and is typified by the common tea kettle on a cook stove. The primary correlation for steady state, pool boiling heat transfer is usually expressed in the form of the boiling curve shown in Figure 1. The rather odd shape of this curve is a result of the fact that it is in actuality composed of four main regimes, each representing a totally different mechanism of heat transfer. In regime I, there is no phase change and the heat transfer is due to natural convection. In this region, the customary free convection heat transfer relationships are quite adequate to predict heat transfer rates.

As the wall temperature is increased such that the excess temperature (this term is customarily used to represent the difference between the wall and the fluid saturation temperatures) approaches point b, phase change begins to occur in the form of bubbles at favored nucleation sites along the surface. The number of such sites is dependent upon several variables; generally the nucleation begins with only one, or at most, a few such sites. For a given surface and fluid, the density of these sites
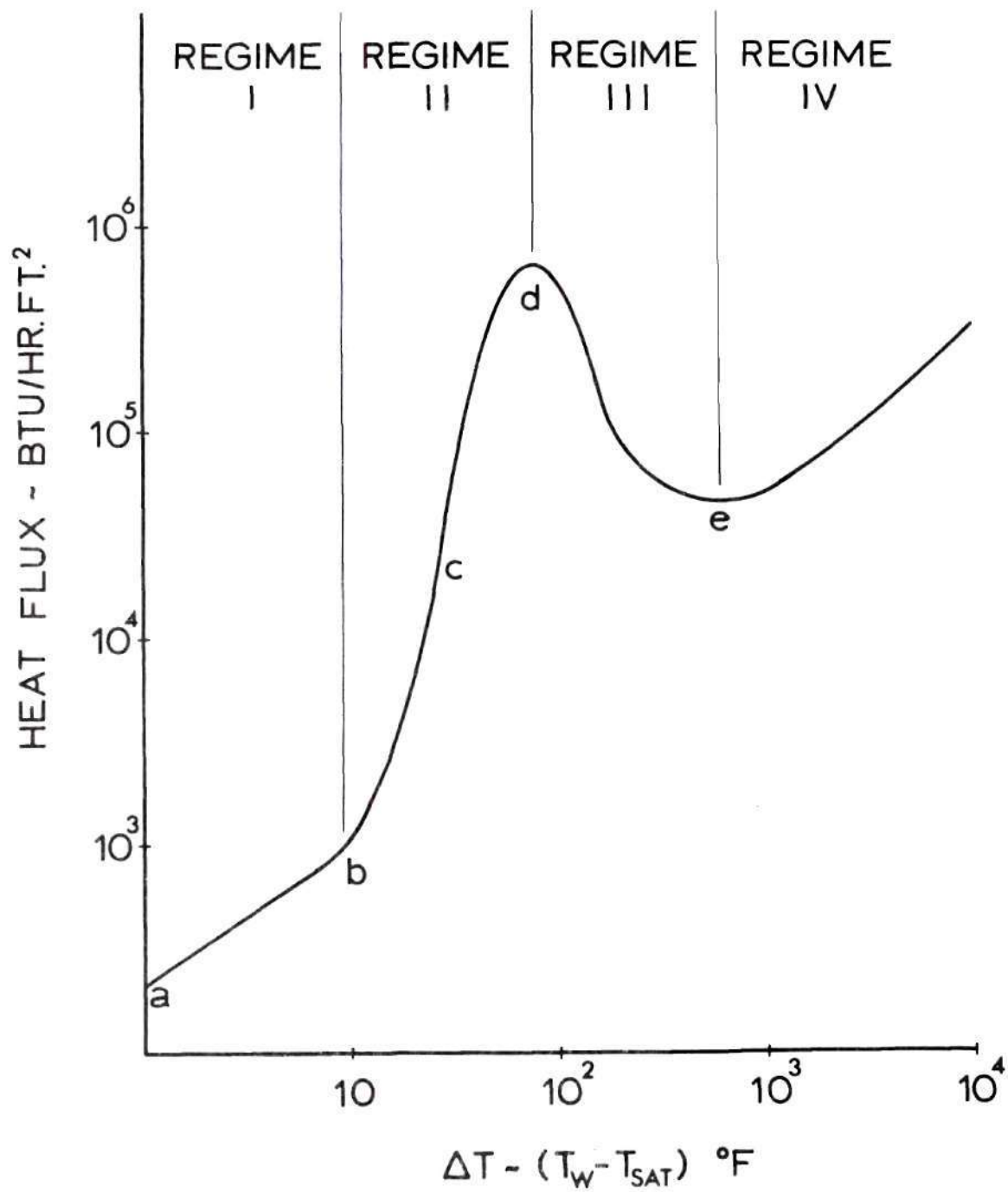
Figure 1.  Typical Pool Boiling Curve for Heat Transfer
from Wire to Water at Atmospheric Pressure.

increases with increasing excess temperature. The mechanism of heat transport in regime II is very complex - heat is being removed from the surface both by the vaporization process and by the high velocity convection currents associated with break-away of the bubbles. Of the many theories concerning nucleate boiling a notable example is the thin film vaporization-condensation mass transfer model proposed by Snyder (2). This has recently been verified and is described in detail in a Ph.D. thesis by Robin (3). For the present purpose, suffice it to say that the heat flux increases with increasing density of nucleating sites until the excess temperature approaches point d.

As the excess temperature passes through point c, an inflection occurs in the curve. This is a result of increased nucleation resulting in the bubbles coalescing to form continuous columns of vapor and thereby causing a reduction in individual site effectiveness. As point d is approached, nucleating sites become so numerous that the interference of columns from individual sites causes a further loss in individual effectiveness. At point d, the site density is so great that it prevents adequate motion of liquid to the heated surface to replenish that leaving by vaporization. Here, the increase in number of sites with increase in excess temperature exactly balances the loss of effectiveness of each site. This results in a maximum value of the heat flux, which is usually referred to as the critical heat flux, the DNB (departure from nucleate boiling), the boiling crisis, or the burnout point. All four of these terms have been used interchangeably throughout the boiling heat transfer literature.

Increase in the excess temperature beyond point d results in transition boiling (also called partial film boiling), regime III of Figure 1.

This is the most unusual part of the boiling curve in that an increase in excess temperature results in a decrease in the heat flux. The actual mechanism, like that of nucleate boiling, is very complex. The phenomenon appears to oscillate between film and nucleate boiling; the surface at times being blanketed by a film and then returning to a nucleating condition. In the case of a heated wire, the film appears to move along the length and then return. There is considerable disagreement among researchers concerning the mechanism of transition boiling. While this is undoubtedly the least understood of the boiling regimes, it is also the least useful; the former is most probably a direct result of the latter.

As the excess temperature is increased to point e, the mechanism of heat transfer changes to one of stable film boiling (regime IV). Here it is generally agreed that the heat transport through the vapor film is by conduction and radiation to the vapor-liquid interface where liquid is being evaporated. It should be noted that the effect of radiation becomes increasingly significant at high surface temperatures, especially when accompanied by high surface emissivity.

For a more complete discussion of boiling heat transfer the reader is referred to the excellent reviews of Jakob (4), Rohsenow (5), Kreith (6), McAdams (7), and to the book devoted solely to boiling by Tong (8).

## Purpose of This Research

This research is intended to investigate the initial regime of transient film boiling from a small diameter, cylindrical surface. The primary objectives are to develop an experimental transient film boiling system which permits quantitative study of the phenomenon, and to develop

an analysis which represents the transient film growth during this initial regime when the film can be described as cylindrical. The secondary objective is to experimentally determine the heat transfer rates from the heated surface, and to compare these with the results of a complimentary analysis.

## Related Literature

While the total research activity in the field of boiling has been quite extensive, a rather limited effort has been directed toward transient boiling. Most of the work that has been undertaken has been concerned with prediction of heating surface temperatures during transients; the majority of which has been further restricted to nucleate boiling. Cole (9) conducted one of the earliest investigations of transient boiling phenomena. He was primarily concerned with the determination of the temperatures developed in a ribbon type heating element. McLean, et al., (10) conducted an experimental investigation of transient boiling on a submerged horizontal wire. They utilized a very high energy flux to the wire of extremely short duration. This was accomplished by means of a square wave alternating current applied to a resistance wire element for a time period of one microsecond. The resulting film growth was recorded using stroboscopic flash photography. No quantitative data were obtained. Rosenthal and Miller (11) conducted an experimental investigation of heat transfer to subcooled water under transient conditions. They employed exponentially increasing heat generation in electrical resistance ribbons of platinum and aluminum. The primary objective of their investigation was to determine the heater surface temperature as a function of time. The range of

experiments included film boiling, but no void formation data are presented in their publication. Hamill and Bankoff (12) postulated an infinite horizontal plate experiencing a step change in wall temperature as the model for their analytical study. They assumed heat to be transferred through a continuous vapor film by conduction and convection. It appears that they employed a plane surface model because of the simplifications resulting in the governing equations, since their work was apparently inspired by the experimental investigation of McLean and his co-workers. No comparison of their solution with experimental data was presented. The same authors (13) also determined theoretical expressions for upper and lower limits of vapor growth for the cases of a) monotonic but arbitrary heat flux and b) monotonic but otherwise arbitrary wall temperature.

H. A. Johnson, et al., (14) obtained experimental values of surface temperatures and volumes of vapor produced during transient nucleate boiling from metal ribbons. Exponentially increasing heat flux rates were employed, and the transient pulses ranged from five to eighty milliseconds. Laurie and Johnson (15) investigated transient boiling on a vertical surface. The region of interest was the non-boiling through the nucleate boiling regimes. An interplay of free convection and nucleate boiling was evidenced. Graham (16) conducted an experimental study of transient nucleate boiling on a horizontal surface. He found evidence of free convection as well as thermal diffusion. For subcooled liquid, considerable surface temperature overshoot was observed, whereas for saturated boiling this did not occur. He studied thermal layer thicknesses in the liquid by means of shadowgraphs and found them to be dependent upon orientation (vertical or horizontal) of the heated surface.

Cooper and Lloyd (17) obtained simultaneous measurements of temperature fluctuations at several points on the surface of a heated glass plate as individual vapor bubbles formed, grew, and left the surface during nucleate boiling. Those fluctuations had been predicted by Snyder (2) using his thin film vaporization model. Temperature measurement was accomplished with small resistance thermometers made of thin films of metal and semiconductor, and transient heat fluxes were deduced. Hall and Harrison (18) investigated transient film boiling on a platinum ribbon which was heated with an exponentially applied electric current. The time duration of the current application ranged from five down to seven-tenths millisecond, and thus afforded an extension of Johnson's earlier work. The heat flux was recorded by means of voltage drops across a standard resistance and the ribbon displayed as a function of time on a dual trace storage oscilloscope. No vapor formation data were recorded.

In summary, for the geometry of the model of the current investigation, there have been no previous experimental investigations which have yielded quantitative film boiling vapor growth rate data, and no prior theoretical analysis exists for transient film growth rate.

CHAPTER II

APPARATUS

## Transient Boiling System

The basic system required for investigation of transient film boiling has three primary requirements; a) provision for rapid transfer of energy to the boiling heater element to minimize time duration in the nucleate regime, b) the capability for determination of the heater element temperature within prescribed limits of accuracy, and c) a means for determination of the rate of vapor formation. The first of these requirements is discussed in the present section, and the remaining two are covered under separate paragraphs of this chapter.

## Electrical Design

Previous research in transient boiling phenomena has utilized electrical heating of the heater element. Most of these investigations, however, have employed electrical transients of the same order of time duration as the entire period of interest of the present investigation. A notable exception to this is the work of McLean and his co-workers (10) but no temperature data for the heated surface were recorded during their investigation.

Obviously, the optimum system would be one which would produce a step-change in the heater element temperature with no change occurring afterwards. The system shown as Figure 2 was designed to accomplish these requirements. The primary elements of this system are:
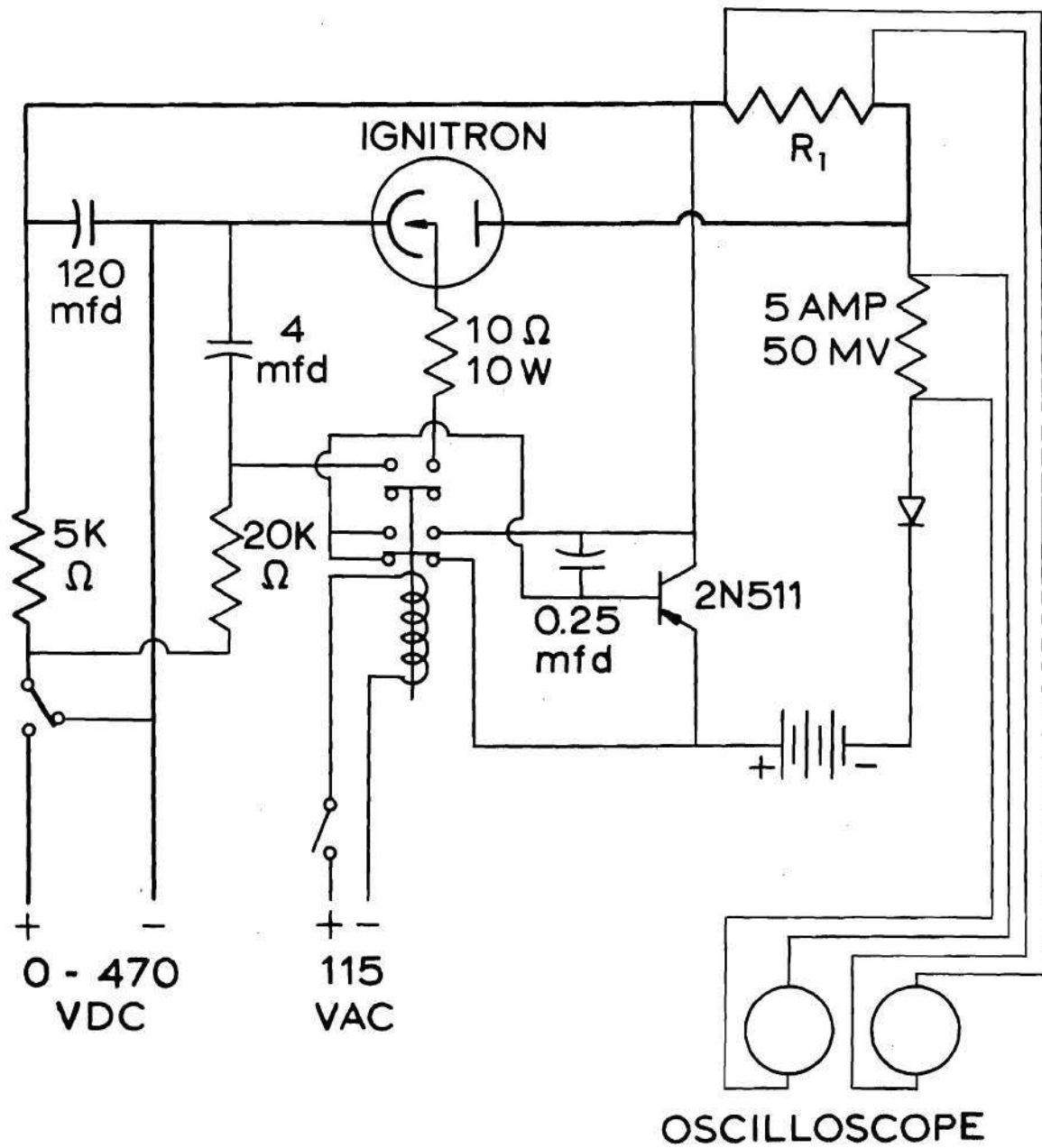
Figure 2. Transient Film Boiling System Electrical Schematic-
Constant Heater Element Temperature Design.

- $R_1$ - the heater element

- 120 microfarad main energy capacitor

- 470 VDC power supply

- Ignitron power tube

- Power transistor

- Low voltage battery

- Silicon rectifier

- Precision shunt

- Oscilloscope - dual trace

This design was constructed and used for preliminary experimental studies. The main capacitor was of the low internal resistance type. All wiring for capacitor energy discharge to the heater element $R_1$ was number ten wire size or larger, and hence the resistance heating element was essentially the total circuit resistance. As a consequence, practically all of the capacitor discharge energy was dissipated in the platinum element except for the losses associated with the Ignitron power tube. The time for wire heat-up is controlled by the time constant of the resistance-capacitance system. A numerical calculation for this is given in Appendix B, where it is shown that the time for discharge is of the order of 50 microseconds.

A major feature of this system was the simultaneous firing of a "holding" current with the discharge of the main capacitor. This was accomplished by actuation of the power transistor to apply a pre-determined low voltage direct current from a lead storage cell. This voltage was calculated to result in a heat dissipation in the heater element approximately equal to the heat flux to the liquid due to film boiling. The

silicon rectifier in the holding circuit prevented discharge of the main capacitor into the storage cell.

With this system, the element temperature could be determined by simultaneous measurement of the current flow and the potential change across the heater element. These measurements in conjunction with a knowledge of the temperature coefficient of electrical resistivity of the heater element could be used to determine the element temperature. This method has several disadvantages which are discussed under the topic of element temperature measurement.

As a consequence of the temperature measurement problem, the system was modified to eliminate the holding current circuit, and to add the Wheatstone bridge of Figure 7. The total circuit is presented as Figure 3. This design permits a temperature decay of the order of 50 degrees Fahrenheit in the element during the transient boiling phenomenon, but this is not of major significance to the current investigation as the element temperatures utilized were from 1245 to 1740 degrees Fahrenheit. The major improvement afforded by this modification is a reduction of at least 50 per cent in temperature measurement error, and direct temperature calibration of the entire system as a unit.

Heater Element Design

The heater element material selected for this investigation was commercially pure platinum wire. This selection was based upon the favorable properties of platinum for use as a resistance thermometer and its low thermal emissivity. The heater element was mounted in a plate glass tank as shown in Figure 4. The large electrodes constitute the only part of the bridge circuit which was not duplicated during the temperature
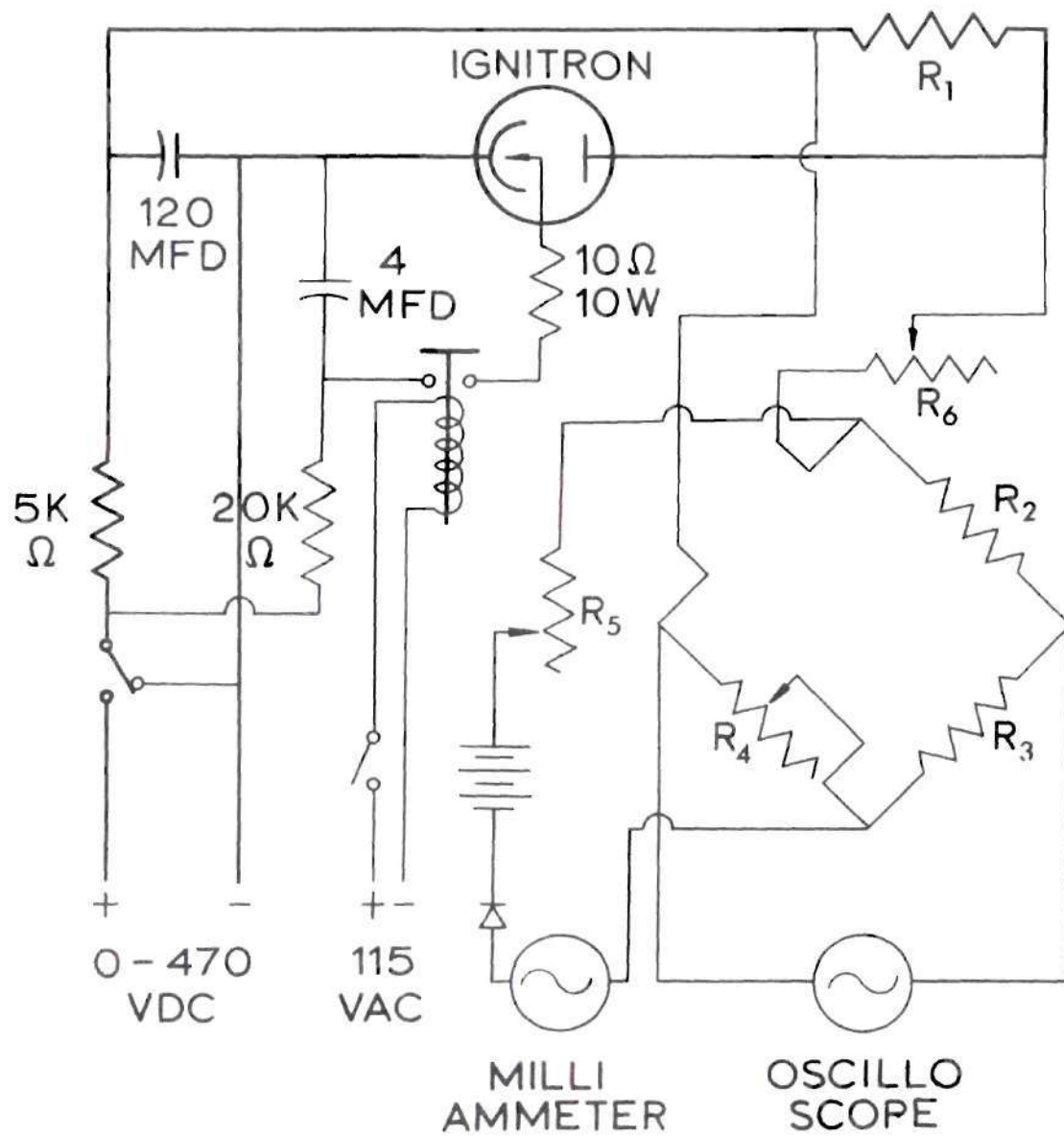
Figure 3. Transient Film Boiling System Electrical
Schematic with Wheatstone Bridge
Temperature Measurement System.
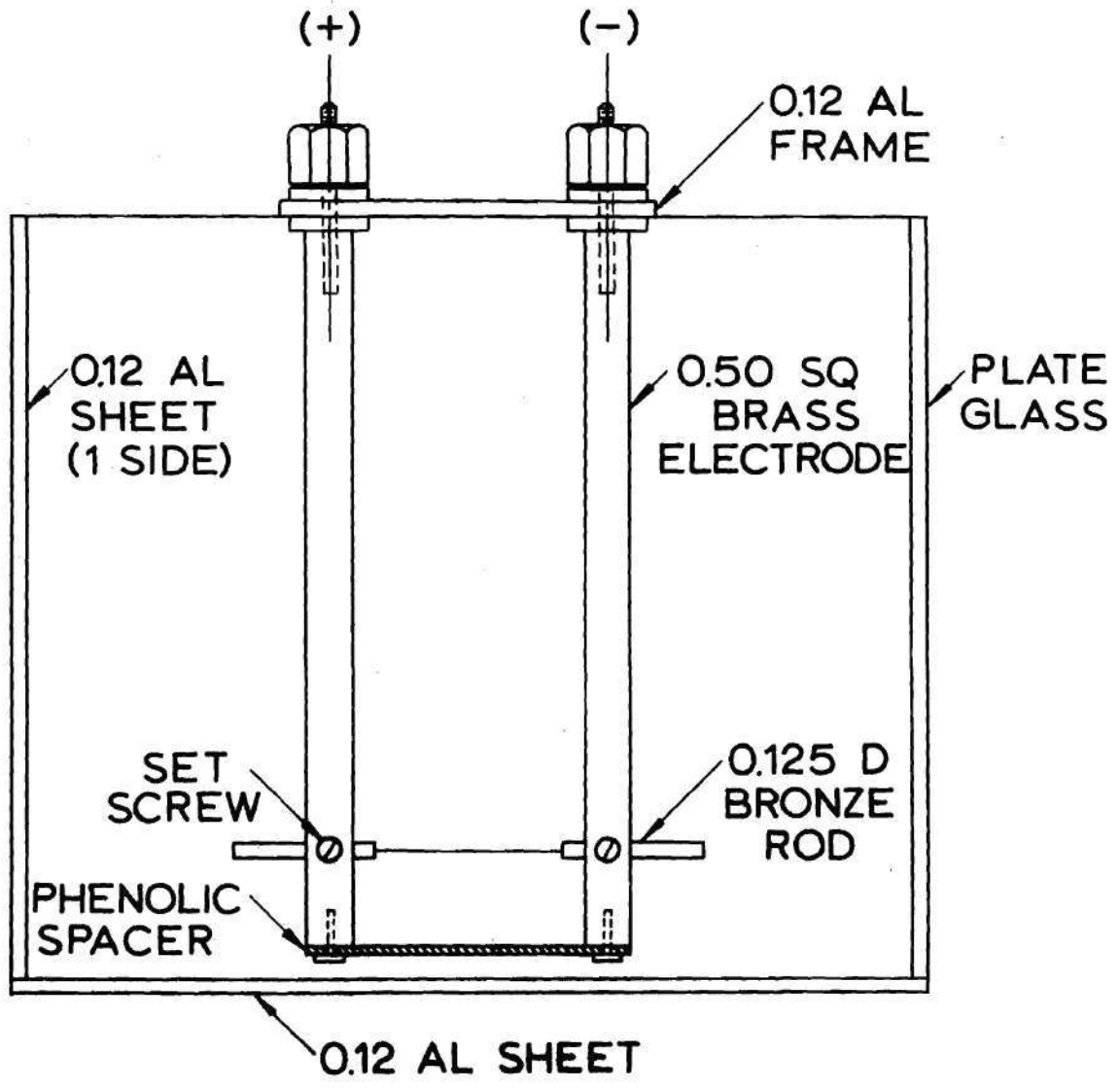
Figure 4.   Test Tank Showing Electrodes and Heater
Element Installation.

calibration. This was rendered insignificant because of the extremely low electrical resistance of these electrodes.

Several designs for mounting the wire in the one-eighth inch diameter bronze holders were tried. The first of these consisted of drilling a hole with a number 80 twist drill in the bronze holder to a depth of approximately one-tenth inch. The slightly smaller diameter platinum wire was inserted into this hole, and the bronze was crimped to secure the wire to the holder. This technique proved to be unsatisfactory due to increasing contact resistance during the rather lengthy temperature calibration. This was attributed to corrosion of the bronze surface at the elevated temperatures of the calibration.

The second technique utilized a similar design except the platinum wire was silver soldered to the bronze holder. This was accomplished by first counter-boring the end of the one-eighth inch rod with a number 30 twist drill to form a pocket to hold the solder and flux. A number 80 drill size hole was then drilled in the center of the counter-bore to an approximate one-tenth inch depth. With the holder in the vertical position, the platinum wire was inserted in the number 80 hole, the counter-bored volume was filled with solder and flux, and the holder was then heated with a small oxy-acetylene flame until the solder melted and formed a bond between the wire and the holder. This design is shown as Figure 5.

This design was acceptable and was used for several heater elements during the experimental program. There was one disadvantage, however, that was overcome by a brazing technique. This concerned the maximum temperature to which the element assembly could be subjected during calibration. In the course of the experimental investigation, it was found
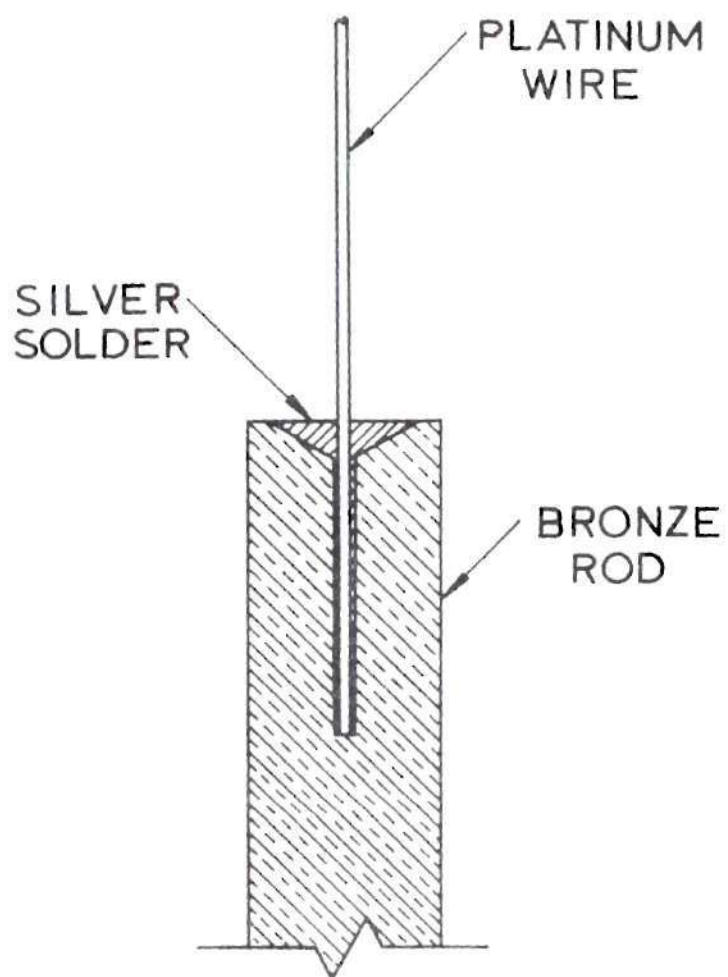
Figure 5.  Heater Wire Design - Silver Soldered
           to Holder.

desirable to collect data for element temperatures in excess of 1700 degrees Fahrenheit. The maximum calibration temperature for a silver-soldered element was approximately 1300 degrees Fahrenheit (because of the melting point of the solder used), and this would have resulted in excessive extrapolation of the calibration data. Consequently, a brazed design was developed.

Since a brazing rod section was being used as the wire holder, a fabrication problem was encountered. Elevation of the rod material to permit brazing to the platinum wire resulted in loss of configuration of the holder to such an extent that it would no longer fit in the prepared electrodes. An attempt to fabricate holders of stainless steel tubing filled by melting a brazing rod inside the tubing proved unsuccessful due to the excessive electrical resistance of the thin shell of stainless steel.

This problem was resolved by installing a short section of one-eighth inch copper tubing over the end of the brazing rod used as the wire holder. Brazing flux was then applied to the end surface of the rod, and heat was applied to the copper sleeve with the small oxy-acetylene flame. The copper, having a melting point in excess of 1900 degrees Fahrenheit, retained the rod material as it became fluid, and the platinum wire was simply inserted to a depth of approximately one-tenth inch into the molten rod. The flame was removed, and the brazed connection was allowed to cool. This configuration is shown as Figure 6. This design, in addition to permitting higher temperature calibration, was found to be easier to fabricate than any other due to the lack of any requirement for drilling very small holes.

The physical size of the heater element was governed by two factors;

PLATINUM WIRE

COPPER SLEEVE

BRONZE ROD
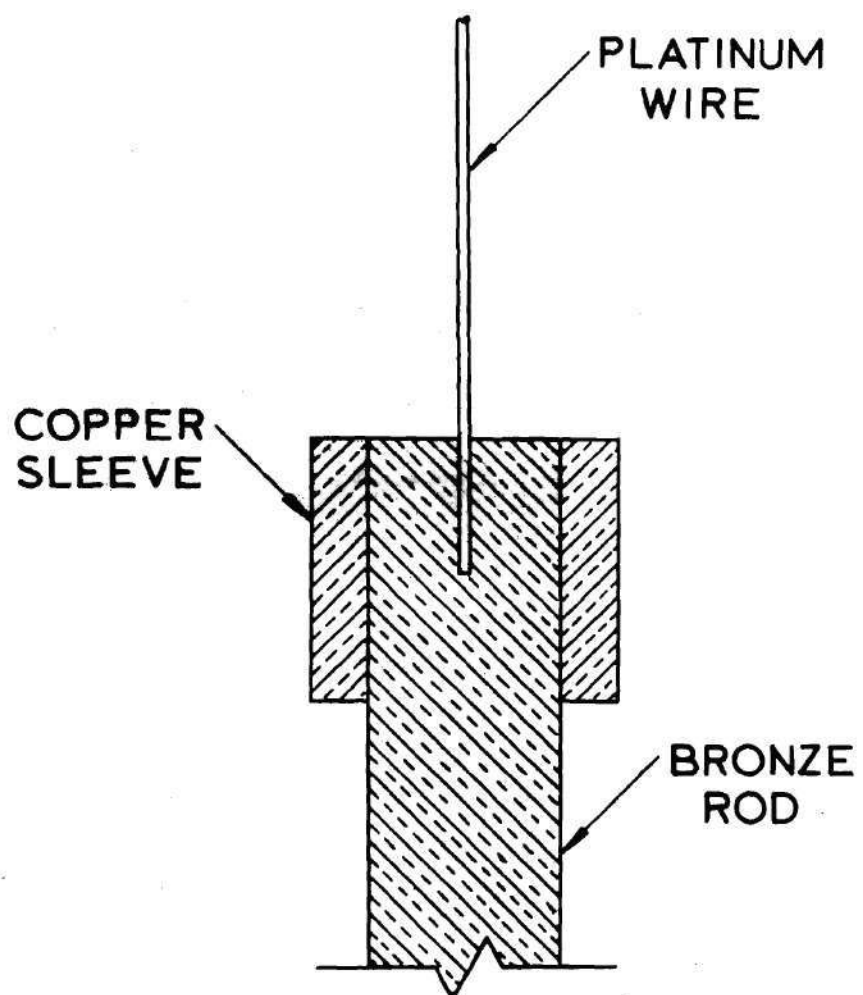
Figure 6. Heater Wire Design - Brazed to Holder.

first, the total energy available for the element temperature step-change, and second, the loss due to end conduction of heat into the wire holders. The energy available to heat the wire is the capacitor charge minus the switching loss. The capacitor charge is given by

$$Q_o = CV^2 \qquad (2.1)$$

The maximum voltage from the power supply is 470 volts d.c., and with the 120 microfarad capacitor, the total energy available is approximately 13.5 joules. Assuming a 25 per cent switching loss, the energy available for heating the element is approximately ten joules. The largest wire size for the present investigation was number 28 (0.0126 inch diameter), and using specific heat and density values

$$C_p = 0.035 \text{ Btu/lb}_m \text{ °F} \qquad (2.2)$$

$$\rho = 0.774 \text{ lb/in}^3 \qquad (2.3)$$

the temperature rise for a two-inch long section of this wire is found from

$$MC_p \Delta T = Q_o \qquad (2.4)$$

From Equation (2.4), the temperature change was calculated to be approximately 1400 degrees Fahrenheit.

The two-inch length was selected to minimize the temperature loss due to end conduction. A numerical calculation for the temperature deviation in the wire due to this effect is accomplished in Appendix B, where it is shown that the average temperature decays approximately 24.

degrees Fahrenheit in a two-inch long wire initially at 1400 degrees and with the ends held at 212 degrees Fahrenheit.

In addition to the foregoing, this wire length resulted in a sufficient resistance to facilitate use of the element as a resistance thermometer.

## Test Tank Design

The boiling test tank was constructed of a combination of one-eighth inch thick plate glass and aluminum. The basic tank frame was salvaged from a nominal two-gallon aquarium which was six inches wide by eight inches deep by ten inches long. The bottom and one end were fabricated of aluminum; this end provided a means of mounting the bulk fluid heater and thermostat. Bulk fluid heating was accomplished by means of 1500 watts of electrical resistance heating which was sufficient to raise the fluid temperature to the saturation point as measured by two ASTM three-inch immersion thermometers mounted in the tank.

## Element Temperature Measurement

### Selection of Method

The conventional steady state temperature measurement techniques are not applicable for a high speed transient phenomena where the time domain of interest is of the order of ten milliseconds. Several investigations in transient nucleate boiling have successfully utilized small thermocouples attached to ribbon type heating elements. The heater element for the present investigation could not use this type of temperature measuring system, since the thermocouple itself would have constituted a significant heat sink. Further, it is very doubtful that adequate transient response could be obtained with a thermocouple.

One of the remaining possibilities was to use the heater element as a resistance thermometer. The most direct approach to this would be to measure a current through and a potential across the element. Then a direct application of Ohm's law would yield the wire resistance. The electric current could be determined by measurement of the potential across a precision shunt; thus, this technique would involve simultaneous measurement of two transient electric potentials. Equipment available in the Georgia Institute of Technology Heat Transfer Laboratory with suffi-ciently rapid response to permit measurement after not more than one mil-lisecond is limited to high quality oscilloscopes. These are nominally accurate to within three per cent, and this naturally introduces the question of accuracy of temperature determination. Assuming for the moment that the wire resistance is a known function of temperature, the possible error due to measurement of the two electrical potentials is given by:

$$\Delta R_{error} = 1 - \frac{1.00 + 0.03}{1.00 - 0.03} = -6.2\% \qquad (2.5)$$

Returning to the wire temperature versus resistance question, it is apparent that a calibration would be required to obtain the maximum precision possible. Here again, the result could be obtained by applica-tion of Ohm's law. These data, however, could be obtained for steady state conditions with reasonably high precision.

The rather large maximum error involved in the preceding method prompted an investigation of other techniques. The method chosen involves the use of the heater wire as one resistance of an unbalanced Wheatstone bridge, in a manner quite analogous to that employed for transient strain

gage measurements. This has the primary advantage that only one oscilloscope reading is required, and that the bridge-wire combination can be calibrated as a unit for direct temperature indication with a conventional thermocouple calibration oven.

System Design

Heater Wire Selection. There are five primary material characteristics which are important for this application. These are:

- large resistance change with temperature

- monotonically increasing (or decreasing) resistance change with temperature

- good brazing qualities

- high melting temperature

- high resistance to corrosion

Several commercial trade-named wires were considered; none of these, however, were as satisfactory with respect to the first two listed characteristics as pure platinum. In addition, pure platinum is more readily available in small quantities than most of the trade name type wires.

Wheatstone Bridge. The bridge design is shown as Figure 7. The salient features of the design are:

- low bridge current resulting in negligible heating of the platinum wire

- low electrical resistance of the platinum wire (approximately one-tenth ohm) compared with any other path for the capacitor energy discharge

- high wattage resistors unaffected by the bridge current

- milliammeter to assure application of constant bridge current regardless of battery condition
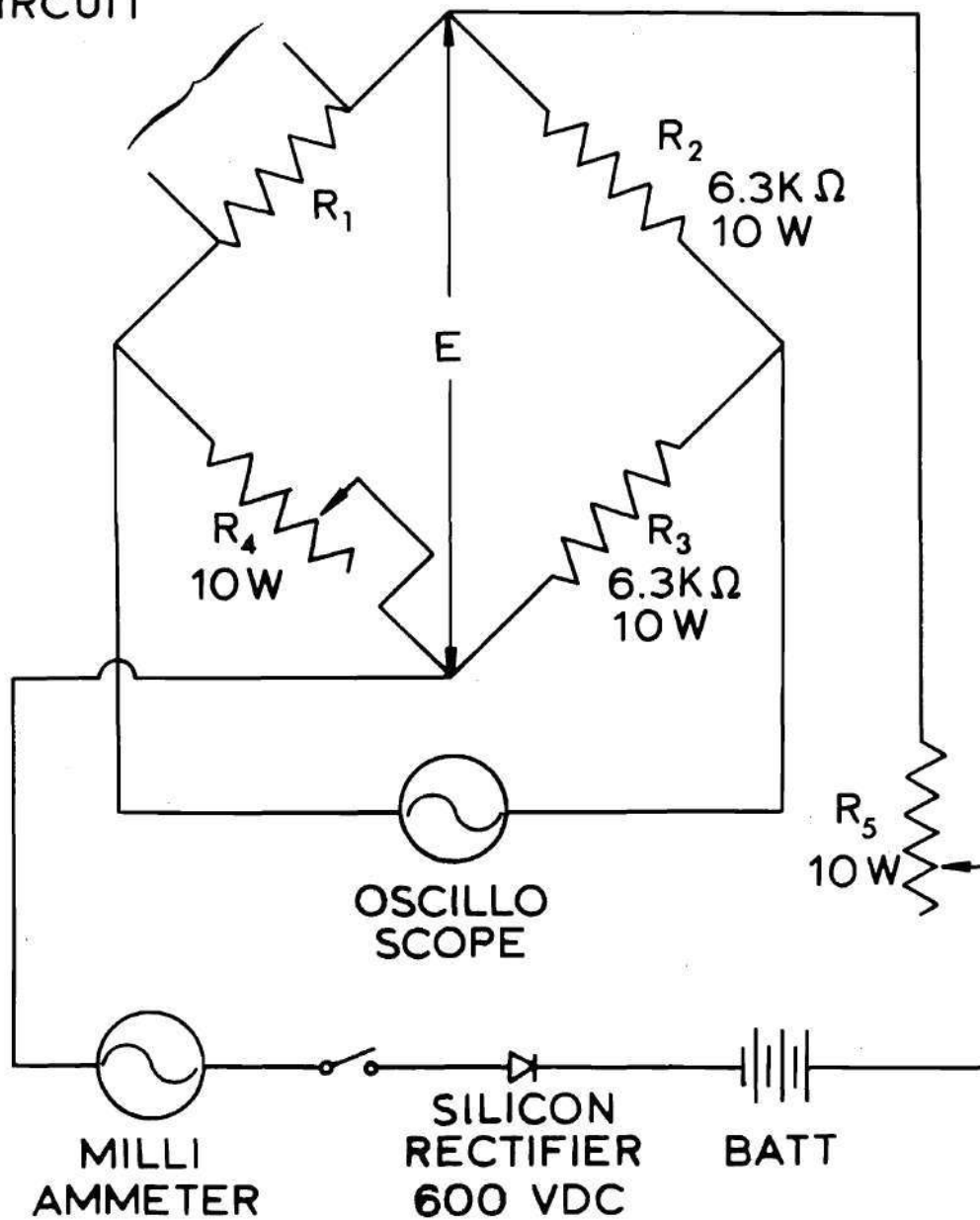
Figure 7.  Schematic Diagram of Wheatstone Bridge.

The design bridge current was on the order of 100 milliamperes. This value was based on a wire temperature rise rate of less than one degree Fahrenheit per second due to the bridge current, and using the highly conservative assumption of no heat transfer from the wire. This assured that the application of the bridge current during calibration in the thermocouple furnace did not significantly alter the wire temperature, as the time period of application was approximately one second. With regard to the effect of this current during actual testing, it was observed that no nucleate boiling would result from indefinite bridge current application with the liquid essentially at saturation conditions.

The resistance of $R_4$ (Figure 7) was adjusted to be slightly less than that of $R_1$, the platinum wire. It can be easily shown (see, e.g., reference 19) that the rate of change of bridge unbalance, e, with change in resistance of $R_1$ is given by

$$\frac{\partial e}{\partial R_1} = \frac{ER_4}{(R_1 + R_4)^2} \qquad (2.6)$$

and is thus independent of $R_2$ and $R_3$ so long as these last two resistances remain constant. This fact permitted the usage of very high value resistors for $R_2$ and $R_3$, and consequently the path for capacitor discharge through $R_2$, $R_3$, and $R_4$ was approximately 12,600 ohms. The path through $R_4$, the silicon rectifier, and $R_5$ could be completely blocked by proper orientation of the capacitor circuit leads, and even if connected so as to permit current flow through the rectifier, this circuit exhibited a resistance of approximately 50 ohms. As a consequence, the total capacitor discharge was essentially dissipated in the platinum wire which offered a

resistance of approximately one-tenth ohm.

By means of the conventional technique of equating the derivative of equation (2.6) with respect to $R_4$ to zero, we obtain

$$\frac{\partial^2 e}{\partial R_4 \partial R_1} = 0 = \frac{E(R_1 + R_4) - 2ER_4}{(R_1 + R_4)^3} \tag{2.7}$$

and hence:

$$R_1 = R_4 \tag{2.8}$$

That this condition yields a maximum rate of change of e with respect to $R_1$ rather than a minimum is apparent from equation (2.6). Thus the resistance of $R_4$ was adjusted to be slightly less than $R_1$ as previously stated, and the valve of e was always positive with respect to the zero current bridge unbalance.

The resistors $R_2$, $R_3$, $R_4$, and $R_5$ were all high wattage type (ten watts or more), and consequently were unaffected by the low bridge current. Further, all calibrations and tests were conducted with the Wheatstone bridge at normal room temperature, and these resistances remained constant for all practical purposes.

The milliammeter, together with resistor $R_5$, provided a means of maintaining a constant bridge current throughout the calibration and the ensuing experiments. Since the maximum resistance change of $R_1$ due to temperature increase was approximately two-tenths ohm, and the battery circuit resistance was approximately 50 ohms, the bridge current should have remained essentially constant. Slight variations, however, occurred,

and these were corrected by means of adjusting $R_5$. These slight varia-
tions were usually negative during a calibration, and were attributed to
diminishing dry cell battery voltage. The important factor is, however,
that the system design permitted both monitoring and regulation of the
bridge supply voltage.

## Temperature Calibration Equipment

The equipment used for calibrating the Wheatstone bridge and
heater element wire combination consisted of the following:

- thermocouple calibrating furnace, Leeds and Northrup Company,
  Philadelphia, Pa., catalog number 9003, serial number 1609778
- certificated platinum versus platinum plus ten per cent rhodium
  thermocouple, Leeds and Northrup Company, Philadelphia, Pa.
- type K - 3 potentiometer, Leeds and Northrup Company, Philadelphia,
  Pa., catalog number 7553-6, serial number 1624632
- electronic null detector, Leeds and Northrup Company, Philadelphia,
  Pa., catalog number 9834.
- unsaturated standard cell, Eppley Laboratory, Inc., Newport, R.I.,
  catalog number 103, serial number B-1608
- storage oscilloscope, Tektronix, Inc., Portland, Oregon, type
  564, serial number 003688
- differential amplifier, Tektronix, Inc., Portland, Oregon, type
  2A63, serial number 006627

Figure 8 is a photograph of the calibration arrangement which was taken
during the calibration of heater element identified as A. The platinum
wire element was mounted in the center of the vertical calibration furnace
by means of two number 10 copper lead wires extending approximately 18
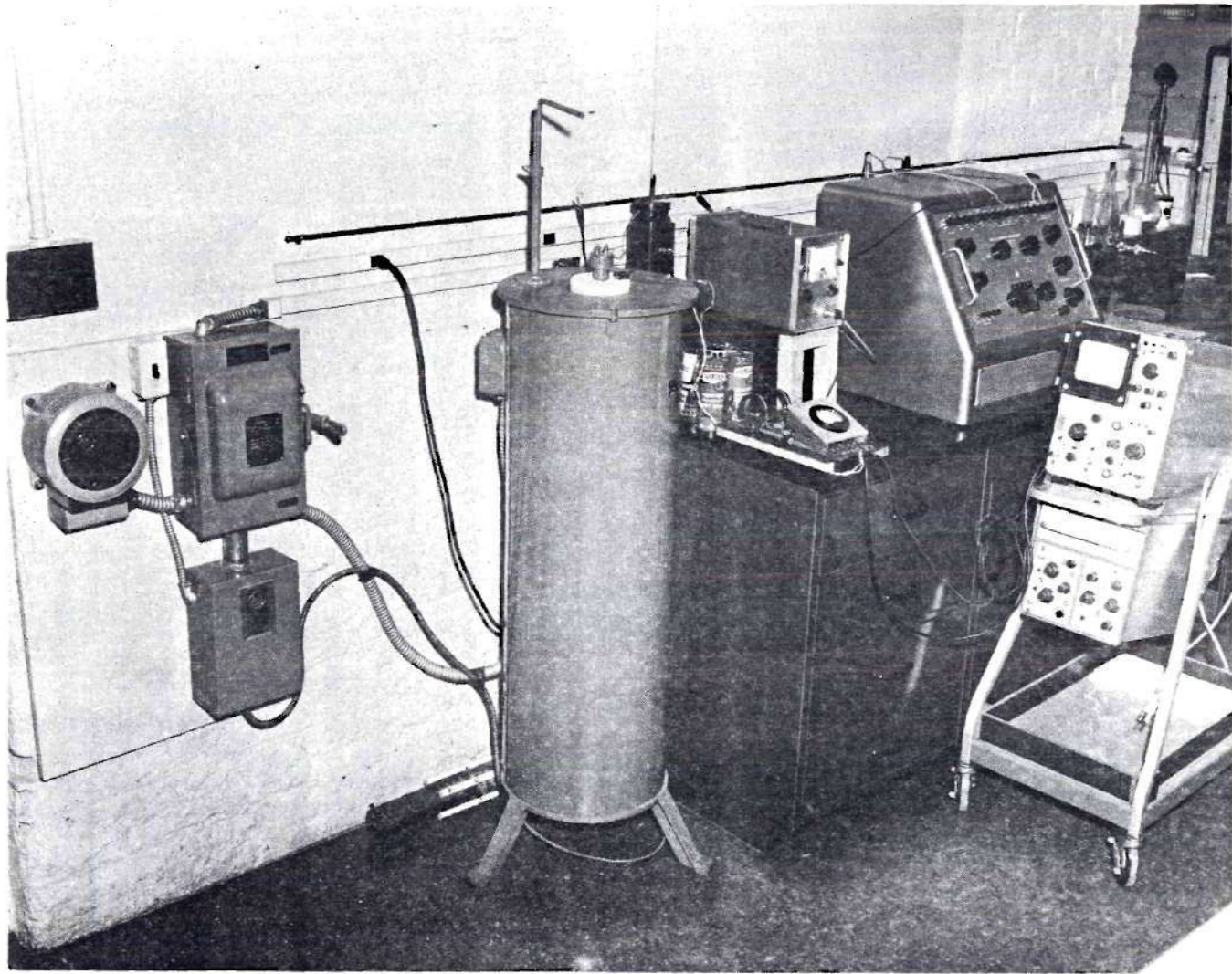
Figure 8.  Photograph of Heater Element Temperature Calibration Arrangement.

inches into the furnace.

The calibration of the potentiometer, standard cell, and electronic null detector combination was based upon the voltage of the standard cell. This cell was calibrated at the Lockheed Aircraft Corporation, Marietta, Georgia, Development Test Laboratory using a secondary standard arrangement consisting of a bank of saturated standard cells and a potentiometer calibrated by the National Bureau of Standards, Washington, D. C.

The K-3 potentiometer and null detector combination was then standardized using this cell, and immediately used to determine the voltage of the same standard cell. The value thus read was never more than 30 microvolts different than the known cell value of 1.01896 volts, and this deviation is considerably less than the error claimed by the manufacturer for this precision potentiometer.

In addition, the potentiometer, standard cell, null detector, and thermocouple combination was compared with standard laboratory thermometers at room temperature, and found to be in agreement within the readability of the thermometers.

The Wheatstone bridge unbalance was read directly on the oscilloscope, which was also used during the boiling experiments. The oscilloscope gain calibration was accomplished by means of the calibrator which is integral to the basic oscilloscope. The accuracy of this calibrator was not verified; this was not deemed necessary since the same oscilloscope was used throughout the program and the amplifier gain was always adjusted by means of the same calibrator.

The values of electromotive force and corresponding temperatures of the platinum versus platinum plus 10 per cent rhodium thermocouple

junction presented in Table 1 were furnished by the Leeds and Northrup Company with this thermocouple, and apply when the reference junctions are maintained at zero degrees centigrade. The accuracy for these data is quoted directly from the manufacturer's certificate which states, "The uncertainties in the above values are not more than 0.75°C in the range 0 to 1100°C...."

## Photographic Equipment

High speed motion picture equipment used in this investigation consisted of a HYCAM model K1004E 16 millimeter camera and accessories marketed by Red Lake Labs., Inc., Santa Clara, California. This is a rotating prism camera capable of framing rates from 10 to 10,000 pictures per second. The unit has a standard film capacity of 400 feet of film of standard thickness, but also accepts ordinary 100 and 200 feet spools of film.

This camera design features an eight-sided rotating prism and segmented disc shutter attached directly to the film sprocket shaft. The design eliminates all gears from the optical system, and enhances picture quality because of better optical compensation than that afforded by the usual 4 sided prism camera design.

Some of the features that were particularly useful in the experimental program are:

- An event synchronizer
- Direct through the lens viewing and focusing
- Standard C mount for lenses
- Built-in timing lights

Table 1. Electromotive Force and Corresponding Temperature
for Platinum vs. Platinum Plus 10 Per
Cent Rhodium Thermocouple

| Absolute Millivolts | International 1948 | |
|---|---|---|
| | Degrees Centigrade | Degrees Fahrenheit |
| 0.000 | 0.0 | 32.0 |
| 0.143 | 25.0 | 77.0 |
| 0.299 | 50.0 | 122.0 |
| 1.000 | 146.5 | 295.7 |
| 2.000 | 264.5 | 508.1 |
| 3.000 | 373.0 | 703.4 |
| 4.000 | 476.8 | 890.2 |
| 5.000 | 577.2 | 1071.0 |
| 6.000 | 674.2 | 1245.6 |
| 7.000 | 768.4 | 1415.1 |
| 8.000 | 859.9 | 1579.8 |
| 9.000 | 948.9 | 1740.0 |
| 10.000 | 1035.8 | 1896.4 |

The built-in timing lights were operated with the Red Lake Model TLG-3 Millimite timing light generator which provides pulses at 10, 100, or 1000 cycles per second. The manufacturer's stated accuracy for this signal generator is two-tenths of one per cent when the unit is maintained at room temperature. This unit was compared with the time base of the Tektronix type 564 oscilloscope, and when adjusted for an output of 1000 cycles per second, the output signal formed exactly ten cycles in ten milliseconds on the oscilloscope screen.

The lens used with this camera was a one inch, f/1.4 Cosmicar Television Lens, serial number 14757, in a focusing mount. This was combined with standard C mount extension tubes to facilitate close-up photography. For approximately one-half of the experiments, a one-half inch extension tube was used, and a one inch tube was used for the other runs. Since a normal day usually resulted in not more than two filmed experiments, this use of two different effective focal lengths served as a secondary identification of the films which were later processed by the school's photographic laboratory.

Data reduction from the processed film was accomplished with a Bell and Howell Model 173 Time and Motion Study Projector, serial number AJ92065. This unit was equipped with a Bell and Howell f/1.9 one inch, Increlite projection lens. The two features of this projector which were of most convenience are the provision for projection of individual frames for periods up to four minutes, and a frame counter directly coupled to the film sprocket.

Photographic lighting was accomplished with a Red Lake Laboratories model RLLi-1 lighting unit which is basically a General Electric

Company 1000 watt quartz iodine lamp. This was augmented by the use of a single photo-BFJ 750 watt photo-flood bulb, or by one, two, or three photo-DXB 500 watt photo-spot bulbs.

Heater element wire diameters were measured with a direct reading micrometer having 0.001 inch scale divisions, and with a Bausch and Lomb Company Model DR-25, direct measuring, pre-calibrated instrument. This unit reads to 0.0001 inch, and permits interpolation to one additional significant figure.

CHAPTER III

EXPERIMENTAL PROCEDURE

Temperature Calibration

The heater element, mounted in the one-eighth inch diameter bronze holders, was attached to number ten bare copper lead wires and placed in the approximate center of the thermocouple calibration furnace. The lead wires were brought out of the furnace through one-half inch diameter holes in a four inch thick ceramic plug which filled the top opening of the furnace. This plug was designed to permit insertion of the calibrated standard platinum versus platinum plus ten per cent rhodium thermocouple so that the junction was located in the center of the furnace. The one-half inch holes through which the bare copper wires passed were closed at both ends with asbestos cloth wrapped tightly around the wire to form a dead air pocket in each passage through the ceramic plug. The two copper lead wires had a combined heated length of 48.5 inches, and corrections to the heater element temperature measuring circuit were made for this during the ensuing tests.

The reference junctions of the standard thermocouple were immersed in an ice water bath maintained in a thermally insulated vacuum bottle. Calibrations were performed both with ice made from distilled water and with ice made from ordinary tap water. No differences were detected in the results from the two grades of ice water.

All instrumentation in Figure 8 was turned on at least 30 minutes prior to recording of calibration data. This is the manufacturers'

recommended warm-up period both for the oscilloscope and the electronic null detector. The oscilloscope was checked for *gain adjustment* using the built-in calibrator in accordance with the manufacturer's recommended procedure. Calibration data were then obtained with no furnace heating as follows:

1) The potentiometer and null detector combination was standardized.

2) The reference junction ice bath was stirred.

3) The Wheatstone bridge current was checked and adjusted as necessary.

4) With the bridge current off, the oscilloscope reference or base line was recorded.

5) With bridge current applied, the oscilloscope reading of bridge unbalance was recorded.

6) The platinum versus platinum plus ten per cent rhodium thermocouple emf was recorded with the potentiometer.

Following this, a power level for furnace heating was selected that would result in a temperature increase of approximately 200 degrees Fahrenheit. The furnace controller provides two modes of operation, full line current for rapid heating and controlled current for temperature stabilization. Using full line current, the temperature was raised to the desired value. Then the unit was placed in the control mode and allowed to stabilize which required from one-half to one hour for a change of 200 degrees. At the new temperature level, the procedure of steps one through six was again employed. This process was repeated to yield about eight calibration points for the temperature range of interest.

During the calibration, two possible sources of error were investigated. The first of these was with regard to possible hystersis. Two of the earliest elements checked were subjected to calibration both during heat-up and during cool-down. In addition, one of these was subjected to a second temperature application in the furnace. No shift in data was observed.

A second possible source of error is introduced by heat loss due to conduction in the lead wires to the element in the furnace. If this error were significant, the platinum wire element could be at a temperature appreciably below the furnace ambient recorded by the standard thermocouple. In order to investigate this, a chromel-alumel thermocouple was imbedded in one of the copper leads at a location adjacent to the attachment of the element holder. During the ensuing calibration, the temperature indicated by this thermocouple agreed within its limits of accuracy with the standard thermocouple up to a temperature of approximately 700 degrees Fahrenheit, at which point it failed due to insulation break-down. Thus at 700 degrees Fahrenheit, the conduction in the copper lead did not noticeably reduce the metal temperature where it connected with the heater element holder, and consequently this problem was considered to be inconsequential.

A total of 12 heater elements were calibrated during the course of this investigation. Only five of these calibrations, however, were actually used in recorded transient boiling experiments. This was a simple consequence of the difficulties encountered during the experimental program; most of the elements failed due to burn-out during preliminary runs. Calibration data for these five elements and element

descriptive information are given in Appendix D. The actual temperature
at any calibration point can be obtained from the thermocouple electromo-
tive force in conjunction with the data of Table 1. A typical element
calibration curve is presented in Figure 9.

## Film Boiling Experiments

The procedure for all experiments was essentially the same, and
can be briefly described as follows: The boiling test tank was filled
with distilled water and the fluid bulk heaters were turned on. The water
was boiled vigorously for a period of not less than one hour to remove
entrained gases. During this period, the camera was critically focused
on the wire element and loaded with film. The camera framing (speed)
rate was selected, and the lighting was adjusted. The quartz-iodine lamp
was normally used for front illumination, and was incident upon the wire
at an angle of approximately 50 degrees from the vertical. One photo-
spot or one photo-flood bulb was located to provide illumination from
the back, and was incident upon the wire at an angle of about 60 degrees
from the vertical. Additional photo-spot lights were used for some of
the runs.

The oscilloscope was allowed to warm-up during the pre-run boil-
ing period. After a minimum of 30 minutes of operation, this item was
calibrated both for vertical deflection gain and for horizontal sweep
rate in accordance with the manufacturer's operational manual. A zero
bridge current reference line was then recorded on the oscilloscope, and
the heater element Wheatstone bridge current was adjusted to the value
used during the element calibration. The direct current power supply
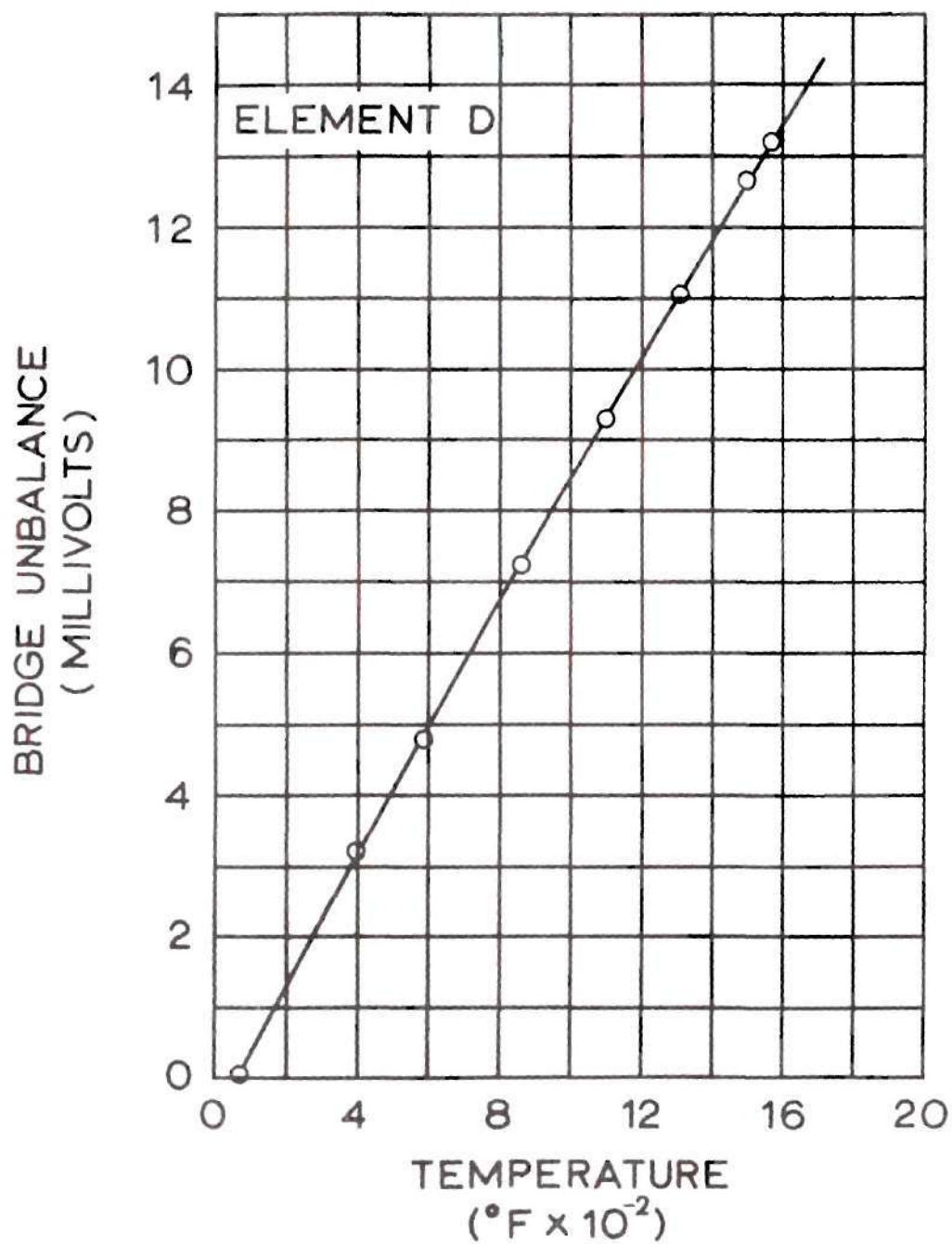
Figure 9. Typical Calibration Curve for Heater Element.

unit was turned on and adjusted to the desired voltage. This was used to charge the main capacitor (Figure 3), and a pre-run firing was accomplished to determine the resultant heater element temperature.

Using this value as a guide, the wiring circuit from the bridge to the heater element was adjusted to add a length of number 10 copper wire having a resistance at room temperature equal to that of the 48.5 inch leads used in the calibration furnace while at the temperature of the element. This corrective adjustment was necessitated by the fact that the only part of the system at the elevated temperature during the experiment was the platinum element, whereas the copper lead wires were also raised to the high temperature during the calibration. The temperature resistance data for the copper wire was taken from the International Critical Tables (20), and the length of number 10 copper wire having the resistance of the 48.5 inch long leads is given as a function of temperature in Figure 10. This length adjustment was accomplished by means of the corrective coil, Figure 11, which was made by coiling approximately 260 inches of number 10 copper wire and providing electrical connectors at stations representing increments of 100 degrees Fahrenheit change in temperature. It should be noted that the total resistance offered by these leads was only about 5 per cent of the resistance of the platinum element at the highest temperature employed; consequently correction to the nearest 100 degrees was adequate.

The complete system was then checked by a second pre-run test. The capacitor was recharged and a zero bridge current reference line recorded on the oscilloscope. The bridge current was adjusted to the proper value, i.e., 80 milliamps for a number of 30 wire size element, or
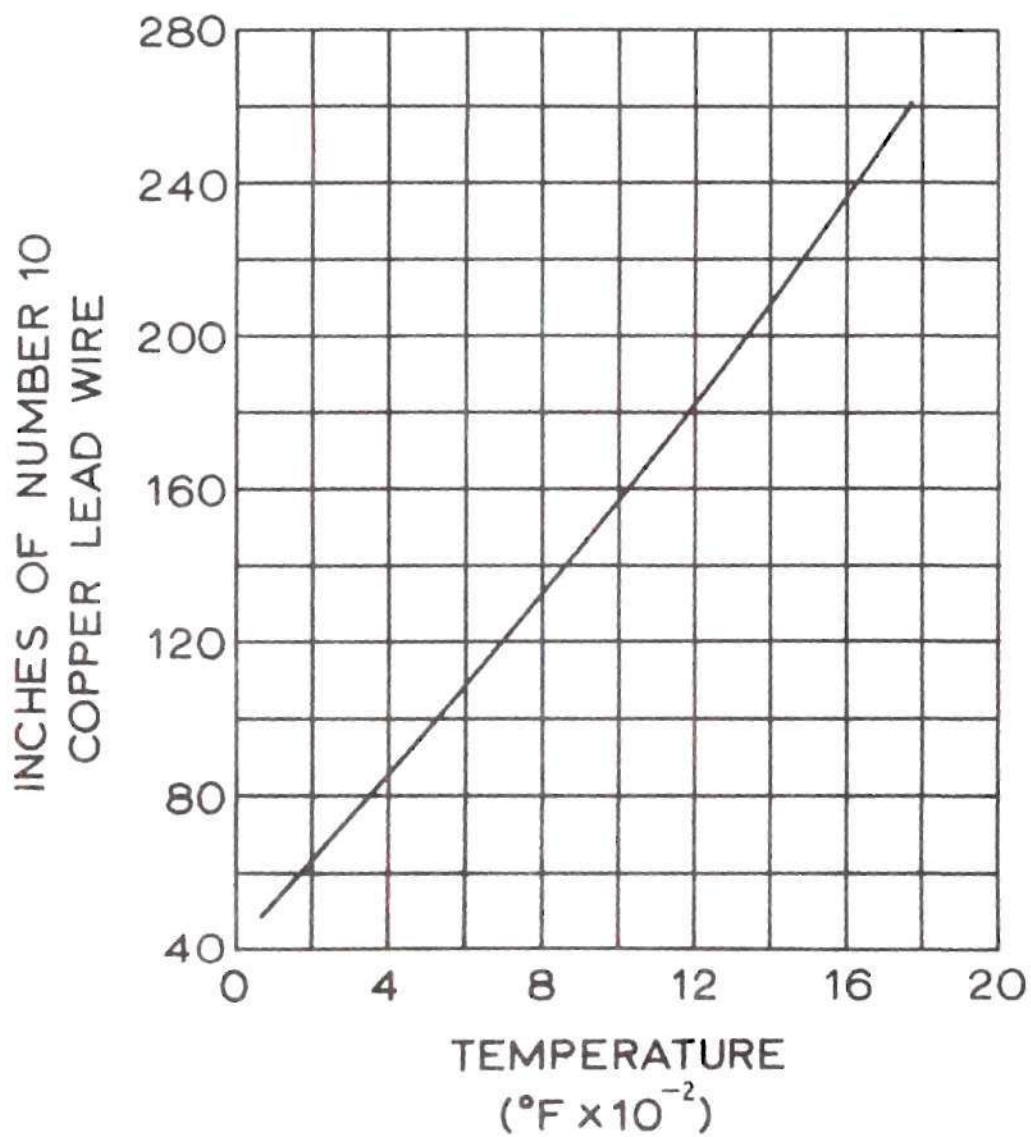
Figure 10.   Length of Number 10 Copper Wire at 70 Degrees
             Fahrenheit Having Electrical Resistance Equal
             to That of 48.5 Inches at Elevated Temperature.
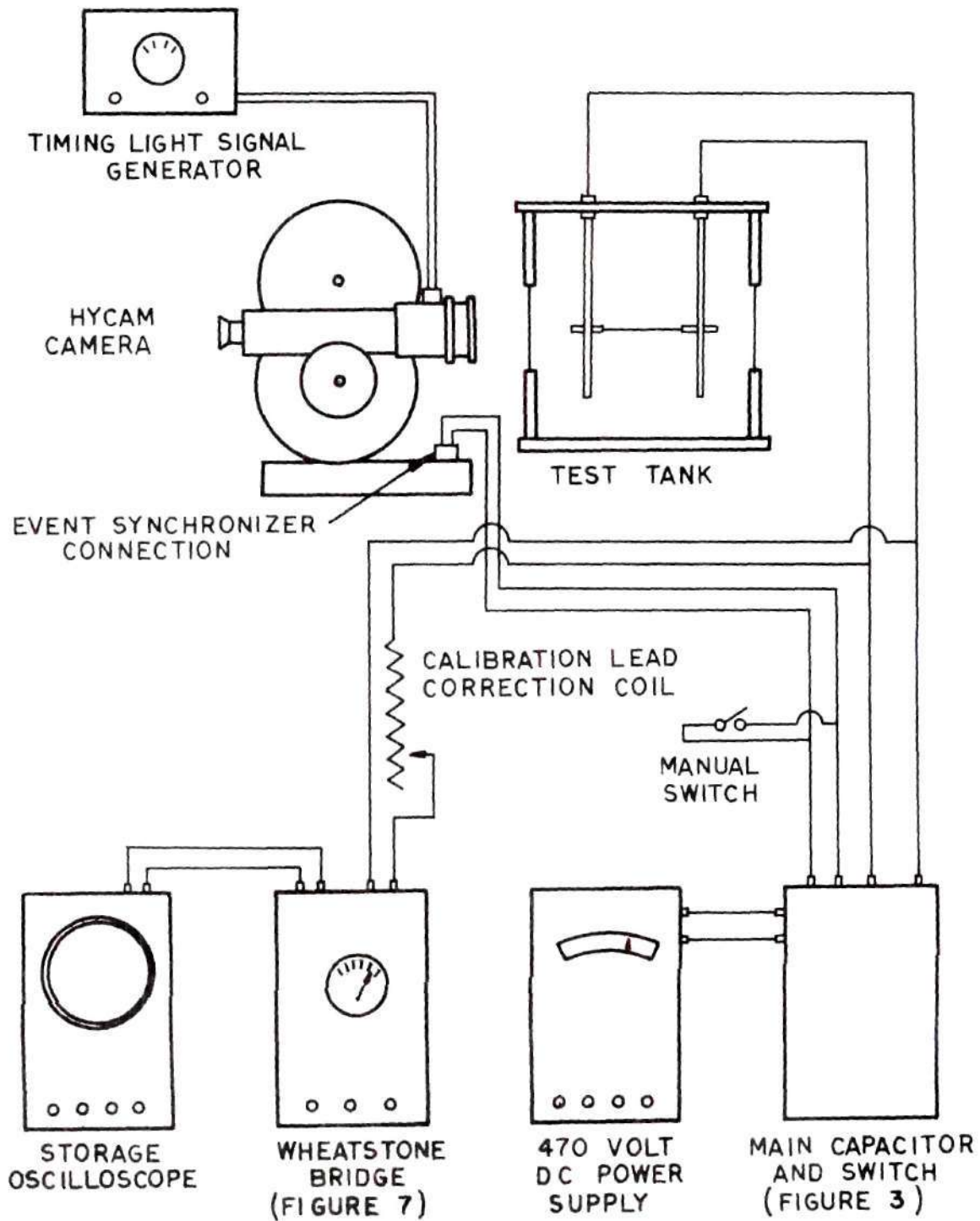
Figure 11. Schematic of General Experiment Arrangement.

120 milliamps for a number 28 wire size element, and the capacitor was discharged by manual closure of the camera synchronizer circuit. This resulted in capacitor discharge through the heater element and automatic triggering of the oscilloscope to record the bridge unbalance as a function of time. Usually several such pre-test runs were required to properly adjust all of the equipment. The most troublesome item was the oscilloscope. Its mode of operation was, of course, single sweep. The unit can be adjusted for either internal or external triggering, but it is very sensitive to stray signals in either mode.

The method of triggering which evolved during the investigation was to use the external mode and feed the actuation signal directly from the electrode connections on the test tank to the oscilloscope trigger connection. This wiring is omitted from Figure 11. Even with this system, false triggering was common, and this resulted in several heater element temperature excursions during the process of adjusting the equipment prior to each recorded test. This factor is mentioned because it had a direct bearing upon the number of element failures experienced during the program. Repetitive heating of the element to temperatures in excess of 1500 degrees Fahrenheit inevitably resulted in element burn-out adjacent to one of the bronze holders. In addition to this detrimental aspect, these pre-run firings undoubtedly accomplished both out-gassing and degassing of the heater element.

Following adjustment of the equipment, a filmed run was made. The data recorded for each test included:

· barometric pressure

· bulk water temperature at time of capacitor discharge

- depth of water above heater element

- type of film

- lens data

- camera nominal speed setting

- lighting data

- Wheatstone bridge unbalance versus time

- capacitor charge voltage

- heater element identification

These data, for each of the reported runs, are presented in Tables 6 and 7 in Appendix D.

A total of 17 filmed tests were conducted. Of these, the results of 12 are reported herein. With regard to the other five, the following comments are offered.

Run 2. This test was conducted at a low element temperature and the resulting boiling was in the transition region.

Run 8. This test was intentionally conducted with the bulk fluid subcooled 17 degrees Fahrenheit and the results will be a part of a following investigation.

Run 11. The heater element burned out during the capacitor discharge, and a significant part of the energy was dissipated at the element failure point.

Run 12. This test was conducted with an uncalibrated gold element for reasons discussed in Chapter V.

Run 13. This was the lowest temperature test undertaken with a number 28 wire size element. The phenomenon appeared to be partially within the transition regime with a higher attendant heat flux.

## Data Reduction

Quantitative data were obtained from the high speed movie films of
the transient film boiling experiments. Preliminary data reduction was
accomplished with a 16 mm movie editor having a screen size of *approxi-*
*mately* four by five inches. This unit afforded a projected view of the
heater element wire as small as 2 millimeters, and since this measurement,
in conjunction with the measured actual wire size, served as the primary
scale factor for vapor volume measurement, a larger projection was needed.
The Bell and Howell model 173 projector provided improved image size, de-
finition, and light intensity. With this, the frame image was magnified
to 11 by 15 inches, and the resulting minimum projected wire size was
greater than two-tenths of an inch.

The transient film growth was not truly cylindrical as can be seen
in Figure 12. Consequently, numerous measurements were required to
determine the vapor volume at any given time. The technique developed
involved the assumption that the vapor bubble could be represented as a
body of revolution. Thus, the volume could be approximated by measuring
the diameter at prescribed intervals along the length of the wire, cal-
culating the area at each of these stations, multiplying this area by the
distance between stations to form a volume, and summing the total of the
incremental volumes thus formed. In mathematical form this is

$$V = \sum_{i=1}^{n} \frac{\pi}{4} D_i^2 \Delta \ell_i \qquad (3.1)$$

where
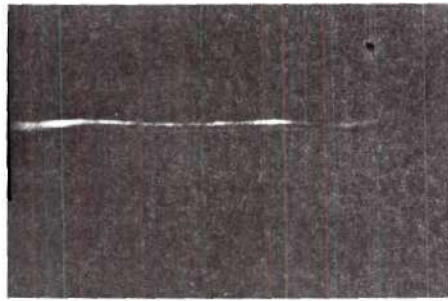
Time:   0.00 x 10$^{-3}$ sec.
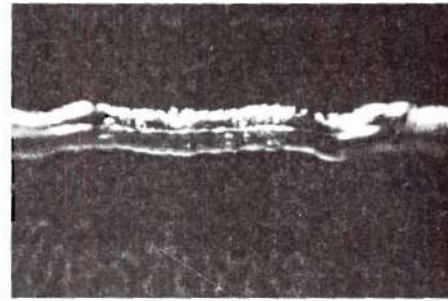
Time:   0.266 x 10$^{-3}$ sec.
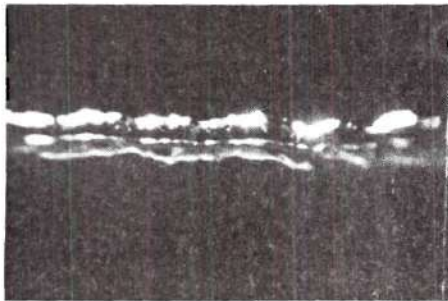
Time:   1.33 x 10$^{-3}$ sec.
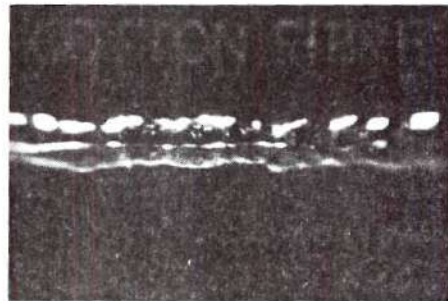
Time:   2.66 x 10$^{-3}$ sec.
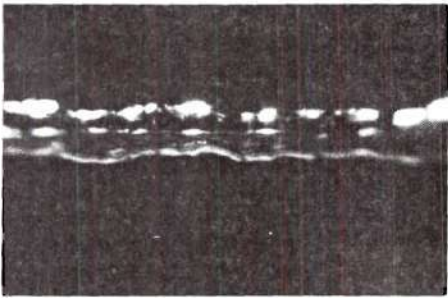
Time:   4.0 x 10$^{-3}$ sec.
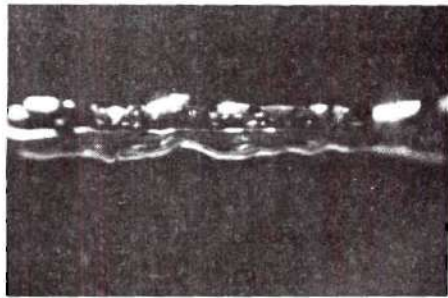
Time:   5.23 x 10$^{-3}$ sec.

Figure 12.   Sequence Photographs of Typical Transient Film
Boiling on a Horizontal Platinum Wire.
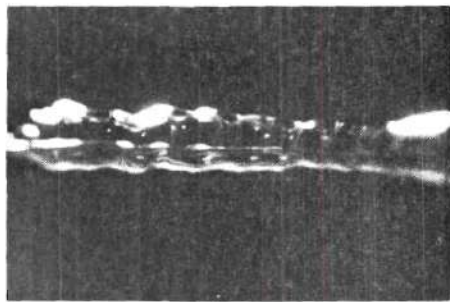
Time: 6.67 x $10^{-3}$ sec.
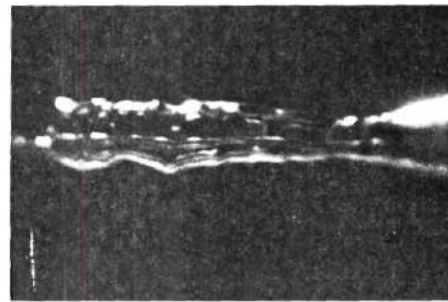


Time: 8.0 x $10^{-3}$ sec.
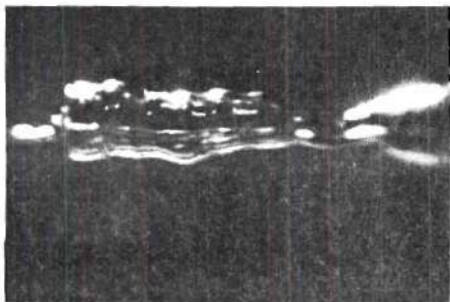


Time: 9.33 x $10^{-3}$ sec.
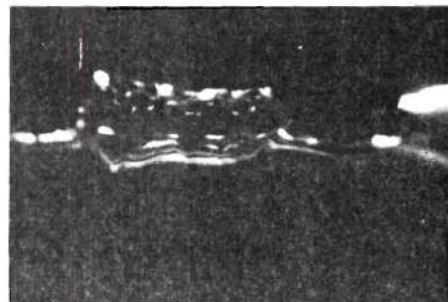


Time: 10.68 x $10^{-3}$ sec.
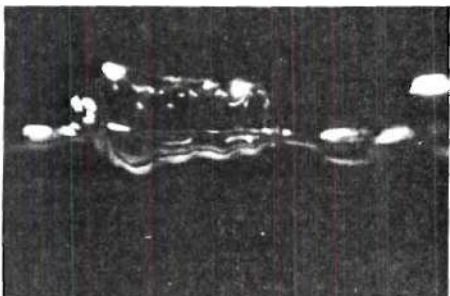


Time: 12.0 x $10^{-3}$ sec.
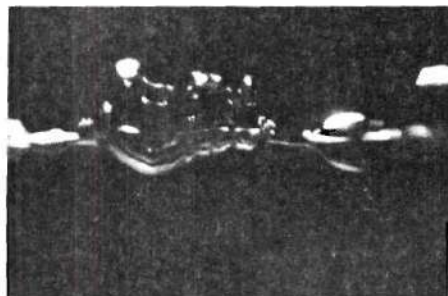


Time: 13.33 x $10^{-3}$ sec.

Figure 12. (Continued) Sequence Photographs of Typical Transient
Film Boiling on a Horizontal Platinum Wire.

$$\Delta \ell_1 = \Delta \ell_2 = \cdots \cdots \qquad (3.2)$$

Now obviously the accuracy of the volume thus determined is dependent upon the non-uniformity of the surface along the length and the size of the incremental length chosen. The error can be reduced simply by increasing the number of measurements, i.e., by reducing the incremental length associated with a specific diameter. For the present investigation, the total filmed length of wire varied from approximately three-eighths to three-quarters of an inch, depending upon the length of the extension tube used with the camera lens. For the longer case, it was found that division into 26 length intervals resulted in a vapor volume which differed with that obtained using 13 intervals by about 3 per cent. As a consequence, it was decided that finer division was unnecessary, and 26 intervals were used for final data reduction for all runs.

A projection screen was prepared from white cardboard with vertical division lines at one-half inch horizontal spacing. The projected picture was adjusted to cover 26 of these lines, and diameter readings were taken only at these stations.

It was decided that vapor volume at one millisecond intervals would suffice to represent the growth rate. Data during the first millisecond following capacitor discharge were highly unreliable due to the nucleate character of the initial vapor formation, and consequently were neglected in the process of data reduction. The zero time point was established as being the last frame on a roll with no vapor formed. Usually, the next frame depicted a large amount of opaque vapor, and since the framing rate for most runs was about 4000 pictures per second,

the maximum time error was of the order of one-fourth millisecond. With
the zero time point thus established, the time for a particular frame was
determined by means of the timing light blip at one millisecond intervals
along the edge of the film. Using this, frames were selected for vapor
volume measurement at intervals close to one millisecond.

The Bell and Howell Model 173 Projector was manually operated to
the desired frame indicated on the continuous frame counter and determined
by subtracting the indicated number of the zero time frame. Then, the 26
diameter measurements were taken with a Keuffel and Esser Company, Para-
gon, Model 1375P-24 scale. This is a white drafting scale with 0.02 inch
black marked graduations, and was found to be ideally suited both with
respect to contrast and with respect to graduation size. This procedure
was repeated for frames at the selected spacing until the configuration
of the vapor bubble indicated serious deviations toward stable film boil-
ing. This change normally occurred at about ten milliseconds, and is
quite obvious in Figure 12. The data thus obtained are presented in
Tables 8 through 19 in Appendix D.

Using these measurements, the void volume for each frame was cal-
culated with Equation (3.1). This volume was divided by the total length,
i.e.,

$$L = \sum_{i=1}^{n} \Delta \ell_i \qquad (3.3)$$

to yield the volume average area of the vapor cylinder. The volume
median diameter was then determined from the volume average area.

Routine computational work was facilitated by use of a Friden

desk calculator for summation of incremental volumes and determination of volume average areas, and by use of a Friden Model 132 Electronic Calculator for extraction of the square roots necessary for determination of volume median diameters.

The final results are presented as Figures 18 through 29 of Appendix D. These depict the vapor growth rate as a plot of vapor bubble volume median diameter versus time for each of the 12 experiments of this investigation.

CHAPTER IV

ANALYSIS

## Film Growth Rate

It is postulated that a horizontal, cylindrical wire submerged in a liquid and at the temperature of the liquid experiences a sudden, large increase in temperature which can be represented as a step change. If this temperature increase is sufficiently large to result in film boiling, we may depict the reaction at the metal-liquid interface as one in which the density of nucleation sites is so great that a continuous vapor film is formed. Thus, the physical model for analysis is that of a uniform vapor film, initially of zero thickness, which increases with time. Eventually, the vapor liquid interface becomes quite distorted, and the model is no longer valid, but the primary concern is with the growth rate during the first ten milliseconds. For this period, the film can be reasonably described as cylindrical. Thus, the problem can be treated as one-dimensional, and is, in actuality, an extension of the Stefan melting-freezing problem.

The physical model assumed is presented in Figure 13. The major assumptions in this model are:

1. The liquid is separated from the metal by a continuous vapor blanket whose thickness is independent of length.

2. The vapor-liquid interface is smooth and continuous.

3. The boiling liquid is at saturation temperature at the liquid-vapor interface.
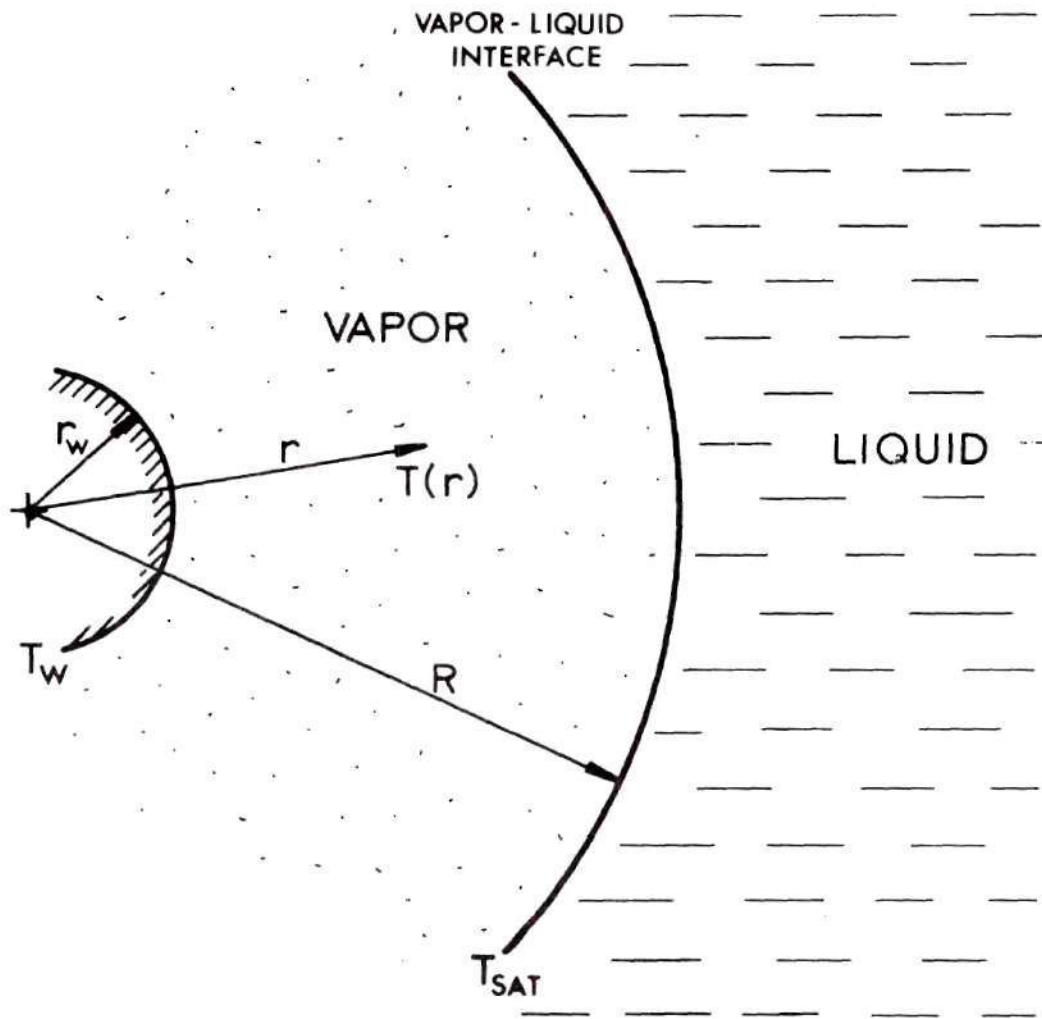
Figure 13. Physical Model for Transient Film Boiling from a
Cylindrical Surface.

The governing equations for the vapor film in cylindrical coordinates are

Energy

$$\rho Cp \left[ \frac{\partial T}{\partial t} + v_r \frac{\partial T}{\partial r} \right] = k \left[ \frac{\partial^2 T}{\partial r^2} + \frac{1}{r} \frac{\partial T}{\partial r} \right] \quad (4.1)$$

Momentum

$$\frac{\partial v}{\partial t} + v_r \frac{\partial v_r}{\partial r} = \frac{\mu}{\rho} \left[ \frac{\partial^2 v_r}{\partial r^2} + \frac{1}{r} \frac{\partial v_r}{\partial r} - \frac{v_r}{r^2} \right] \quad (4.2)$$

$$+ \frac{\lambda + \mu}{\rho} \frac{\partial}{\partial r} \left[ \frac{1}{r} \frac{\partial}{\partial r} (rv_r) \right]$$

Continuity

$$\frac{\partial \rho}{\partial t} + \frac{1}{r} \frac{\partial}{\partial r} (\rho r v_r) = 0 \quad (4.3)$$

where the following assumptions have been made:

a) axial symmetry

b) no velocity or thermal variation with length

c) negligible work of compression

d) negligible viscous dissipation

e) negligible radiation to the vapor

f) no heat generation in the vapor

g) negligible body forces in the vapor

h) constant viscosity

i) constant thermal conductivity

j) no radial pressure gradient

These equations are readily obtainable from the more complete forms by application of the listed assumptions, and this is accomplished in Appendix A.

The boundary conditions on the energy equation a

$$r = r_w : T(r_w, t) = T_w \tag{4.4}$$

$$r = R : T(R, t) = T_{sat} \tag{4.5}$$

The interfacial temperature at the vapor-liquid boundary is the saturation value regardless of the liquid bulk temperature. The boundary conditions on the momentum equation are:

$$r = r_w : v(r_w, t) = 0 \tag{4.6}$$

$$r = R : v(R, t) = \dot{R} \tag{4.7}$$

where the last condition can be shown to apply if the density of the vapor is negligible in comparison with the density of the liquid. Equations (4.1) through (4.3) constitute a set of three equations in three unknowns, density, velocity, and temperature. The boundary conditions, however, introduce an additional unknown, R, the position of the vapor-liquid phase change front. As a consequence, an additional equation is necessary. This may be obtained from a conservation of energy at the vapor-liquid interface which can be expressed as:

$$\rho h_{fg} \dot{R} = -k_v \left. \frac{\partial T}{\partial r} \right|_R + k_\ell \left. \frac{\partial T}{\partial r} \right|_R + \varepsilon_w a_\ell \sigma T_w^4 \left. \frac{r_w}{r} \right|_R \tag{4.8}$$

This expression relates the energy required to vaporize the liquid to the algebraic sum of the energy conducted to the interface through the vapor, the energy conducted away from the interface through the liquid, and the radiant energy from the wire absorbed at the moving front. Equation (4.8) is also derived in Appendix A.

Turning to the case of saturated film boiling, the term in Equation (4.8) representing the energy conducted into the liquid disappears. Further, for the case of platinum wires, the low metal emissivity renders the radiant energy term negligible for the temperatures of the present investigation, and this equation reduces to

$$\rho h_{fg} \dot{R} = -k_v \left. \frac{\partial T}{\partial r} \right|_R \tag{4.9}$$

Since the vapor properties are known functions of temperature and pressure, a knowledge of the temperature as a function of radius would suffice to determine $\dot{R}$, and consequently would completely determine the growth history of the film.

Retention of both convective and conductive terms in the energy equation would necessitate the simultaneous solution of it with the momentum equation. The most promising approach to this would be the use of a digital computer program. The question naturally arises as to whether convective energy is significant in this problem or not. If not, the possibility of obtaining a closed form solution of the energy equation is introduced, and this factor is deemed important by the present author.

There is precedent for the assumption that the phenomenon is primarily controlled by conduction. Bromley (21) in his pioneering work on stable film boiling states as an assumption for his theory, "Heat travels through vapor film by conduction and radiation." Several other researchers have indicated that the primary mode of heat transfer in the vapor during film boiling is by conduction. The stable film boiling process is characterized by growth of film until large bubbles break away, and then the

growth at that point begins again with a thin film. Thus, the mechanism of stable film boiling should be very similar to that for transient film boiling.

<u>Transient Conduction Solution</u>

Assuming convective terms to be negligible, the energy equation for the vapor reduces to

$$\frac{\partial T}{\partial t} = \alpha \left[ \frac{\partial^2 T}{\partial r^2} + \frac{1}{r} \frac{\partial T}{\partial r} \right] \tag{4.10}$$

Introducing the dimensionless temperature defined by

$$\theta = \frac{T_w - T}{T_w - T_{sat}} \tag{4.11}$$

the energy equation becomes

$$\frac{\partial \theta}{\partial t} = \alpha \left[ \frac{\partial^2 \theta}{\partial r^2} + \frac{1}{r} \frac{\partial \theta}{\partial r} \right] \tag{4.12}$$

Under the transformation

$$\eta \equiv \frac{r}{2\sqrt{\alpha t}} \tag{4.13}$$

where it is assumed that

$$T = T(\eta) \tag{4.14}$$

Equation (4.12) becomes:

$$\frac{\partial^2 \theta}{\partial \eta^2} + (2\eta + \frac{1}{\eta}) \frac{\partial \theta}{\partial \eta} = 0 \qquad (4.15)$$

The solution to equation (4.15) may be taken from Kamke (22), and is:

$$\theta = \beta_1 + \beta_2 \int e^{-\int (2\eta + \frac{1}{\eta}) d\eta} d\eta \qquad (4.16)$$

Integrating Equation (4.16) yields

$$\theta = \beta_1 + \beta_3 \int \frac{e^{-\eta^2}}{\eta} d\eta \qquad (4.17)$$

which after multiplication and division of the integrand may be expressed as

$$\theta = \beta_1 + \beta_4 \int \frac{e^{-\eta^2}}{\eta^2} d\eta^2 \qquad (4.18)$$

Examination of the definition of $\eta$, Equation (4.13) reveals that

$$\lim_{t \to 0} \eta = \infty \qquad (4.19)$$

and for any finite value of $t$, the limiting value is simply $\eta$. Thus, for the present problem Equation (4.18) may be expressed as

$$\theta = \beta_1 + \beta_5 \int_{\infty}^{\eta^2} \frac{e^{-y}}{y} dy \qquad (4.20)$$

or, in terms of $E_i(-\eta^2)$ defined by

$$-E_i(-\eta^2) = \int_{\eta^2}^{\infty} \frac{e^{-y}}{y} \, dy \qquad (4.21)$$

the dimensionless temperature is given by:

$$\theta = \beta_1 + \beta_5 E_i(-\eta^2) \qquad (4.22)$$

Returning to the $(r,t)$ coordinate system, the dimensionless temperature at any specific time, $\tau$, is given by

$$\theta = C_1 + C_2 E_i\left(\frac{-r^2}{4\alpha\tau}\right) \qquad (4.23)$$

with boundary conditions

$$\theta(r_w,\tau) = 0 \qquad (4.24)$$

and

$$\theta(R,\tau) = 1 \qquad (4.25)$$

Applying the boundary condition of Equation (4.24) to Equation (4.23) yields

$$C_1 = -C_2 E_i\left(\frac{-r_w^2}{4\alpha\tau}\right) \qquad (4.26)$$

and

$$\theta = C_2\left[E_i\left(\frac{-r^2}{4\alpha\tau}\right) - E_i\left(\frac{-r_w^2}{4\alpha\tau}\right)\right] \qquad (4.27)$$

In order to apply the boundary condition of Equation (4.25), an assumed

expression for the phase growth law must be introduced. In melting-freezing problems it is customary to assume the distance moved by the interface to be proportional to the square root of the time. In addition to this classical application, it is noteworthy that this type expression was used by Dyer and Sunderland (23) to represent the motion of the interface during sublimation dehydration of beef, and Hamill and Bankoff (12) obtained the same type expression for the growth of a mass of vapor on a rapidly heated plane surface, i.e., transient film boiling from a plate. For the current investigation, this assumption is modified to account for the finite initial radius and becomes

$$R = b\sqrt{t} + r_w \qquad (4.28)$$

Inclusion of the $r_w$ term complicates the analysis somewhat, but it is a significant term in the case of the present experimental investigation and should be included here. Applying Equations (4.25) and (4.28) to Equation (4.27) at a specific time yields:

$$C_2 = \cfrac{1}{E_i\left[\cfrac{-(b\sqrt{\tau} + r_w)^2}{4\alpha\tau}\right] - E_i\left[\cfrac{-r_w^2}{4\alpha\tau}\right]} \qquad (4.29)$$

Defining for convenience

$$\zeta = \frac{b\sqrt{\tau} + r_w}{2\sqrt{\alpha\tau}} \qquad (4.30)$$

the dimensionless temperature profile at time $\tau$ is

$$\theta = \frac{E_i\left(-\frac{r^2}{4\alpha\tau}\right) - E_i\left(-\frac{r_w^2}{4\alpha\tau}\right)}{E_i(-\zeta^2) - E_i\left(-\frac{r_w^2}{4\alpha\tau}\right)} \qquad (4.31)$$

In order to apply Equation (4.9) the required derivatives are obtained from Equations (4.28 and (4.31). Differentiating Equation (4.28) yields

$$\frac{dR}{dt} = \frac{1}{2\sqrt{t}} \, b + \sqrt{t} \ \frac{db}{dt} \qquad (4.32)$$

where the possibility of b depending upon time has been retained. Examination of the two coefficients of the terms in b for the current problem reveals a major simplification. The average time of interest is of the order of five milliseconds, i.e., the total growth time is ten milliseconds. Thus,

$$\frac{1}{2\sqrt{t}} \cong 7 \qquad (4.33)$$

and

$$\sqrt{t} \cong .07 \qquad (4.34)$$

and the coefficient of the first term is seen to be two orders of magnitude larger than the second. Assuming the rate of change of b with respect to time to be within one order of magnitude of the value of b, Equation (4.32) reduces to

$$\frac{dR}{dt} = \frac{1}{2\sqrt{t}} \, b \qquad (4.35)$$

Expressing Equation (4.31) in integral form and differentiating with respect to r yields

$$\frac{d\theta}{dr} = \frac{1}{E_i(-\zeta^2) - E_i(\frac{-r_w^2}{4\alpha\tau})} \frac{d}{dr} \int_{\infty}^{\frac{r^2}{4\alpha\tau}} \frac{e^{-y}}{y} dy \qquad (4.36)$$

Applying Leibnitz's rule for differentiation under the integral gives

$$\frac{d\theta}{dr} = \frac{2}{E_i(-\zeta^2) - E_i(\frac{-r_w^2}{4\alpha\tau})} \frac{e^{\frac{-r^2}{4\alpha\tau}}}{r} \qquad (4.37)$$

Substitution of the derivative of Equation (4.37) evaluated at the vapor-liquid interface and the derivative of Equation (4.35) evaluated at time $\tau$ into Equation (4.9) yields the following expression for b:

$$b = \frac{2k(T_w - T_{sat})}{\rho h_{fg}\sqrt{\alpha}\left[E_i(-\zeta^2) - E_i(\frac{-r_w^2}{4\alpha\tau})\right]} \frac{e^{-\zeta^2}}{\zeta} \qquad (4.38)$$

This transcendental equation in b is the major result of the present analysis. This equation is solved for all cases of the present experimental program. The results are presented in Appendix D, where the growth rate of Equation (4.28) is compared with experimental data for all runs. In addition, an example of the solution of this equation is presented in Appendix B.

CHAPTER V

DISCUSSION OF RESULTS

The experimental equipment and procedures have been described in considerable detail in Chapters II and III. This was considered to be significant since a major contribution of this investigation was the simultaneous determination of both heater element temperature and void volume as a function of time during transient film boiling.

## Temperature Determination

The measurement of element temperature by means of the Wheatstone bridge and oscilloscope system was satisfactory for the purpose of correlating vapor growth data. The wire temperature decay rate data, however, were somewhat disappointing. The measurement of quantitative transient heat transfer rates, which was the secondary experimental objective of this investigation, was initially predicated upon accurate determination of the wire temperature as a function of time. The difficulty encountered in accomplishing this is highlighted in Figure 14, which is a plot of temperature versus time for a typical experiment (run number 5). The apparent indicated wire temperature decay during the ten millisecond period of boiling is about 95 degrees Fahrenheit. Unfortunately, the maximum error in temperature measurement is about 60 degrees and the probable error is about 30 degrees (see Appendix C). This smaller figure has been displayed as vertical lines over each data point of Figure 14. This uncertainty, coupled with the element temperature
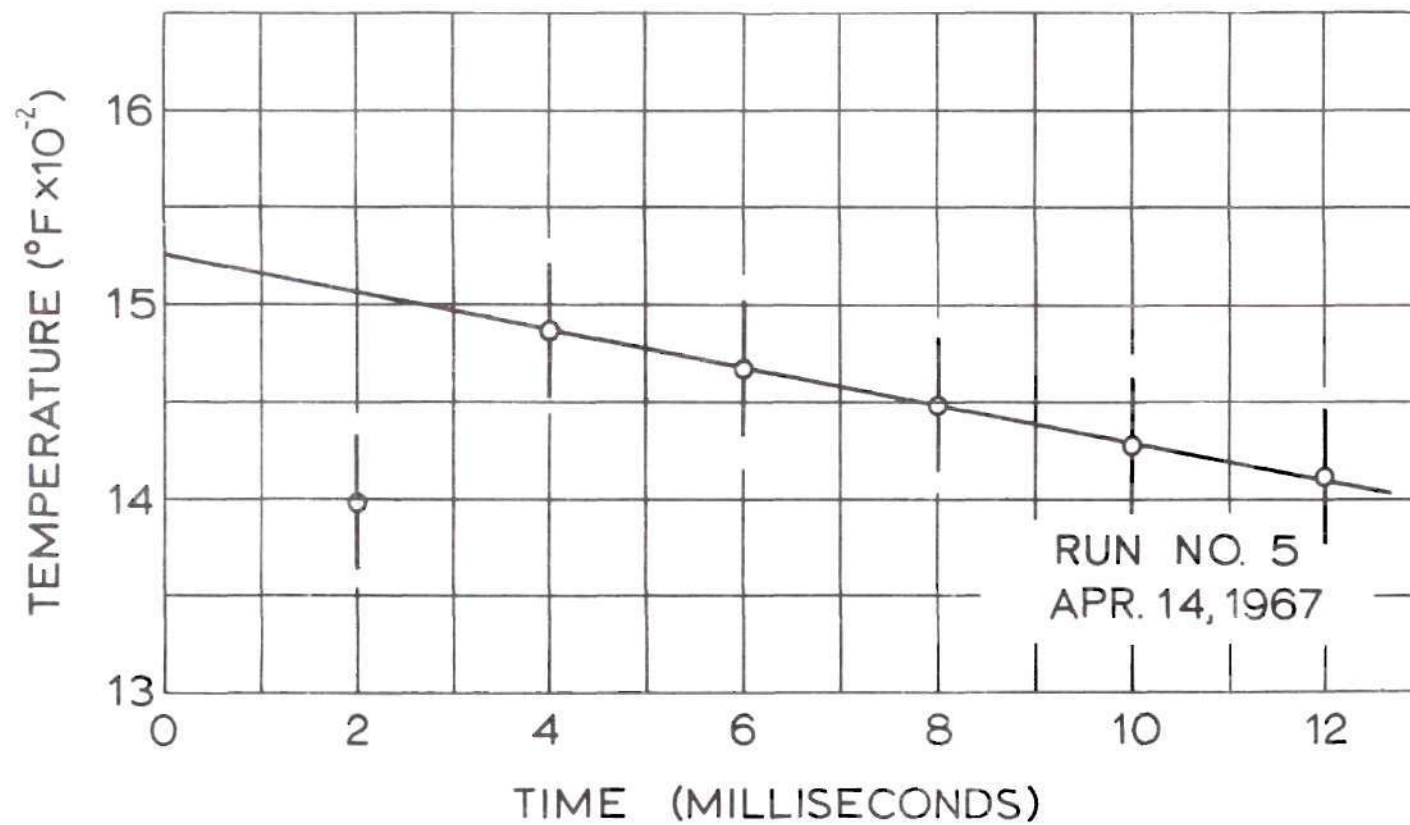
Figure 14. Heater Element Temperature versus Time Recorded During Run 5.

loss of approximately 24 degrees due to end conduction effects (see Appendix B) obviates all possibility of obtaining transient heat flux data in this manner.

The data of Figure 14 are quite typical of results obtained with number 30 size platinum wires with respect to the low value of indicated temperature during the first two to three milliseconds following the capacitor discharge. This is attributable to the main capacitor voltage remaining above the bridge millivolt potential level for this short time period. The element temperature change is governed by the capacitor discharge, and this is better than 99 per cent complete at the end of 100 microseconds. As a consequence, the best representation of temperature is obtained by extrapolation of the linear data points back to time zero, or 100 microseconds.

This indicated low initial temperature was markedly different for all experiments with the number 28 size platinum wire where the reduced electrical resistance allowed the main capacitor to discharge down to the bridge millivolt level much faster. Results for runs 14, 15, 15A, and 16 allow direct temperature measurement (without data extrapolation) as early as one-half millisecond after capacitor discharge.

In view of the foregoing uncertainty in element temperature at a specific time, the recorded temperature data were used to obtain a mean element temperature for each run. This mean temperature is defined as the indicated temperature five milliseconds following capacitor discharge, and determined from a graph of the temperature for each run, similar to Figure 14. This is the element temperature used in the vapor growth calculations and reported throughout this thesis.

An additional check on the accuracy and repeatability of element temperature data can be inferred from electrical energy considerations. Assuming the capacitor discharge switching loss to be proportional to the energy transferred, the resulting element temperature rise should be proportional to the capacitor charge for a given element heat capacity. Now elements A, B, C, and D were all of the same material and very nearly identical in size. Thus, the capacitor charge versus temperature rise for all tests using these elements is given in Figure 15. Similarly, these data for all runs (including run 13) with element E, the number 28 wire size element, are presented as Figure 16.

It is quite interesting that the maximum deviation from the line representing the mean of these data for Figure 15 is about 40 degrees Fahrenheit, and this agrees well with the value of the most probable error from Appendix C. The deviation from the mean in Figure 16 is considerably less; this may be attributable to the fact that only one element is represented, and hence difference in element mounting resistances and element lengths do not exist.

### Experimental Vapor Growth Data

The experimental vapor formation data are summarized in Table 2 which gives the cylinder diameter at nine milliseconds following capacitor discharge for each of the 12 film boiling experiments. These data were obtained by drawing a "best fit" curve through the experimental data points of Figures 18 through 29, Appendix D.

The filmed results for each run showed an initial burst of vapor occurring at the beginning of each experiment. This vapor is completely opaque, as opposed to the transparency of the vapor evident in the later
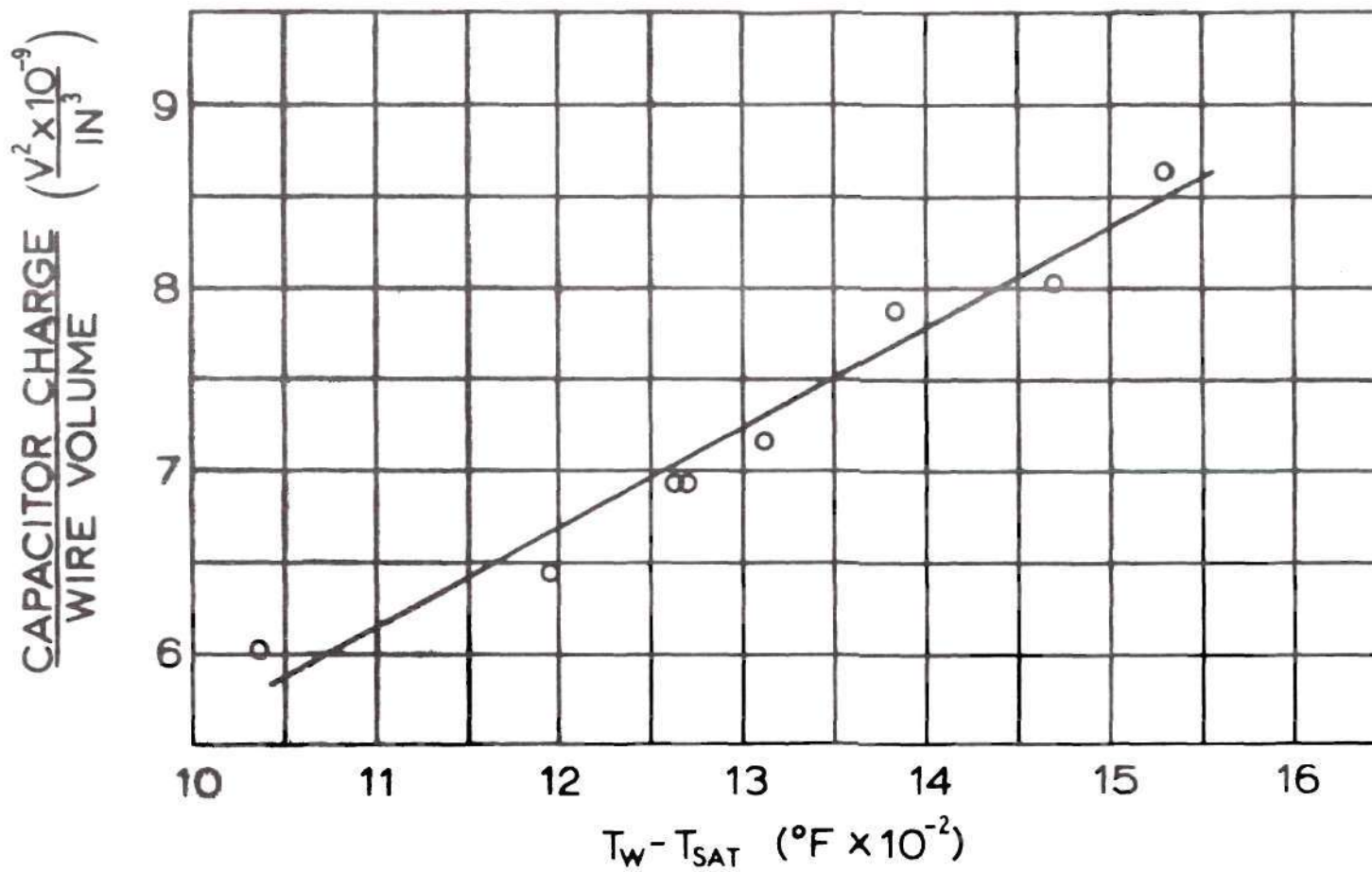
Figure 15.   Correlation of Element Mean Temperature with Capacitor
Charge Voltage for Experiments 1 through 10.

64
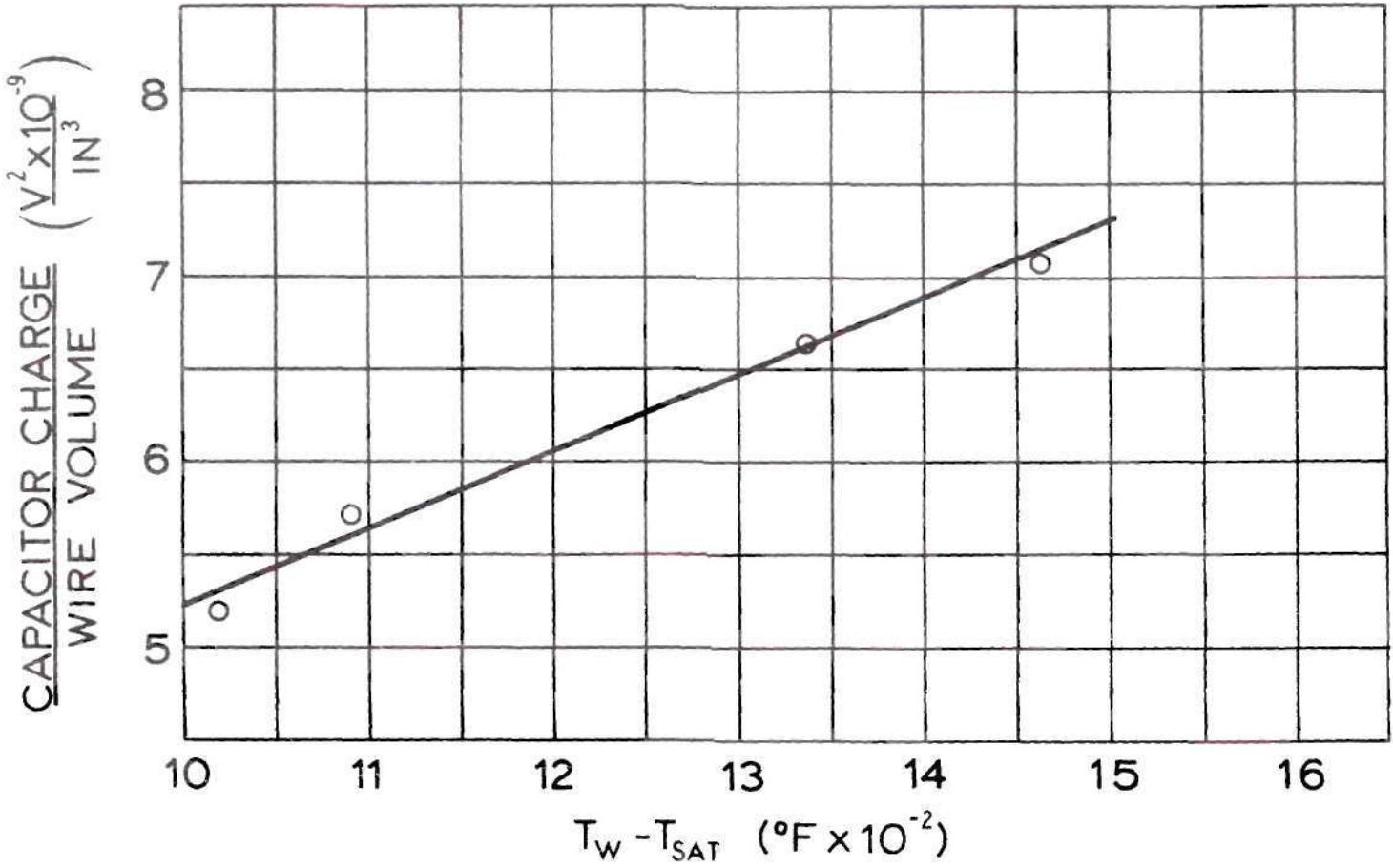
Figure 16. Correlation of Element Mean Temperature with Capacitor
Charge Voltage for Experiments 13 through 16

Table 2. Experimental Vapor Cylinder Diameter Summary

| $\Delta T$ $(T_w - T_{sat})$ $^\circ F$ | Wire Diameter inch | Run Number | Vapor Cylinder Dia. at 9 millisec inch |
|---|---|---|---|
| 1034 | 0.0098 | 1 | 0.050 |
| 1194 | 0.0098 | 6 | 0.0495 |
| 1266 | 0.0098 | 5 | 0.0522 |
| 1266 | 0.0098 | 3 | 0.0590 |
| 1310 | 0.0098 | 7 | 0.0520 |
| 1384 | 0.0098 | 4 | 0.0619 |
| 1469 | 0.0098 | 9 | 0.0660 |
| 1529 | 0.0098 | 10 | 0.0523 |
| 1092 | 0.0126 | 14 | 0.0585 |
| 1337 | 0.0126 | 15 | 0.0607 |
| 1337 | 0.0126 | 15A | 0.0615 |
| 1462 | 0.0126 | 16 | 0.0700 |

frames for each experiment. Close inspection indicates that this initial vapor is nucleate in character. This is clearly evident in one of the motion pictures filmed at a rate of approximately 5000 frames per second. Also, the surface of the cylinder in the initial frame in several runs is clearly composed of very small vapor bubbles. As a consequence, the initial vapor cylinder contains a significant liquid content, and the average diameter actually decreases during the first millisecond, i.e., for two to three frames following the first frame in the case of a 4000 frame per second camera speed. During some of the runs, the vapor quality was questionable throughout the first millisecond, and consequently no early diameter measurements were undertaken.

The question arose during the investigation as to whether this initial nucleation was peculiar to a platinum surface? In order to resolve this question, run number 12 was filmed using a number 30 size gold wire, 99.99 per cent pure. This was not thermometrically calibrated because of the relatively low electrical resistance of gold. The initial vapor formation during this experiment was, however, phenomenologically identical with that observed during the tests with platinum wires.

This initial nucleation had a decided effect upon the ensuing vapor cylinder growth rate; the latter growth occurring due to heat conduction through the vapor film to the vapor-liquid interface. That the initial nucleation was not a highly ordered process such as would have resulted in good correlation of initial vapor cylinder diameter with excess temperature is evident from Figures 18 through 29, Appendix D. The prediction of nucleate boiling heat flux or vapor formation is notoriously difficult due to the large number of variables involved. Non-repeatibility

of this initial phenomenon is considered to be the major reason for deviation of the experimental data from the analytical solution for the vapor growth rate.

Examination of the data of Table 2 reveals that the vapor cylinder is generally an increasing function of the excess temperature, a result which was, of course, anticipated. Further, it is noted that adjustment of these measurements by less than the probable error in bubble diameter measurement (see Appendix C) would result in the diameter being a monotonically increasing function of excess temperature with the single exception of run 10, which would be slightly low.

Runs 3 and 5 were intentionally conducted with the same capacitor charge, but using different elements of the same wire size. The results were measurably different. This was considered to be a consequence of difference in initial nucleation. Runs 15 and 15A were also intended to be identical tests. The results of this comparison were much better, there being practically no difference in the resulting vapor formation.

## Analytical Solution for Vapor Growth

The results of the analysis, Chapter IV, Equations (4.28) and (4.38), have been applied to each transient film boiling experiment of this program. As previously mentioned in this chapter, the wire temperature for each run is taken as the mean temperature five milliseconds after capacitor discharge and is treated as a constant in the analysis.

The initial nucleation previously discussed results in a relatively large amount of vapor surrounding the wire as early as one millisecond following the capacitor discharge. It was discovered by trial and error

that the analysis would well represent the data if the time were adjusted by the addition of four milliseconds to account for this initial vapor. This is equivalent to applying the solution of the analysis to the growth of a vapor film that has been growing due to pure conduction (see model of analysis, Chapter IV) for four milliseconds. Stated differently, this means that the average vapor volume due to the initial nucleation is the same amount that would result from the continuous growth of a smooth vapor film beginning with zero thickness and growing for four milliseconds by transfer of heat through the film due to conduction.

From Equation (4.38) it is evident that there is a dependence of b upon time. This was taken into consideration in the calculation of b for the first run, and it was discovered that the b's resulting for one and ten milliseconds were 0.174 and 0.166, respectively. Since this would result in only approximately two per cent change in vapor diameter from that obtained by use of a mean b evaluated at the mid-point of the time interval, it was neglected for the remaining calculations. Also, it is noted that

$$\frac{db}{dt} \cong \frac{\Delta b}{\Delta \tau} \cong 0.8/\text{sec} \tag{5.1}$$

and the value of b is 0.17, thus b and db/dt are of the same order of magnitude which substantiates the assumption made in the analysis and permits approximation of the solution by the transcendental algebraic Equation (4.38) rather than a differential equation.

A major item of interest in application of any thermal analysis concerns the temperature for evaluation of properties. In the present analysis, the thermal properties involved are the thermal conductivity,

the thermal diffusivity, the density, and the heat of vaporization. The thermal diffusivity enters the analysis in the solution of the temperature profile within the vapor, i.e., in the solution of the energy equation. Consequently, it has been evaluated at a mean temperature, defined for convenience as the arithmetic mean between the heater element and the fluid saturation temperatures.

The density enters in the application of a boundary energy conservation equation, but eventually represents the bulk of the vapor being formed. Thus, it also was evaluated at the arithmetic mean of element and saturation temperatures.

The appearance of the heat of vaporization is due to a boundary phenomenon, and it was evaluated at the fluid saturation temperature. The thermal conductivity likewise enters due to the boundary heat transfer at the liquid-vapor interface, and was evaluated at the fluid saturation temperature.

The value of b has been determined for each of the runs reported herein using property values from Kreith (24) and from Keenan and Keyes (25). The vapor cylinder diameters computed from Equation (4.28) have been plotted on Figures 18 through 29 to facilitate comparison with the reduced experimental data. Also, a sample solution of the transcendental equation (4.38) involving only the use of a slide rule and tabulated values of $E_i(-x)$ for very small values of the argument is presented in Appendix B.

## Heat Transfer Rates

The heat transfer rate based on a nine millisecond interval has

been calculated for each of runs one through ten from vapor formation data. This was done using both the experimental data of Table 2 and the analytical solution for vapor cylinder diameters at nine milliseconds presented in Figures 18 through 29.

This was accomplished with the approximative equation

$$\dot{q} = \frac{\rho V\left[h_{fg} + C_p (T_m - T_{sat})\right]}{A_w \Delta\tau} \tag{5.2}$$

where V represents the volume of vapor produced per unit length of wire in time, $\Delta\tau$. $A_w$ is the wire surface area per unit length, $h_{fg}$ is the heat of vaporization at the saturation temperature, $T_{sat}$, and $C_p$ is the mean specific heat evaluated at $T_m$, the arithmetic mean between the wire and saturation temperatures.

The results of these calculations are presented in Figure 30. Calculations of this type are not presented for the larger wire diameter since only four experiments were conducted with it. The deviation in heat transfer rates based on experimental vapor diameter from those calculated using the analytical vapor cylinder diameter reaches a amximum of 33 per cent. Although this is rather high, these data are considered to be of reportable value since considerable data scatter is usually obtained in boiling heat transfer experiments even at steady state conditions. It is noted that these values of the heat flux are only slightly higher than those reported in the literature for steady-state film boiling from small resistance wires.

# CHAPTER VI

## CONCLUSIONS AND RECOMMENDATIONS

The conclusions reached in this investigation may be stated as follows:

1. Vapor film growth in transient film boiling of saturated water from small diameter cylindrical surfaces of low thermal emissivity is primarily controlled by conduction heat transfer within the vapor film.

2. The minimum wall temperature for formation of a cylindrical growth of vapor in boiling of saturated water from a small diameter wire of low emissivity is approximately 1000 degrees Fahrenheit above the liquid saturation temperature.

3. The average time for cylindrical growth of a vapor film in transient film boiling of saturated water from a small platinum wire to its maximum size is approximately ten milliseconds; after this, the on-set of large bubble formation at nodes along the wire due to Taylor-Helmholtz instability is apparent.

4. Film boiling is preceded by vigorous nucleation for heating surface temperature changes occurring in as short a time span as 50 microseconds; this nucleation has a pronounced effect upon the ensuing rate of vapor formation.

5. Time averaged transient heat transfer rates for a nine milli-second interval ranged from approximately 50,000 to 90,000 Btu/hr.-ft$^2$ for excess temperatures from 1043 to 1529 degrees Fahrenheit during transient film boiling of saturated water from small diameter

platinum wires, which is very close to steady-state values reported in the literature.

6. The use of a capacitance discharge into a resistive heating element is a satisfactory method for accomplishing a step-change input to a heating surface for heat transfer investigations.

7. The use of a Wheatstone bridge and resistive heater element system for recording transient element temperatures is a satisfactory approach.

8. Accuracy of heater element temperature determination is primarily controlled by the metal temperature coefficient of resistance and the accuracy and readability of the recording equipment.

Specific recommendations concerning future investigations of this type include:

1. The effects of subcooling of the liquid should be investigated both analytically and experimentally.

2. The effects of radiation from heater element surfaces of relatively high thermal emissivity should be investigated and would be an interesting area for experimental work.

3. The present analysis should be confirmed for other liquids.

4. An investigation should be made of the region of vigorous nucleation at the onset of film boiling. This would be valuable and informative; such experimental work, however, would require equipment of a significantly greater degree of sophistication than that used in the present study.

APPENDIX A

DERIVATION OF GOVERNING EQUATIONS

Momentum Equation

Energy Equation in Vapor

Energy Conservation Equation at Vapor-Liquid
Interface

Derivation of the governing equations is accomplished by the assumptions of Chapter IV to the well known more general forms of these equations. The expression for energy conservation at the vapor-liquid interface is derived using the "shell" method of reference (27).

## Momentum Equation

From reference (26), the radial direction momentum equation for a fluid with constant viscosity is

$$\rho \left[ \frac{Dv_r}{Dt} - \frac{v_\varphi^2}{r} \right] = \frac{\partial p}{\partial r} + F_r + \mu \left[ \nabla^2 v_r - \frac{v_r}{r^2} - \frac{2}{r^2} \frac{\partial v_\varphi}{\partial \varphi} \right]$$

$$+ (\lambda + \mu) \frac{\partial}{\partial r} (\nabla \cdot V) \qquad (A.1)$$

where

$$\nabla^2 = \frac{\partial^2}{\partial r^2} + \frac{1}{r} \frac{\partial}{\partial r} + \frac{1}{r^2} \frac{\partial^2}{\partial \varphi^2} + \frac{\partial^2}{\partial z^2} \qquad (A.2)$$

$$\nabla \cdot V = \frac{1}{r} \frac{\partial}{\partial r} (rv_r) + \frac{1}{r} \frac{\partial v_\varphi}{\partial \varphi} + \frac{\partial v_z}{\partial z} \qquad (A.3)$$

$$\frac{D}{Dt} = \frac{\partial}{\partial t} + v_r \frac{\partial}{\partial r} + \frac{v_\varphi}{r} \frac{\partial}{\partial \varphi} + v_z \frac{\partial}{\partial z} \qquad (A.4)$$

and $\lambda$ is the second coefficient of viscosity. The assumptions of axial symmetry and no velocity variation with length eliminate the $\varphi$ and z-direction momentum equations. Further application of these two assumptions yields

$$\rho \left[ \frac{\partial v_r}{\partial t} + v_r \frac{\partial v_r}{\partial r} \right] = - \frac{\partial p}{\partial r} + F_r + \mu \left[ \frac{\partial^2 v_r}{\partial r^2} + \frac{1}{r} \frac{\partial v_r}{\partial r} - \frac{v_r}{r^2} \right]$$

$$+ (\lambda + \mu) \frac{\partial}{\partial r} \left[ \frac{1}{r} \frac{\partial}{\partial r} (r v_r) \right] \tag{A.5}$$

For no radial pressure gradient and negligible body forces, Equation (A.5) reduces to

$$\frac{\partial v_r}{\partial t} + v_r \frac{\partial v_r}{\partial r} = \frac{\mu}{\rho} \left[ \frac{\partial^2 v_r}{\partial r^2} + \frac{1}{r} \frac{\partial v_r}{\partial r} - \frac{v_r}{r^2} \right]$$

$$+ \frac{(\lambda + \mu)}{\rho} \frac{\partial}{\partial r} \left[ \frac{1}{r} \frac{\partial}{\partial r} (r v_r) \right] \tag{A.6}$$

### Energy Equation

From reference (27) the energy equation in cylindrical coordinates for a Newtonian fluid with constant thermal properties and negligible radiation is:

$$\rho C_p \left( \frac{\partial T}{\partial t} + v_r \frac{\partial T}{\partial r} + \frac{v_\varphi}{r} \frac{\partial T}{\partial \varphi} + v_z \frac{\partial T}{\partial z} \right) = k \left[ \frac{1}{r} \frac{\partial}{\partial r} \left( r \frac{\partial T}{\partial r} \right) + \frac{1}{r^2} \frac{\partial^2 T}{\partial \varphi^2} + \frac{\partial^2 T}{\partial z^2} \right]$$

$$+ 2\mu \left\{ \left( \frac{\partial v_r}{\partial r} \right)^2 + \left[ \frac{1}{r} \left( \frac{\partial v_\varphi}{\partial \varphi} + v_r \right) \right]^2 + \left( \frac{\partial v_z}{\partial z} \right)^2 \right\} + \mu \left\{ \left( \frac{\partial v_\varphi}{\partial z} + \frac{1}{r} \frac{\partial v_z}{\partial \varphi} \right)^2 \right.$$

$$\left. + \left( \frac{\partial v_z}{\partial r} + \frac{\partial v_r}{\partial z} \right)^2 + \left[ \frac{1}{r} \frac{\partial v_r}{\partial \varphi} + r \frac{\partial}{\partial r} \left( \frac{v_\varphi}{r} \right) \right]^2 \right\} \tag{A.7}$$

For negligible viscous dissipation, the terms within the $\left\{ \right\}$ brackets disappear. For axial symmetry and no thermal variation with length, the energy equation reduces to

$$\rho C_p \left(\frac{\partial T}{\partial t} + v_r \frac{\partial T}{\partial r}\right) = k\left[\frac{1}{r} \frac{\partial}{\partial r} \left(r \frac{\partial T}{\partial r}\right)\right] \tag{A.8}$$

Carrying out the indicated differentiation, this may be written as

$$\rho C_p \left[\frac{\partial T}{\partial t} + v_r \frac{\partial T}{\partial r}\right] = k\left[\frac{\partial^2 T}{\partial r^2} + \frac{1}{r} \frac{\partial T}{\partial r}\right] \tag{A.9}$$

which is the desired form.

### Equation of Energy Conservation at Vapor-Liquid Interface

With reference to Figure 17, the energy stored within the control volume in time $\Delta\tau$, assuming a mean temperature, is

$$\frac{\rho h_{fg} (R\Delta\varphi)\Delta R}{\Delta\tau} \tag{A.10}$$

Summing the energy flux entering and leaving the control volume and equating this to the rate of energy stored yields

$$\frac{\rho h_{fg}(R\Delta\varphi)\Delta R}{\Delta\tau} = -\left[\frac{k_v(R\Delta\varphi)\Delta T}{\Delta R}\bigg|_{R+\Delta R} - \frac{k_v(R\Delta\varphi)\Delta T}{\Delta R}\bigg|_{R}\right]$$

$$+ \left[\frac{k_\ell(R\Delta\varphi)\Delta T}{\Delta R}\bigg|_{R+\Delta R} - \frac{k_\ell(R\Delta\varphi)\Delta T}{\Delta R}\bigg|_{R}\right]$$

$$+ \varepsilon_w a_\ell \sigma T_w^4 (r_w \Delta\varphi)\bigg|_{R} \tag{A.11}$$

Dividing by $R\Delta\varphi$ and taking the limit as $\Delta R$ and $\Delta\tau$ approach zero yields

$$\rho h_{fg} \frac{dR}{dt} = -k_v \frac{\partial T}{\partial r}\bigg|_{R} + k_\ell \frac{\partial T}{\partial r}\bigg|_{R} + \varepsilon_w a_\ell \sigma T_w^4 \frac{r_w}{r}\bigg|_{R} \tag{A.12}$$

$$\left. \dfrac{-k_v (r\Delta\phi)\Delta T}{\Delta r} \right|_R$$

$$\left. \dfrac{-k_v (r\Delta\phi)\Delta T}{\Delta r} \right|_{R+\Delta R}$$

VAPOR-LIQUID
INTERFACE

$$\left. \dfrac{-k_\ell (r\Delta\phi)\Delta T}{\Delta r} \right|_R$$

$$\left. \dfrac{-k_\ell (r\Delta\phi)\Delta T}{\Delta r} \right|_{R+\Delta R}$$

$$\epsilon_w a_1 \sigma T_w^4 (r_w \Delta\phi)$$

R

R+ΔR
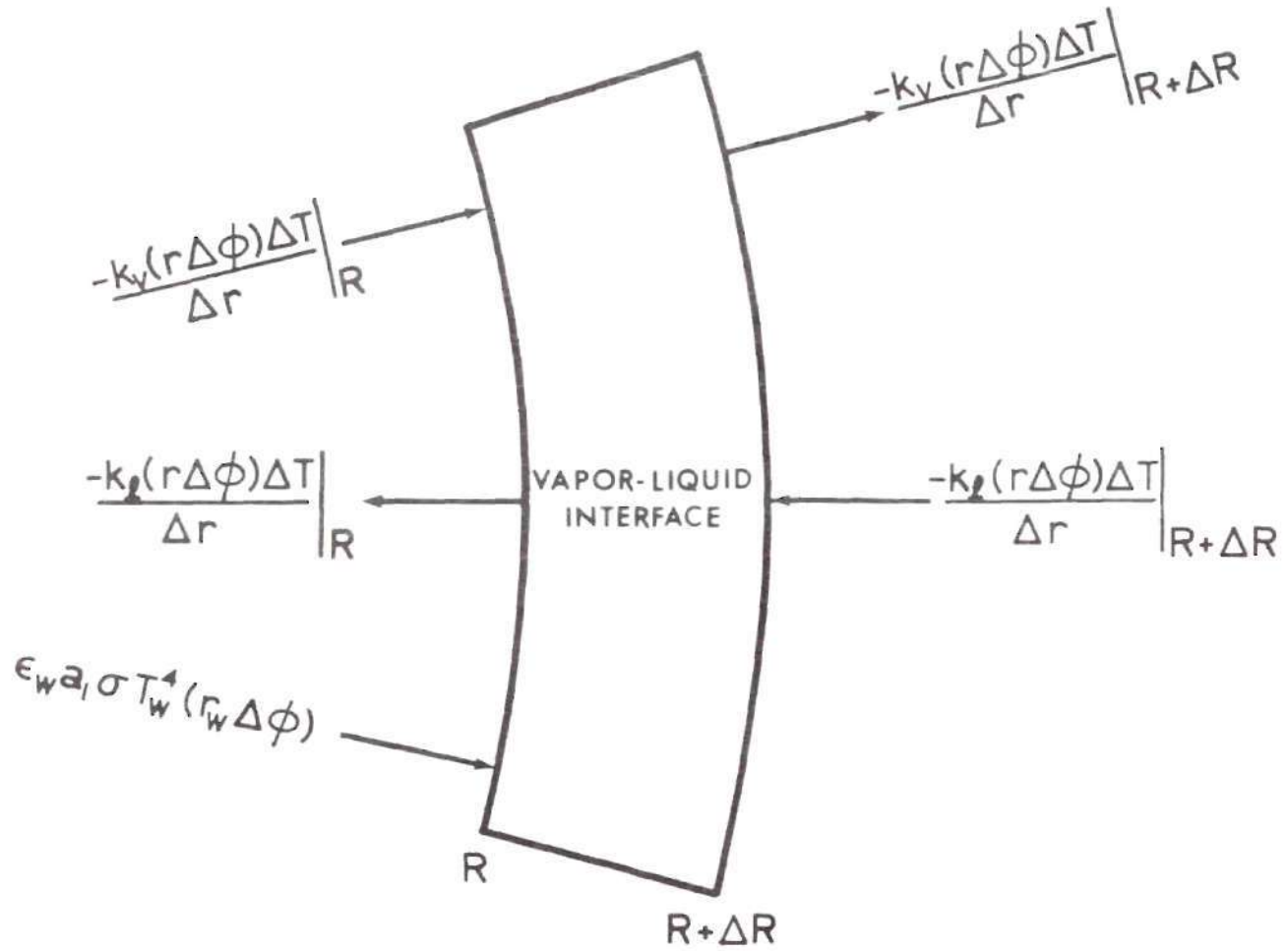
Figure 17. Control Volume for Derivation of Equation of
Energy Conservation at Vapor-Liquid Interface.

The term on the left is the rate of energy storage within the vapor. The first term on the right represents the rate of energy conducted through the vapor to the interface; the second term represents the rate of energy conducted away from the interface in the liquid, and the third term represents the rate of energy radiated from the wire to the liquid at the interface.

APPENDIX B

SAMPLE CALCULATIONS


Wire Temperature Decay Due to End Conduction Effects

Capacitor Discharge Time

Solution of Transcendental Equation for Phase Growth
       Constant of Proportionality

<u>Wire Temperature Decay Due to End Conduction</u>

Assuming no heat loss in the radial direction, the temperature in the wire of length $2\ell$, initially at temperature $T_0$, and losing heat by conduction to the bronze holders maintained at the bulk fluid temperature may be determined from

$$T_{av} = T_0 - 2T_0 \left(\frac{\alpha t}{\ell^2}\right)^{1/2} \left[\pi^{-1/2} + 2 \sum_{n=1}^{\infty} (-1)^n \; ierfc \frac{n\ell}{\sqrt{\alpha t}}\right] \qquad (B.1)$$

which is taken from reference (28). Using property values for platinum from reference (20), for a two-inch long wire at 10 milliseconds

$$\frac{\alpha t}{\ell^2} = \frac{(0.208 \; cm^2/sec)(10^{-2} sec)}{(2.54 \; cm)^2} = 0.0323 \times 10^{-2} \qquad (B.2)$$

or

$$\frac{\ell}{(\alpha t)^{1/2}} = 55.6 \qquad (B.3)$$

Now

$$ierfc(x) = \frac{1}{\sqrt{\pi}} \, e^{-x^2} - x erfcx \qquad (B.4)$$

Also, for large values of the argument, $erfc(x)$ may be approximated by

$$erfc(x) = \frac{1}{\sqrt{\pi}} \, e^{-x^2} \left(\frac{1}{x} - \frac{1}{2x^3} + \frac{1}{4x^5} - \frac{1 \times 3 \times 5}{8x^7} + \ldots\right) \qquad (B.5)$$

Thus, for large x,

$$\text{ierfc}(x) = \frac{1}{\sqrt{\pi}} e^{-x^2} - \frac{xe^{-x^2}}{\sqrt{\pi}} \left(\frac{1}{x} - \frac{1}{2x^3} + \cdots\right) \qquad (B.6)$$

and consequently, for $x = 55.6$,

$$\text{ierfc}(x) \cong 0 \qquad (B.7)$$

This term is insignificant when compared with $1/\sqrt{\pi}$, and the average temperature in the wire after 10 milliseconds is given by

$$T_{av} = T_0 - \frac{2T_0}{\sqrt{\pi}} \left(\frac{\alpha t}{\ell^2}\right)^{1/2} \qquad (B.8)$$

As a specific example, the average wire temperature after 10 milliseconds for an initial temperature of 1188 degrees Fahrenheit above the end value, i.e., 1400 degrees Fahrenheit wire temperature, is

$$T_{av} = 1188 - \frac{2(1188)}{1.773} \times \frac{1}{55.6} = 1164°F \qquad (B.9)$$

which is a decay of 24 degrees Fahrenheit during the period of interest.

## Capacitor Discharge Time

The electrical charge on a condenser decreases exponentially with time according to

$$Q = Q_0 e^{-t/RC} \qquad (B.10)$$

where $Q_0$ is the initial charge, t is the time in seconds, R is the circuit resistance in ohms, and C is the capacitance in farads. For the present application, the capacitance was 120 microfarads. The resistance of the circuit was primarily due to the platinum element alone. Data of

reference (20) show that the electrical resistivity of pure platinum varies from about $9.83 \times 10^{-6}$ to $32.8 \times 10^{-6}$ ohm-cm over a range of 20 to 760 degrees centigrade. For an average temperature of 800 degrees Fahrenheit, the resistivity is $23.5 \times 10^{-6}$ ohm-cm.

Thus a number 28 platinum wire, two inches long, has a mean resistance of

$$R_m = \frac{23.5 \times 10^{-6} \times 5.08}{8.13 \times 10^{-4}} = 0.147 \text{ ohm} \qquad (B.11)$$

during a typical boiling experiment. Approximating the time constant, i.e., the product RC, by use of a constant effective resistance equal to the mean resistance of the platinum wire, the system time constant is

$$RC)_m = 0.147 \times 120 \times 10^{-6} = 17.6 \times 10^{-6} \text{ seconds} \qquad (B.12)$$

Thus, by Equation (B.10), the charge remaining in the capacitor after 50 microseconds is approximately 6 per cent of the initial value; after 100 microseconds this is only 0.3 per cent.

### Solution of Transcendental Equation for Phase Growth Constant of Proportionality

The specific example presented here is for run number 6. The pertinent parameters for solution of Equation (4.38) are

$$T_w - T_{sat} = 1405 - 210.6 = 1194.4°F$$

$$T_m = 807.8°F$$

Using property values from references (24) and (25),

$$\frac{2k(T_w - T_{sat})}{\rho h_{fg}} = \frac{0.1467}{2} \tag{B.13}$$

and

$$2\alpha = \frac{0.541}{2} \tag{B.14}$$

where the dimensions of distance and time are inches and seconds, respectively. Computing b for a time of 6 milliseconds, the adjusted time is $\tau_{adj}$ = 0.010 seconds. Thus,

$$\sqrt{\tau_{adj}} = 0.1 \tag{B.15}$$

For a trial solution, assume b = 0.18. This yields, from Equation (4.30)

$$\zeta = \frac{0.18 \times 0.1 + 0.0049}{0.7356 \times 0.1} = 0.0967 \tag{B.16}$$

and

$$\frac{e^{-\zeta^2}}{\zeta} = 2.9195 \tag{B.17}$$

Thus, using values of $E_i$ from Table 3, page 86,

$$E_i(-\zeta^2) = -1.853 \tag{B.18}$$

Now

$$\frac{r_w^2}{4\alpha\tau} = 0.00444 \tag{B.19}$$

and

$$E_i\left(-\frac{r_w^2}{4a\tau}\right) = -4.845 \tag{B.20}$$

From Equation (4.38)

$$b = \frac{0.1467 \times 2.9195}{0.7356(4.845 - 1.853)} = 0.1947 \tag{B.21}$$

which is slightly higher than the assumed value. Assuming b = 0.186 and repeating the calculations yields

$$\zeta = 0.3193 \tag{B.22}$$

$$\frac{e^{-\zeta^2}}{\zeta} = 2.828 \tag{B.23}$$

$$E_i(-\zeta^2) = -1.805 \tag{B.24}$$

and thus

$$b = \frac{0.1467 \times 2.828}{0.7356(4.845 - 1.805)} = 0.186 \tag{B.25}$$

In practice, the use of graphical values of $E_i(-x)$ for the range of the arguments encountered, i.e., $0.003 < x < 0.14$, as well as a graph of $e^{-\zeta^2}/\zeta$ for $0.28 < \zeta < 0.35$, were found to be very helpful in the computational work.

Table 3. Values of $E_i(-x)$ for Small Values
of the Argument (Abramowitz (29))

| x | $-E_i(-x)$ | x | $-E_i(-x)$ |
|---|---|---|---|
| .001 | 6.3315 | .03 | 2.9591 |
| .002 | 5.6394 | .04 | 2.6813 |
| .003 | 5.2349 | .05 | 2.4679 |
| .004 | 4.9482 | .06 | 2.2953 |
| .005 | 4.7261 | .07 | 2.1508 |
| .006 | 4.5448 | .08 | 2.0269 |
| .007 | 4.3916 | .09 | 1.9187 |
| .008 | 4.2591 | .10 | 1.8229 |
| .009 | 4.1423 | .11 | 1.7371 |
| .010 | 4.0379 | .12 | 1.6595 |
| .02 | 3.3547 | .13 | 1.5889 |
|  |  | .14 | 1.5241 |

APPENDIX C

ERROR ANALYSES

Element Temperature Measurement Error

Vapor Cylinder Diameter Measurement Error

## Element Temperature

The maximum error associated with determination of the arbitrary function $\psi$ is given by

$$\Delta \psi = \sum \frac{\partial \psi}{\partial m_i} \Delta m_i \qquad (C.1)$$

where the $m_i$'s are the variables of measurement. For the case of the element temperature, the variables are:

1) bridge current, I

2) oscilloscope gain, G

3) oscilloscope reading error, S

4) oscilloscope drift between reference reading and data reading, B

5) potentiometer error, H

6) standard platinum versus platinum plus 10 per cent rhodium thermocouple error, P

Items one through four occur twice in any temperature measurement; once during calibration and once during the boiling experiment. Thus, the maximum error in element temperature measurement is given by

$$\Delta T = 2 \frac{\partial T}{\partial I} \Delta I + 2 \frac{\partial T}{\partial G} \Delta G + 2 \frac{\partial T}{\partial S} \Delta S$$

$$+ 2 \frac{\partial T}{\partial B} \Delta B + \frac{\partial T}{\partial H} \Delta H + \frac{\partial T}{\partial P} \Delta P \qquad (C.2)$$

The bridge current was adjusted to within one-half milliampere for each reading. The current was nominally 70 milliamperes for most

tests, and an error of one milliampere could result in

$$\frac{\Delta T}{\Delta I} = \frac{1}{70} \times 1700 \cong 24°F/\text{milliampere} \qquad (C.3)$$

and thus

$$2 \frac{\partial T}{\partial I} \Delta I \cong 24°F \qquad (C.4)$$

The oscilloscope gain was adjusted and controlled to within one-tenth of the smallest grid division on the scope screen. Thirty-five of these divisions represented as much as 1700 degrees Fahrenheit. Consequently,

$$\frac{\Delta T}{\Delta G} = \frac{1}{35} \times 1700 \cong 48°F/\text{div} \qquad (C.5)$$

and

$$2 \frac{\partial T}{\partial G} \Delta G \cong 2 \times 48 \times \frac{1}{10} \cong 9.6°F \qquad (C.6)$$

The oscilloscope reading error was also held to within one-tenth of the smallest division of the grid for each reading. Two readings were required for each temperature measurement, i.e., bridge unbalance voltage and zero bridge current reference, thus

$$\frac{\Delta T}{\Delta S} = \frac{1}{35} \times 1700 \cong 48°F/\text{div.} \qquad (C.7)$$

and

$$2 \frac{\partial T}{\partial S} \Delta S \cong 19.2°F \qquad (C.8)$$

The oscilloscope drift was constantly checked, both during

calibration and during boiling tests. This was accomplished by repeating
the zero bridge current reference reading and observing any change in
value. This was also held to within one-tenth of the smallest grid divi-
sion, and

$$2 \frac{\partial T}{\partial B} \Delta B \cong 9.6°F \tag{C.9}$$

The manufacturer's stated error for the K-3 potentiometer is 0.015
per cent plus 0.5 microvolts. The emf error at 1700 degrees Fahrenheit is
approximately

$$\Delta H \cong 0.00015 \times 8.625 + 0.5 \times 10^{-3} \cong 1.8 \times 10^{-3} \tag{C.10}$$

and

$$\frac{\Delta T}{\Delta H} \cong \frac{1700}{8.625} \cong 197°F/\text{millivolt} \tag{C.11}$$

thus,

$$\frac{\partial T}{\partial H} \Delta H \cong 197 \times 1.8 \times 10^{-3} \cong 0.35°F \tag{C.12}$$

The manufacturer's stated deviation for the platinum versus plat-
inum plus 10 per cent rhodium thermocouple is 0.75 degrees Centigrade, or

$$\frac{\partial T}{\partial P} \Delta P = 1 \times (0.75 \times 1.8) = 1.35°F \tag{C.13}$$

Hence, by Equation (C.2) the maximum error in element temperature is

$$\Delta T = 24 + 9.6 + 19.2 + 9.6 + 0.35 + 1.35 = 64.1°F \tag{C.14}$$

and the maximum per cent error is

$$\frac{\Delta T}{T} = \frac{64.1}{1700} = 3.77\% \tag{C.15}$$

Assuming a normal (Gaussian) distribution of errors, the probable error in an arbitrary function is

$$\Delta \psi_p = \left[ \sum (\frac{\partial \psi}{\partial m_i} \Delta m_i)^2 \right]^{1/2} \tag{C.16}$$

Applying this expression to the element temperature yields for the probable error

$$\Delta T_p = \lfloor (24)^2 + (9.6)^2 + (19.2)^2 + (9.6)^2 + (0.35)^2$$
$$+ (1.35)^2 \rfloor^{1/2} = 33.6°F \tag{C.17}$$

or, the probable per cent error is

$$\frac{\Delta T_p}{T} = \frac{33.6}{1700} = 1.98\% \tag{C.18}$$

### Vapor Cylinder Diameter

The variables of measurement are:

1) wire actual diameter

2) wire projected diameter

3) individual projection station diameter

4) definition of vapor-liquid interface

In addition, it is assumed (see text, Chapter III) that not more than three per cent error is introduced by the approximation of the actual

irregular vapor bubble by 26 short cylinders.  Thus, Equation (C.1) is modified to

$$\Delta\psi = 0.03\psi + \sum \frac{\partial\psi}{\partial m_i} \Delta m_i \tag{C.19}$$

In terms of the variables of measurement, Equation (C.19) becomes

$$\frac{\Delta D}{D} = \frac{0.03D}{D} + \frac{\partial D}{\partial d_1}\frac{\Delta d_1}{D} + \frac{\partial D}{\partial d_2}\frac{\Delta d_2}{D} + \frac{\partial D}{\partial d_3}\frac{\Delta d_3}{D} + \frac{\partial D}{\partial d_4}\frac{\Delta d_4}{D} \tag{C.20}$$

The wire diameter was measured with two instruments (see Chapter II) and for the number 30 wire was found to be 0.0098 plus or minus 0.00005 inch.  The bubble diameter measurement is a linear function of the wire diameter.  Thus for the smallest projected wire diameter of 0.21 inch

$$\frac{\partial D}{\partial d_1} = \frac{0.21}{0.0098} \tag{C.21}$$

and

$$\frac{\partial D}{\partial d_1}\frac{\Delta d_1}{D} = \frac{0.21}{0.0098} \times \frac{0.00005}{0.21} = 0.0051 \tag{C.22}$$

The projected wire diameter was measured to within one- one hundredth of an inch, thus for the worst case

$$\frac{\partial D}{\partial d_2}\frac{\Delta d_2}{D} = \frac{0.01}{0.21} = 0.0476 \tag{C.23}$$

The average vapor cylinder projected diameter was on the order of one and one-half inches.  Consequently, an error of one-one hundredth inch in measurement resulted in

$$\frac{\partial D}{\partial d_3} \frac{\Delta d_3}{D} = 1 \times \frac{0.01}{1.5} = 0.00666 \qquad (C.24)$$

The projected vapor-liquid interface was usually defined to within 0.02 inches at any point. Thus, for the average diameter

$$\frac{\partial D}{\partial d_4} \frac{\Delta d_4}{D} = 1 \times \frac{0.02}{1.5} = 0.01333 \qquad (C.25)$$

and by equation (C.20), the maximum per cent error in the vapor cylinder volume median diameter is

$$\frac{\Delta D}{D} = 0.03 + 0.0051 + 0.0476 + 0.00666 + 0.01333 \cong 0.1027 \quad (C.26)$$

or, 10.27 per cent. Again assuming a normal distribution of errors, the probable error in vapor cylinder diameter is

$$\frac{\Delta D}{D} \Big)_p = [\, (0.03)^2 + (0.0051)^2 + (0.0476)^2 + (0.00666)^2$$
$$+ (0.01333)^2 \,]^{1/2} = 0.0585 \qquad (C.27)$$

or approximately six per cent.

APPENDIX D

DATA

Calibration and Descriptive Data for Heater Elements

General Test Data for Each Transient Boiling Experiment

Vapor Growth Rate Data

Transient Heat Flux Data

Table 4.  Temperature Calibration Data for All Heater Elements

| Element | Date | Thermocouple EMF millivolts | Bridge Unbalance millivolts | Bridge Current milliamps |
|---------|------|-----------------------------|-----------------------------|--------------------------|
| A | 2-21-67 | 0.1368 | 0.36 | 80 |
| A | 2-21-67 | 0.7268 | 1.90 | 80 |
| A | 2-21-67 | 1.2545 | 3.06 | 80 |
| A | 2-21-67 | 1.6080 | 3.74 | 80 |
| A | 2-21-67 | 2.9289 | 6.00 | 80 |
| A | 2-21-67 | 3.6766 | 7.28 | 80 |
| A | 2-21-67 | 4.7005 | 8.80 | 80 |
| A | 2-21-67 | 5.2680 | 9.66 | 80 |
| B | 4-4-67 | 0.1504 | 0.70 | 80 |
| B | 4-4-67 | 0.8802 | 2.66 | 80 |
| B | 4-4-67 | 1.5715 | 4.14 | 80 |
| B | 4-4-67 | 2.4406 | 5.80 | 80 |
| B | 4-4-67 | 3.4603 | 7.60 | 80 |
| B | 4-4-67 | 4.4565 | 9.28 | 80 |
| B | 4-4-67 | 5.6711 | 11.34 | 80 |
| B | 4-4-67 | 5.4370 | 10.94 | 80 |
| C | 4-29-67 | 0.3188 | 1.08 | 80 |
| C | 4-29-67 | 1.5122 | 4.00 | 80 |
| C | 4-29-67 | 2.3940 | 5.75 | 80 |
| C | 4-29-67 | 4.0070 | 8.76 | 80 |
| C | 4-29-67 | 5.2672 | 10.88 | 80 |
| C | 4-29-67 | 6.3301 | 12.52 | 80 |
| D | 5-5-67 | 0.1365 | 0.06 | 80 |
| D | 5-5-67 | 1.4630 | 3.20 | 80 |
| D | 5-5-67 | 2.3691 | 4.80 | 80 |
| D | 5-5-67 | 3.8355 | 7.26 | 80 |
| D | 5-5-67 | 5.1489 | 9.30 | 80 |
| D | 5-5-67 | 6.3586 | 11.06 | 80 |
| D | 5-5-67 | 7.4940 | 12.66 | 80 |
| D | 5-5-67 | 7.9204 | 13.20 | 80 |
| E | 5-26-67 | 0.1367 | 0.60 | 120 |
| E | 5-26-67 | 1.4502 | 3.34 | 120 |
| E | 5-26-67 | 2.3185 | 4.66 | 120 |
| E | 5-26-67 | 3.8370 | 6.85 | 120 |
| E | 5-26-67 | 5.1180 | 8.56 | 120 |
| E | 5-26-67 | 6.1620 | 9.90 | 120 |
| E | 5-26-67 | 7.3101 | 11.34 | 120 |
| E | 5-26-67 | 7.9891 | 12.22 | 120 |

Table 5.  Heater Element Descriptive Data

| Element | Description |
|---------|-------------|
| A | Number 30 (0.0098 inch) diameter, commercially pure platinum wire, 2.12 inches long, silver soldered in one-eighth inch diameter bronze holders |
| B | Number 30 (0.0098 inch) diameter, commercially pure platinum wire, 2.18 inches long, silver soldered in one-eighth inch diameter bronze holders |
| C | Number 30 (0.0098 inch) diameter, commercially pure platinum wire, 2.00 inches long, silver soldered in one-eighth inch diameter bronze holders |
| D | Number 30 (0.0098 inch) diameter, commercially pure platinum wire, 2.03 inches long, brazed in one-eighth inch diameter bronze holders |
| E | Number 28 (0.0126 inch) diameter, commercially pure platinum wire, 1.94 inches long, brazed in one-eighth inch diameter bronze holders |

Table 6.  General Data for Transient Boiling Tests

| Run No. | Bulk Water Temperature (°F) | Water Depth (in.) | Film Type | Lens Data f/stop | Ext. Tube (in.) | Barometric Pressure (in.Hg.) |
|---|---|---|---|---|---|---|
| 1 | 208.5 | | Dupont 931A | 1.4 | 1.0 | 29.17 |
| 3 | 210.0 | 3.38 | Kodak Tri-X | 1.4 | 0.5 | 29.40 |
| 4 | 211.0 | 2.50 | Kodak Tri-X | 1.4 | 0.5 | 29.30 |
| 5 | 211.0 | 1.75 | Kodak Tri-X | 1.4 | 1.0 | 29.30 |
| 6 | 210.5 | 2.50 | Dupont 931A | 1.4 | 1.0 | 29.12 |
| 7 | 209.0 | 1.75 | Dupont 931A | 1.4 | 0.5 | 29.36 |
| 9 | 209.5 | 1.70 | Dupont 931A | 1.4 | 0.5 | 29.32 |
| 10 | 209.5 | 1.60 | Dupont 931A | 1.4 | 1.0 | 29.03 |
| 14 | 210.5 | 1.26 | Dupont 931A | 1.4 | 0.5 | 29.20 |
| 15 | 210.2 | 1.40 | Dupont 931A | 1.4 | 0.5 | 29.20 |
| 15A | 210.2 | 1.40 | Dupont 931A | 1.4 | 0.5 | 29.20 |
| 16 | 210.2 | 0.7 | Dupont 931A | 1.4 | 1.0 | 29.20 |

Table 7. Heater Element Temperature Data for Transient Boiling Tests

| Run No. | Element | Capacitor Voltage | Time Millisec. | Bridge Unbalance - Millivolts | | | | | | | | | |
|---|---|---|---|---|---|---|---|---|---|---|---|---|---|
| | | | | 1 | 2 | 3 | 4 | 5 | 6 | 7 | 8 | 9 | 10 |
| 1 | A | 350 | | | 10.60 | | 10.70 | | 10.66 | | 10.60 | | 10.56 |
| 3 | A | 375 | | | 12.50 | | 12.56 | | 12.50 | | 12.46 | | 12.40 |
| 4 | A | 400 | | | 13.44 | | 13.50 | | 13.50 | | 13.46 | | 13.44 |
| 5 | B | 375 | | | 13.28 | | 13.84 | | 13.68 | | 13.52 | | 13.34 |
| 6 | B | 362 | | | 12.94 | | 13.28 | | 13.06 | | 12.88 | | 12.76 |
| 7 | C | 370 | | 13.80 | 14.94 | 15.10 | 15.02 | 14.90 | 14.76 | 14.74 | 14.68 | 14.64 | 14.58 |
| 9 | D | 395 | | 12.20 | 14.00 | 14.10 | 14.08 | 14.10 | 14.04 | 14.00 | 13.96 | 13.90 | 13.80 |
| 10 | D | 410 | | 13.36 | 14.72 | 14.76 | 14.70 | 14.68 | 14.50 | 14.48 | 14.36 | 14.12 | 14.00 |
| 14 | E | 420 | | 10.24 | 10.26 | 10.22 | 10.20 | 10.16 | 10.16 | 10.12 | 10.10 | 10.04 | 9.92 |
| 15 | E | 452 | | 12.08 | 12.12 | 12.10 | 12.04 | 11.96 | 11.88 | 11.76 | 11.66 | 11.54 | 11.40 |
| 15A | E | 452 | | 12.08 | 12.12 | 12.10 | 12.04 | 11.96 | 11.88 | 11.76 | 11.66 | 11.54 | 11.40 |
| 16 | E | 466 | | 13.20 | 13.14 | 13.08 | 12.86 | 12.76 | 12.72 | 12.64 | 12.54 | 12.42 | 12.30 |

Table 8.  Film Growth Rate Data for Run Number 1

| Frame No. | Frame Station | Vapor Bubble Projected Diameter - Inches | | | | | | | | | | | | |
|---|---|---|---|---|---|---|---|---|---|---|---|---|---|---|
| | | 1 14 | 2 15 | 3 16 | 4 17 | 5 18 | 6 19 | 7 20 | 8 21 | 9 22 | 10 23 | 11 24 | 12 25 | 13 26 |
| wire | | 0.41 | 0.39 | 0.40 | 0.40 | 0.41 | 0.38 | 0.39 | 0.40 | | | | | |
| 2 | | 1.70 | 1.57 | 1.26 | 1.20 | 1.10 | 1.18 | 1.24 | 1.34 | 1.26 | 1.18 | 1.49 | 1.68 | 1.74 |
| | | 1.97 | 1.90 | 1.86 | 1.46 | 1.25 | 1.11 | 1.68 | 1.44 | 1.72 | 1.90 | 2.02 | | |
| 4 | | 0.69 | 0.69 | 0.85 | 1.16 | 1.27 | 1.09 | 0.56 | 0.58 | 0.99 | 0.76 | 0.48 | 1.58 | 1.84 |
| | | 2.25 | 2.60 | 2.12 | 1.40 | 0.64 | 0.66 | 0.65 | 1.21 | 1.46 | 1.72 | 1.80 | | |
| 6 | | 0.88 | 0.70 | 1.43 | 1.50 | 1.70 | 1.00 | 0.76 | 1.33 | 1.38 | 0.72 | 0.46 | 2.15 | 2.88 |
| | | 2.65 | 2.50 | 1.14 | 0.55 | 0.82 | 0.78 | 0.56 | 0.98 | 1.78 | 2.36 | 2.28 | | |
| 8 | | 1.00 | 0.75 | 1.20 | 1.87 | 1.70 | 1.37 | 1.13 | 1.32 | 1.44 | 0.94 | 0.48 | 0.84 | 2.83 |
| | | 3.26 | 2.76 | 2.27 | 0.74 | 0.65 | 0.62 | 0.66 | 1.12 | 1.34 | 2.76 | 2.78 | | |
| 10 | | 0.98 | 1.27 | 1.68 | 1.68 | 1.71 | 1.82 | 1.81 | 1.40 | 0.52 | 0.65 | 1.00 | 2.45 | 3.12 |
| | | 3.00 | 2.54 | 1.22 | 0.68 | 0.72 | 0.74 | 1.00 | 1.26 | 1.70 | 1.68 | 1.72 | | |
| 12 | | 1.32 | 1.24 | 1.42 | 1.78 | 2.18 | 2.43 | 2.45 | 1.02 | 0.48 | 0.60 | 1.79 | 2.62 | 2.78 |
| | | 2.70 | 2.42 | 2.10 | 0.62 | 0.84 | 0.74 | 1.20 | 2.30 | 2.62 | 2.72 | 2.48 | | |
| 14 | | 1.40 | 1.46 | 1.60 | 1.90 | 2.26 | 2.62 | 2.12 | 1.00 | 0.46 | 1.16 | 2.47 | 2.64 | 2.68 |
| | | 2.68 | 2.44 | 2.30 | 1.40 | 0.64 | 0.76 | 1.86 | 2.10 | 2.30 | 2.54 | 2.66 | | |
| 16 | | 1.10 | 1.54 | 1.96 | 2.56 | 2.70 | 2.45 | 1.74 | 0.70 | 0.60 | 1.77 | 2.16 | 2.38 | 2.59 |
| | | 2.52 | 2.38 | 2.34 | 1.76 | 1.00 | 0.67 | 1.47 | 1.85 | 2.46 | 2.58 | 2.60 | | |
| 18 | | 1.40 | 2.20 | 2.84 | 2.86 | 2.56 | 2.30 | 1.72 | 1.12 | 1.23 | 1.67 | 2.12 | 2.58 | 2.67 |
| | | 2.50 | 2.27 | 1.96 | 1.40 | 0.88 | 0.98 | 1.63 | 2.35 | 2.36 | 2.60 | 2.14 | | |
| 20 | | 1.55 | 1.88 | 2.36 | 3.12 | 2.70 | 1.95 | 1.70 | 1.37 | 1.44 | 1.66 | 2.08 | 2.43 | 2.46 |
| | | 2.44 | 1.94 | 1.42 | 1.11 | 0.98 | 1.20 | 1.66 | 2.19 | 2.28 | 2.42 | 2.52 | | |

Framing Speed:    23 Frames = 13.0 milliseconds

Table 9. Film Growth Rate Data for Run Number 3

| Frame No. | Frame Station | Vapor Bubble Projected Diameter - Inches | | | | | | | | | | | | |
|---|---|---|---|---|---|---|---|---|---|---|---|---|---|---|
| | | 1<br>14 | 2<br>15 | 3<br>16 | 4<br>17 | 5<br>18 | 6<br>19 | 7<br>20 | 8<br>21 | 9<br>22 | 10<br>23 | 11<br>24 | 12<br>25 | 13<br>26 |
| wire | | 0.22 | 0.23 | 0.24 | 0.22 | 0.23 | 0.22 | 0.23 | 0.22 | | | | | |
| | | 0.23 | 0.23 | 0.23 | 0.22 | 0.23 | 0.23 | | | | | | | |
| 5 | | 1.00 | 0.92 | 0.84 | 0.70 | 0.62 | 0.54 | 0.62 | 0.70 | 0.84 | 0.84 | 0.64 | 0.63 | 1.06 |
| | | 1.24 | 1.12 | 0.70 | 0.52 | 0.28 | 0.74 | 0.80 | 0.90 | 0.84 | 1.02 | 0.66 | 0.64 | 0.92 |
| 10 | | 0.60 | 1.04 | 0.98 | 0.85 | 0.71 | 0.56 | 0.32 | 0.70 | 0.90 | 0.92 | 0.64 | 0.67 | 1.40 |
| | | 1.50 | 1.42 | 0.34 | 0.72 | 0.39 | 0.27 | 1.24 | 1.16 | 0.82 | 0.98 | 0.82 | 0.47 | 0.96 |
| 15 | | 0.62 | 1.28 | 1.22 | 1.06 | 0.74 | 0.34 | 0.41 | 0.40 | 1.08 | 1.10 | 0.67 | 0.28 | 1.30 |
| | | 1.76 | 1.67 | 0.62 | 0.52 | 0.23 | 0.32 | 1.45 | 1.34 | 0.93 | 1.02 | 1.62 | 0.43 | 1.03 |
| 20 | | 0.32 | 1.40 | 1.45 | 1.25 | 0.80 | 0.34 | 0.52 | 0.45 | 1.16 | 1.43 | 0.82 | 0.38 | 1.30 |
| | | 1.86 | 1.78 | 0.60 | 0.36 | 0.50 | 0.29 | 1.30 | 1.67 | 1.24 | 0.94 | 0.45 | 0.48 | 1.24 |
| 25 | | 0.40 | 1.58 | 1.74 | 1.28 | 0.33 | 0.47 | 0.41 | 0.64 | 1.50 | 1.56 | 0.86 | 0.29 | 1.00 |
| | | 2.07 | 1.70 | 0.52 | 0.42 | 0.70 | 0.60 | 1.37 | 1.73 | 1.68 | 0.70 | 0.38 | 0.72 | 1.00 |
| 30 | | 0.40 | 1.44 | 1.62 | 1.45 | 0.30 | 0.47 | 0.42 | 0.83 | 1.52 | 1.67 | 1.00 | 0.27 | 1.56 |
| | | 2.16 | 1.62 | 0.30 | 0.36 | 0.55 | 0.72 | 1.42 | 1.88 | 1.90 | 0.60 | 0.40 | 0.58 | 1.20 |
| 35 | | 0.60 | 1.42 | 1.93 | 1.32 | 0.38 | 0.40 | 0.33 | 1.01 | 1.70 | 1.76 | 1.18 | 0.29 | 1.38 |
| | | 2.11 | 1.90 | 0.68 | 0.38 | 0.36 | 0.66 | 1.26 | 1.88 | 2.07 | 0.70 | 0.36 | 0.45 | 1.22 |
| 40 | | 0.90 | 1.62 | 1.88 | 1.54 | 0.40 | 0.57 | 0.34 | 1.01 | 1.82 | 1.78 | 1.22 | 0.30 | 1.52 |
| | | 2.10 | 2.00 | 0.86 | 0.42 | 0.44 | 0.38 | 1.38 | 2.06 | 2.00 | 0.90 | 0.52 | 0.52 | 1.32 |
| 45 | | 1.30 | 1.78 | 1.80 | 1.50 | 0.52 | 0.68 | 0.40 | 1.48 | 1.84 | 1.75 | 0.92 | 0.90 | 1.66 |
| | | 2.03 | 1.88 | 1.02 | 0.33 | 0.40 | 0.40 | 1.08 | 2.20 | 1.92 | 1.24 | 0.56 | 0.64 | 1.42 |
| 50 | | 1.50 | 1.78 | 1.80 | 1.56 | 1.00 | 0.44 | 0.47 | 1.53 | 1.96 | 1.70 | 0.98 | 1.01 | 1.72 |
| | | 1.83 | 1.85 | 1.25 | 0.40 | 0.74 | 0.58 | 1.24 | 2.13 | 1.94 | 1.42 | 0.66 | 0.50 | 1.46 |

Framing Speed: 47 Frames = 9.0 milliseconds

Table 10. Film Growth Rate Data for Run Number 4

Vapor Bubble Projected Diameter – Inches

| Frame Station | Frame No. 1 / 14 | 2 / 15 | 3 / 16 | 4 / 17 | 5 / 18 | 6 / 19 | 7 / 20 | 8 / 21 | 9 / 22 | 10 / 23 | 11 / 24 | 12 / 25 | 13 / 26 |
|---|---|---|---|---|---|---|---|---|---|---|---|---|---|
| wire | 0.23 (0.22) | 0.23 | 0.21 | 0.22 | 0.21 | 0.22 | 0.22 | 0.21 | 0.22 | 0.21 | 0.22 | 0.23 | 0.21 |
| 8 | 1.08 | 0.52 | 0.91 | 0.98 | 1.16 | 1.16 | 1.03 | 0.66 | 0.66 | 0.80 | 0.80 | 0.60 | 0.97 |
| 12 | 1.10 | 0.42 | 0.60 | 0.78 | 1.00 | 1.08 | 0.96 | 0.88 | 0.87 | 0.83 | 0.80 | 0.70 | 1.18 |
| 16 | 1.34 | 0.38 | 0.48 | 0.90 | 1.06 | 1.07 | 0.95 | 0.76 | 0.94 | 0.97 | 0.69 | 0.76 | 1.28 |
| 20 | 1.43 | 0.40 | 0.30 | 0.86 | 1.12 | 1.14 | 1.12 | 0.86 | 0.72 | 1.00 | 0.95 | 0.66 | 1.34 |
| 24 | 1.55 | 0.62 | 0.37 | 0.40 | 1.18 | 1.24 | 1.22 | 1.29 | 1.10 | 1.13 | 0.86 | 0.78 | 1.40 |
| 28 | 1.76 | 0.30 | 0.26 | 0.23 | 1.30 | 1.32 | 1.40 | 1.32 | 0.90 | 0.94 | 0.62 | 0.70 | 1.48 |
| 32 | 1.88 | 0.50 | 0.50 | 0.42 | 1.34 | 1.66 | 1.66 | 1.36 | 0.92 | 1.00 | 0.66 | 0.66 | 1.54 |
| 36 | 2.07 | 0.51 | 0.60 | 0.30 | 1.10 | 1.92 | 1.81 | 1.46 | 1.04 | 1.00 | 0.80 | 0.50 | 1.62 |
| 40 | 2.06 | 0.73 | 0.92 | 0.24 | 0.60 | 2.05 | 2.12 | 1.56 | 0.99 | 0.50 | 0.40 | 0.37 | 1.58 |

Framing Speed:  31 Frames = 8.0 milliseconds

Table 11. Film Growth Rate Data for Run Number 5

| Frame No. | Frame Station | Vapor Bubble Projected Diameter - Inches | | | | | | | | | | | | |
|---|---|---|---|---|---|---|---|---|---|---|---|---|---|---|
| | | 1 14 | 2 15 | 3 16 | 4 17 | 5 18 | 6 19 | 7 20 | 8 21 | 9 22 | 10 23 | 11 24 | 12 25 | 13 26 |
| wire | | 0.42 | 0.44 | 0.42 | 0.41 | 0.43 | 0.42 | 0.42 | 0.43 | 0.43 | | | | |
| 4 | | 1.44 | 1.30 | 1.21 | 1.14 | 1.01 | 1.44 | 1.46 | 1.63 | 1.76 | 1.38 | 1.23 | 0.94 | 0.95 |
| | | 1.38 | 1.44 | 1.26 | 1.04 | 1.22 | 1.22 | 1.43 | 1.62 | 1.20 | 1.80 | 1.92 | 1.46 | |
| 8 | | 1.80 | 1.64 | 1.08 | 0.78 | 0.89 | 1.22 | 1.76 | 2.02 | 1.78 | 1.56 | 0.90 | 0.46 | 0.58 |
| | | 0.98 | 1.28 | 1.38 | 1.07 | 0.84 | 1.08 | 1.41 | 1.70 | 2.10 | 2.04 | 1.89 | 1.86 | |
| 12 | | 2.07 | 1.82 | 1.30 | 0.86 | 0.75 | 0.86 | 1.90 | 1.93 | 2.00 | 1.60 | 1.05 | 0.44 | 0.52 |
| | | 1.06 | 1.48 | 1.34 | 1.24 | 1.22 | 1.16 | 1.52 | 1.72 | 2.10 | 2.20 | 2.08 | 2.16 | |
| 16 | | 2.28 | 1.90 | 1.31 | 0.82 | 0.76 | 0.78 | 1.64 | 2.41 | 2.07 | 1.60 | 0.48 | 0.70 | |
| | | 0.70 | 0.72 | 1.31 | 1.61 | 1.64 | 1.12 | 1.23 | 1.74 | 2.18 | 2.36 | 2.42 | 2.45 | 2.42 |
| 20 | | 2.63 | 2.24 | 1.04 | 0.64 | 0.58 | 1.32 | 2.42 | 2.72 | 2.38 | 1.40 | 0.44 | 0.64 | 0.70 |
| | | 0.48 | 0.53 | 1.02 | 1.25 | 1.30 | 1.52 | 2.00 | 2.62 | 3.10 | 3.20 | 2.20 | 2.65 | |
| 24 | | 2.96 | 2.21 | 0.96 | 0.58 | 0.61 | 1.56 | 2.78 | 2.78 | 2.38 | 1.70 | 0.60 | 1.04 | |
| | | 1.26 | 0.99 | 0.68 | 0.66 | 0.58 | 0.72 | 1.56 | 2.40 | 3.16 | 3.42 | 3.40 | 3.00 | 2.62 |
| 28 | | 2.82 | 2.48 | 1.26 | 0.65 | 1.06 | 2.10 | 2.88 | 3.06 | 2.72 | 1.96 | 1.22 | 1.07 | 1.23 |
| | | 1.25 | 0.56 | 0.79 | 0.92 | 0.66 | 0.80 | 2.90 | 3.22 | 3.46 | 3.40 | 3.20 | 3.00 | |
| 32 | | 2.62 | 2.04 | 1.42 | 0.78 | 1.26 | 2.04 | 2.80 | 2.84 | 1.62 | 2.16 | 1.64 | 1.27 | 0.52 |
| | | 0.78 | 0.64 | 0.78 | 0.86 | 0.68 | 0.90 | 3.70 | 3.69 | 3.40 | 3.10 | 2.63 | 2.88 | |
| 36 | | 2.62 | 2.22 | 1.50 | 1.57 | 1.51 | 2.38 | 2.69 | 2.76 | 2.71 | 2.76 | 2.12 | 1.15 | 0.68 |
| | | 0.98 | 1.04 | 0.60 | 0.62 | 0.62 | 1.50 | 3.14 | 3.65 | 3.72 | 3.50 | 2.10 | 2.88 | |

Framing Speed:  41 Frames = 11.0 milliseconds

Table 12. Film Growth Rate Data for Run Number 6

Vapor Bubble Projected Diameter – Inches

| Frame Station | Frame No. | 1 / 14 | 2 / 15 | 3 / 16 | 4 / 17 | 5 / 18 | 6 / 19 | 7 / 20 | 8 / 21 | 9 / 22 | 10 / 23 | 11 / 24 | 12 / 25 | 13 / 26 |
|---|---|---|---|---|---|---|---|---|---|---|---|---|---|---|
| wire | frames | 0.38 | 0.38 | 0.38 | 0.38 | 0.40 | 0.40 | 0.40 | 0.40 | | | | | |
| 4 | 1–13 | 0.50 | 0.81 | 0.89 | 0.75 | 0.98 | 1.36 | 1.92 | 1.70 | 1.44 | 1.40 | 1.21 | 1.05 | 1.05 |
| 4 | 14–26 | 0.96 | 0.58 | 0.62 | 0.61 | 1.12 | 1.62 | 1.77 | 1.87 | 1.84 | 1.43 | 1.22 | 1.28 | 0.64 |
| 8 | 1–13 | 0.64 | 0.72 | 0.88 | 0.69 | 0.79 | 1.44 | 2.17 | 2.20 | 2.10 | 1.80 | 1.44 | 0.64 | 0.65 |
| 8 | 14–26 | 0.61 | 0.91 | 1.06 | 0.56 | 0.50 | 1.52 | 2.30 | 2.17 | 1.90 | 1.50 | 0.72 | 0.92 | 0.95 |
| 12 | 1–13 | 0.68 | 0.86 | 0.95 | 0.65 | 0.68 | 1.37 | 2.14 | 2.42 | 2.51 | 2.16 | 1.50 | 0.63 | 0.57 |
| 12 | 14–26 | 0.73 | 0.84 | 0.79 | 0.72 | 0.73 | 1.77 | 2.36 | 2.62 | 2.75 | 2.29 | 1.60 | 0.64 | 0.84 |
| 16 | 1–13 | 0.66 | 1.40 | 1.85 | 1.00 | 1.42 | 2.18 | 2.77 | 2.96 | 2.64 | 1.60 | 0.64 | 0.54 | 0.54 |
| 16 | 14–26 | 0.95 | 1.06 | 0.93 | 0.63 | 0.69 | 1.48 | 2.51 | 2.96 | 3.07 | 2.26 | 1.68 | 0.73 | 1.27 |
| 20 | 1–13 | 0.77 | 1.46 | 1.56 | 1.42 | 1.08 | 1.54 | 2.31 | 2.60 | 2.67 | 2.56 | 1.28 | 0.60 | 0.53 |
| 20 | 14–26 | 0.88 | 0.90 | 1.34 | 0.90 | 0.42 | 1.24 | 2.76 | 3.12 | 3.14 | 2.80 | 1.91 | 0.92 | 1.08 |
| 24 | 1–13 | 0.88 | 0.90 | 1.24 | 1.68 | 2.02 | 2.24 | 2.40 | 2.52 | 2.37 | 2.04 | 1.07 | 0.62 | 0.64 |
| 24 | 14–26 | 0.64 | 1.66 | 1.70 | 1.04 | 0.52 | 1.50 | 2.56 | 3.08 | 3.00 | 2.84 | 2.22 | 1.00 | 0.66 |
| 28 | 1–13 | 0.90 | 0.70 | 0.53 | 0.58 | 2.32 | 2.46 | 2.54 | 2.57 | 2.46 | 2.30 | 1.92 | 1.00 | 0.62 |
| 28 | 14–26 | 1.40 | 1.30 | 1.02 | 1.14 | 1.50 | 2.03 | 2.36 | 2.78 | 3.14 | 2.92 | 2.52 | 1.40 | 0.62 |
| 32 | 1–13 | 0.77 | 0.84 | 0.59 | 0.92 | 2.00 | 2.80 | 2.87 | 2.79 | 2.46 | 2.24 | 1.85 | 1.00 | 0.80 |
| 32 | 14–26 | 0.66 | 0.62 | 0.50 | 0.80 | 2.02 | 2.08 | 2.62 | 2.84 | 2.77 | 2.80 | 2.34 | 1.44 | 0.72 |
| 36 | 1–13 | 0.81 | 0.74 | 0.62 | 1.40 | 2.28 | 2.95 | 3.14 | 3.18 | 2.80 | 1.74 | 0.92 | 1.14 | 1.58 |

Framing Speed: 58 Frames = 16.0 milliseconds

Table 13. Film Growth Rate Data for Run Number 7

| Frame No. | Frame Station | Vapor Bubble Projected Diameter - Inches | | | | | | | | | | | | |
|---|---|---|---|---|---|---|---|---|---|---|---|---|---|---|
| | | 1<br>14 | 2<br>15 | 3<br>16 | 4<br>17 | 5<br>18 | 6<br>19 | 7<br>20 | 8<br>21 | 9<br>22 | 10<br>23 | 11<br>24 | 12<br>25 | 13<br>26 |
| wire | | 0.22 | 0.22 | 0.23 | 0.24 | 0.24 | 0.24 | | | | | | | |
| 4 | | 0.84 | 0.90 | 0.94 | 0.96 | 0.88 | 0.83 | 0.76 | 0.55 | 0.57 | 0.76 | 0.60 | 0.58 | 0.74 |
| | | 0.66 | 0.76 | 0.72 | 0.75 | 0.72 | 0.81 | 0.62 | 0.70 | 0.80 | 0.72 | 0.78 | 0.80 | 0.70 |
| 8 | | 0.94 | 1.04 | 1.16 | 1.20 | 1.14 | 0.92 | 0.78 | 0.52 | 0.68 | 0.78 | 0.73 | 0.76 | 0.78 |
| | | 0.71 | 0.82 | 0.86 | 0.88 | 0.80 | 0.76 | 0.71 | 0.78 | 0.88 | 0.96 | 1.00 | 0.98 | 0.96 |
| 12 | | 1.08 | 1.16 | 1.27 | 1.38 | 1.30 | 1.06 | 0.62 | 0.48 | 0.30 | 0.85 | 0.91 | 0.93 | 0.84 |
| | | 0.76 | 0.82 | 0.92 | 1.02 | 0.82 | 0.75 | 0.70 | 0.75 | 0.94 | 1.00 | 1.08 | 1.04 | 0.80 |
| 16 | | 1.08 | 1.32 | 1.42 | 1.48 | 1.34 | 0.82 | 0.50 | 0.70 | 0.31 | 0.30 | 0.92 | 0.86 | 0.78 |
| | | 0.82 | 0.92 | 1.04 | 1.15 | 1.08 | 0.80 | 0.62 | 0.82 | 0.94 | 1.06 | 1.07 | 0.94 | 0.84 |
| 20 | | 1.20 | 1.32 | 1.61 | 1.56 | 1.50 | 0.44 | 0.72 | 0.92 | 0.49 | 0.28 | 0.88 | 0.83 | 0.72 |
| | | 0.85 | 0.96 | 1.13 | 1.22 | 1.05 | 0.82 | 0.46 | 0.70 | 1.05 | 1.20 | 1.04 | 1.00 | 0.84 |
| 24 | | 1.26 | 1.44 | 1.66 | 1.66 | 1.20 | 0.30 | 0.78 | 1.09 | 0.78 | 0.26 | 0.48 | 0.96 | 0.93 |
| | | 0.87 | 1.12 | 1.32 | 1.41 | 1.17 | 0.86 | 0.42 | 0.50 | 1.18 | 1.30 | 1.21 | 1.12 | 0.94 |
| 28 | | 1.40 | 1.56 | 1.60 | 1.83 | 1.26 | 1.00 | 1.00 | 1.23 | 0.72 | 0.28 | 0.28 | 0.98 | 0.98 |
| | | 0.82 | 1.18 | 1.42 | 1.60 | 1.40 | 1.02 | 0.40 | 0.40 | 0.76 | 0.38 | 1.52 | 1.32 | 1.06 |
| 32 | | 1.44 | 1.63 | 2.00 | 1.81 | 1.20 | 0.32 | 0.70 | 1.32 | 0.76 | 0.36 | 0.36 | 0.29 | 0.79 |
| | | 0.80 | 1.22 | 1.70 | 1.82 | 1.56 | 0.92 | 0.33 | 0.46 | 0.42 | 1.42 | 1.66 | 1.52 | 1.30 |
| 36 | | 1.66 | 1.62 | 2.07 | 1.84 | 0.72 | 0.40 | 0.82 | 1.47 | 1.08 | 0.40 | 0.38 | 0.39 | 0.40 |
| | | 0.93 | 1.29 | 1.80 | 2.00 | 1.70 | 0.96 | 0.44 | 0.64 | 0.50 | 1.20 | 1.70 | 1.66 | 1.47 |
| 40 | | 1.75 | 2.18 | 2.06 | 1.70 | 0.60 | 0.42 | 1.32 | 1.48 | 1.20 | 0.30 | 0.42 | 0.66 | 0.50 |
| | | 1.02 | 1.46 | 1.92 | 2.00 | 1.84 | 0.50 | 0.62 | 0.96 | 0.59 | 0.50 | 1.68 | 1.72 | 1.66 |

Framing Speed: 41 Frames = 11.0 milliseconds

Table 14. Film Growth Rate Data for Run Number 9

| Frame No. | Frame Station | 1 14 | 2 15 | 3 16 | 4 17 | 5 18 | 6 19 | 7 20 | 8 21 | 9 22 | 10 23 | 11 24 | 12 25 | 13 26 |
|---|---|---|---|---|---|---|---|---|---|---|---|---|---|---|
| | | | | | | Vapor Bubble Projected Diameter - Inches | | | | | | | | |
| wire | | 0.22 | 0.22 | 0.22 | 0.22 | | | 0.22 | 0.21 | 0.21 | 0.22 | 0.21 | | |
| | | 0.21 | 0.21 | 0.21 | 0.21 | 0.21 | 0.21 | 0.22 | 0.21 | 0.21 | | | | |
| 4 | | 1.06 | 0.88 | 0.96 | 1.00 | 0.94 | 0.92 | 0.98 | 1.00 | 0.90 | 0.80 | 1.00 | 0.83 | 0.78 |
| | | 0.78 | 0.78 | 0.94 | 1.06 | 1.08 | 0.84 | 1.00 | 0.92 | 0.98 | 0.92 | 1.08 | 0.96 | 0.92 |
| 8 | | 1.16 | 1.02 | 1.02 | 0.96 | 1.01 | 1.08 | 1.14 | 1.26 | 0.84 | 0.88 | 0.96 | 0.86 | 0.88 |
| | | 0.66 | 0.70 | 0.92 | 1.08 | 1.12 | 1.07 | 1.10 | 1.10 | 1.06 | 1.08 | 1.10 | 1.04 | 0.90 |
| 12 | | 1.18 | 1.14 | 1.06 | 1.10 | 1.12 | 1.12 | 1.34 | 1.38 | 1.12 | 0.78 | 0.88 | 1.00 | 1.00 |
| | | 0.78 | 0.59 | 0.86 | 1.18 | 1.16 | 1.10 | 0.97 | 1.16 | 1.12 | 1.24 | 1.10 | 0.96 | 1.10 |
| 16 | | 1.16 | 1.18 | 1.23 | 1.14 | 1.27 | 1.34 | 1.36 | 1.32 | 1.00 | 0.84 | 0.90 | 0.88 | 0.58 |
| | | 0.52 | 0.53 | 0.84 | 1.28 | 1.43 | 1.26 | 1.14 | 1.14 | 1.28 | 1.30 | 1.28 | 1.16 | 1.00 |
| 20 | | 1.26 | 1.28 | 1.10 | 1.30 | 1.32 | 1.44 | 1.52 | 1.47 | 1.33 | 1.00 | 0.72 | 0.52 | 0.41 |
| | | 0.40 | 0.30 | 1.01 | 1.46 | 1.66 | 1.54 | 1.44 | 1.40 | 1.42 | 1.37 | 1.30 | 1.18 | 0.98 |
| 24 | | 1.40 | 1.28 | 1.28 | 1.18 | 1.35 | 1.57 | 1.57 | 1.64 | 1.45 | 0.82 | 0.38 | 0.38 | 0.74 |
| | | 0.82 | 0.42 | 0.40 | 1.44 | 1.68 | 1.64 | 1.50 | 1.52 | 1.42 | 1.50 | 1.30 | 1.12 | 0.98 |
| 28 | | 1.42 | 1.36 | 1.22 | 1.24 | 1.54 | 1.72 | 1.76 | 1.64 | 1.30 | 0.62 | 0.50 | 0.36 | 1.04 |
| | | 1.24 | 0.56 | 0.23 | 1.42 | 1.82 | 1.64 | 1.50 | 1.62 | 1.68 | 1.59 | 1.50 | 1.36 | 1.36 |
| 32 | | 1.52 | 1.40 | 1.28 | 1.40 | 1.46 | 1.66 | 1.70 | 1.72 | 1.06 | 0.36 | 0.50 | 0.50 | 1.22 |
| | | 1.42 | 0.86 | 0.28 | 0.66 | 1.98 | 1.97 | 2.00 | 1.87 | 1.82 | 1.74 | 1.58 | 1.38 | 1.20 |
| 36 | | 1.44 | 1.42 | 1.34 | 1.38 | 1.58 | 1.77 | 1.83 | 1.56 | 0.32 | 0.42 | 0.41 | 0.46 | 1.42 |
| | | 1.68 | 1.32 | 0.34 | 0.34 | 1.88 | 2.14 | 2.12 | 1.96 | 1.86 | 1.86 | 1.64 | 1.40 | 1.28 |

Framing Speed:  27 frames = 7.0 milliseconds

Table 15.  Film Growth Rate Data for Run Number 10

Vapor Bubble Projected Diameter - Inches

| Frame Station | 1 / 14 | 2 / 15 | 3 / 16 | 4 / 17 | 5 / 18 | 6 / 19 | 7 / 20 | 8 / 21 | 9 / 22 | 10 / 23 | 11 / 24 | 12 / 25 | 13 / 26 |
|---|---|---|---|---|---|---|---|---|---|---|---|---|---|
| wire | 0.40 | 0.38 | 0.38 | 0.38 | 0.38 | 0.39 | 0.40 | 0.40 | 0.39 | | | | |
| | 0.38 | 0.38 | 0.40 | 0.39 | 0.38 | 0.38 | 0.40 | | | | | | |
| 4 | 1.36 | 1.48 | 1.58 | 1.48 | 1.54 | 1.62 | 1.52 | 1.27 | 1.28 | 1.67 | 1.60 | 1.46 | 1.24 |
| | 1.57 | 1.50 | 1.40 | 1.56 | 1.42 | 1.51 | 1.45 | 1.52 | 1.52 | 1.70 | 1.80 | 1.70 | 1.72 |
| 8 | 1.68 | 1.50 | 1.68 | 1.76 | 1.58 | 1.74 | 1.62 | 1.55 | 1.48 | 1.53 | 1.60 | 1.63 | 1.64 |
| | 1.66 | 1.48 | 1.58 | 1.64 | 1.60 | 1.52 | 1.62 | 1.62 | 1.52 | 1.72 | 1.80 | 1.88 | 1.94 |
| 12 | 1.88 | 1.92 | 1.68 | 1.86 | 1.78 | 1.77 | 1.69 | 1.86 | 1.74 | 1.62 | 1.76 | 1.74 | 1.82 |
| | 1.48 | 1.66 | 1.73 | 1.68 | 1.76 | 1.69 | 1.48 | 1.52 | 1.76 | 1.74 | 1.56 | 1.88 | 2.20 |
| 16 | 1.92 | 1.96 | 2.13 | 1.86 | 1.84 | 1.89 | 1.80 | 1.79 | 1.88 | 1.88 | 1.80 | 1.70 | 1.74 |
| | 1.86 | 1.70 | 1.74 | 1.72 | 1.71 | 1.63 | 1.64 | 1.70 | 1.67 | 1.58 | 1.44 | 2.06 | 2.13 |
| 20 | 1.72 | 2.22 | 2.24 | 2.14 | 2.00 | 2.01 | 1.92 | 1.92 | 1.80 | 2.01 | 1.80 | 1.91 | 1.92 |
| | 1.98 | 1.88 | 1.75 | 1.65 | 1.66 | 1.68 | 1.60 | 1.56 | 1.50 | 1.70 | 1.78 | 2.00 | 2.20 |
| 24 | 0.90 | 1.87 | 2.32 | 2.40 | 2.16 | 2.07 | 2.06 | 2.10 | 2.10 | 2.14 | 2.08 | 2.24 | 2.16 |
| | 1.93 | 1.96 | 1.88 | 1.73 | 1.64 | 1.62 | 1.80 | 1.65 | 1.60 | 1.73 | 1.91 | 2.18 | 2.43 |
| 28 | 0.60 | 1.20 | 2.08 | 2.38 | 2.23 | 2.34 | 2.14 | 2.13 | 2.15 | 2.30 | 2.30 | 2.28 | 2.17 |
| | 2.09 | 2.00 | 1.90 | 1.82 | 1.74 | 1.60 | 1.51 | 1.58 | 1.63 | 1.74 | 1.94 | 2.26 | 2.52 |
| 32 | 0.60 | 0.68 | 0.92 | 2.30 | 2.52 | 2.58 | 2.42 | 2.26 | 2.24 | 2.40 | 2.46 | 2.26 | 2.20 |
| | 2.10 | 2.05 | 1.92 | 1.84 | 1.81 | 1.63 | 1.30 | 1.26 | 1.36 | 1.80 | 2.20 | 2.38 | 2.83 |
| 36 | 0.68 | 0.69 | 0.70 | 0.98 | 2.36 | 2.90 | 2.90 | 2.78 | 2.64 | 2.42 | 2.36 | 2.47 | 2.48 |
| | 2.34 | 2.12 | 2.04 | 1.86 | 1.36 | 1.34 | 1.22 | 1.20 | 1.52 | 1.59 | 2.20 | 2.65 | 2.82 |

Framing Speed:  30 frames = 8.0 milliseconds

Table 16.  Film Growth Rate Data for Run Number 14

| Frame No. | Frame Station | 1 14 | 2 15 | 3 16 | 4 17 | 5 18 | 6 19 | 7 20 | 8 21 | 9 22 | 10 23 | 11 24 | 12 25 | 13 26 |
|---|---|---|---|---|---|---|---|---|---|---|---|---|---|---|
| wire | | 0.26 | 0.26 | 0.25 | 0.26 | 0.24 | 0.27 | | | | | | | |
| | | 0.26 | 0.26 | 0.25 | 0.25 | 0.24 | 0.24 | 0.26 | 0.26 | 0.26 | | | | |
| 5 | | 0.40 | 0.88 | 0.94 | 0.84 | 0.88 | 0.75 | 0.71 | 0.81 | 0.88 | 0.78 | 0.80 | 1.00 | 1.09 |
| | | 0.98 | 0.92 | 0.62 | 0.72 | 0.72 | 0.71 | 0.76 | 0.76 | 0.82 | 0.72 | 0.48 | | |
| 10 | | 0.60 | 0.82 | 0.93 | 0.96 | 0.40 | 0.46 | 0.82 | 1.06 | 0.98 | 0.76 | 0.96 | 1.16 | 1.24 |
| | | 1.16 | 1.00 | 0.46 | 0.38 | 0.61 | 0.66 | 0.76 | 0.93 | 1.00 | 1.06 | 0.82 | | |
| 15 | | 0.40 | 0.75 | 1.36 | 0.96 | 0.40 | 0.47 | 0.29 | 1.16 | 1.07 | 0.86 | 1.03 | 1.31 | 1.45 |
| | | 1.38 | 0.90 | 0.38 | 0.36 | 0.56 | 0.70 | 0.84 | 1.06 | 1.16 | 1.20 | 0.99 | | |
| 20 | | 0.40 | 1.04 | 1.50 | 1.30 | 0.62 | 0.50 | 0.36 | 1.02 | 1.16 | 0.92 | 1.16 | 1.39 | 1.53 |
| | | 1.26 | 0.30 | 0.60 | 0.57 | 0.56 | 0.66 | 0.89 | 1.21 | 1.31 | 1.16 | 0.97 | | |
| 25 | | 0.38 | 0.90 | 1.58 | 1.34 | 0.42 | 0.40 | 0.28 | 0.66 | 1.18 | 1.06 | 1.29 | 1.42 | 1.74 |
| | | 1.52 | 0.27 | 0.80 | 0.86 | 0.32 | 0.32 | 0.60 | 1.36 | 1.66 | 1.50 | 1.20 | | |
| 30 | | 0.38 | 1.22 | 1.61 | 1.22 | 0.32 | 0.67 | 0.47 | 0.40 | 1.08 | 1.27 | 1.38 | 1.78 | 1.95 |
| | | 1.08 | 0.32 | 0.98 | 0.62 | 0.40 | 0.35 | 0.35 | 1.32 | 1.66 | 1.85 | 1.28 | | |
| 35 | | 0.38 | 1.12 | 1.54 | 1.44 | 0.93 | 0.40 | 0.44 | 0.37 | 0.30 | 1.36 | 1.44 | 1.65 | 1.65 |
| | | 1.40 | 0.47 | 1.07 | 0.93 | 0.68 | 0.58 | 0.42 | 0.33 | 1.42 | 1.81 | 1.64 | | |
| 40 | | 0.36 | 0.84 | 1.67 | 1.50 | 1.14 | 0.36 | 0.60 | 0.46 | 0.52 | 0.56 | 1.62 | 1.86 | 2.00 |
| | | 1.55 | 0.51 | 0.81 | 1.19 | 0.84 | 0.31 | 0.34 | 0.87 | 1.94 | 1.70 | 1.06 | | |
| 45 | | 0.42 | 0.92 | 1.78 | 1.39 | 1.10 | 0.36 | 0.30 | 0.45 | 0.29 | 0.41 | 1.90 | 2.12 | 1.94 |
| | | 1.35 | 0.68 | 0.72 | 1.13 | 0.70 | 0.28 | 0.36 | 1.25 | 1.82 | 1.56 | 1.00 | | |

Framing Speed:   33 frames = 7.0 milliseconds

Table 17   Film Growth Rate Data for Run Number 15

| Frame No. | Frame Station | Vapor Bubble Projected Diameter - Inches | | | | | | | | | | | | |
|---|---|---|---|---|---|---|---|---|---|---|---|---|---|
| | | 1 14 | 2 15 | 3 16 | 4 17 | 5 18 | 6 19 | 7 20 | 8 21 | 9 22 | 10 23 | 11 24 | 12 25 | 13 26 |
| wire | | 0.28 | 0.27 | 0.27 | 0.28 | 0.26 | 0.28 | 0.26 | 0.27 | 0.28 | 0.28 | | | |
| | | 0.27 | 0.26 | 0.26 | 0.25 | 0.27 | 0.26 | 0.26 | 0.26 | 0.27 | 0.27 | 0.27 | | |
| 5 | | 0.96 | 0.95 | 0.92 | 0.82 | 0.84 | 0.70 | 1.02 | 0.72 | 0.91 | 0.79 | 0.86 | 0.72 | 0.88 |
| | | 0.96 | 0.92 | 0.87 | 0.95 | 0.78 | 0.73 | 0.76 | 0.92 | 0.92 | 0.93 | 0.83 | | |
| 10 | | 0.94 | 0.96 | 0.80 | 0.77 | 0.92 | 0.98 | 0.90 | 0.93 | 0.83 | 0.93 | 0.90 | 0.80 | 0.99 |
| | | 1.28 | 1.04 | 0.96 | 0.87 | 0.82 | 0.79 | 0.84 | 0.90 | 0.90 | 1.00 | 0.97 | | |
| 15 | | 1.00 | 1.00 | 0.92 | 0.92 | 1.01 | 1.06 | 1.00 | 0.78 | 0.84 | 0.98 | 1.00 | 1.02 | 1.04 |
| | | 1.16 | 1.18 | 0.85 | 0.78 | 0.88 | 0.80 | 0.87 | 0.94 | 1.03 | 1.16 | 1.00 | | |
| 20 | | 1.15 | 1.06 | 1.00 | 0.92 | 0.98 | 1.12 | 0.96 | 0.87 | 1.04 | 1.21 | 1.06 | 1.07 | 1.18 |
| | | 1.30 | 1.16 | 1.14 | 0.86 | 0.70 | 0.90 | 1.02 | 1.03 | 1.19 | 1.16 | 1.22 | | |
| 25 | | 1.13 | 1.12 | 0.97 | 1.00 | 1.15 | 1.19 | 0.96 | 0.80 | 0.93 | 1.16 | 1.16 | 1.17 | 1.37 |
| | | 1.32 | 1.34 | 1.05 | 0.65 | 0.48 | 0.75 | 1.02 | 1.07 | 1.28 | 1.12 | 1.46 | | |
| 30 | | 1.24 | 1.02 | 0.87 | 1.04 | 1.16 | 1.20 | 0.98 | 0.74 | 0.90 | 1.12 | 1.17 | 1.28 | 1.30 |
| | | 1.38 | 1.38 | 1.06 | 0.35 | 0.33 | 0.44 | 1.03 | 1.17 | 1.48 | 1.60 | 1.56 | | |
| 35 | | 1.22 | 1.21 | 0.94 | 1.07 | 1.14 | 1.12 | 0.79 | 0.90 | 0.92 | 1.11 | 1.23 | 1.36 | 1.52 |
| | | 1.66 | 1.50 | 0.95 | 0.40 | 0.67 | 0.35 | 0.92 | 1.38 | 1.62 | 1.70 | 1.34 | | |
| 40 | | 1.30 | 1.26 | 1.16 | 1.13 | 1.17 | 1.17 | 0.98 | 0.94 | 1.06 | 1.12 | 1.38 | 1.48 | 1.63 |
| | | 1.64 | 1.55 | 0.35 | 0.43 | 0.83 | 0.86 | 0.40 | 1.55 | 1.80 | 1.90 | 1.50 | | |
| 45 | | 1.38 | 1.36 | 1.32 | 1.14 | 1.31 | 1.26 | 0.87 | 0.84 | 0.88 | 1.13 | 1.43 | 1.68 | 1.86 |
| | | 1.85 | 1.74 | 0.58 | 0.36 | 0.96 | 0.65 | 0.37 | 0.92 | 2.06 | 2.00 | 1.82 | | |

Framing Speed:   29 frames = 6.0 milliseconds

Table 18. Film Growth Rate Data for Run Number 15A

| Frame No. | Frame Station | Vapor Bubble Projected Diameter - Inches | | | | | | | | | | | | |
|---|---|---|---|---|---|---|---|---|---|---|---|---|---|---|
| | | 1 | 2 | 3 | 4 | 5 | 6 | 7 | 8 | 9 | 10 | 11 | 12 | 13 |
| | | 14 | 15 | 16 | 17 | 18 | 19 | 20 | 21 | 22 | 23 | 24 | 25 | 26 |
| wire | | 0.25 | 0.25 | 0.26 | 0.25 | 0.25 | 0.25 | 0.26 | 0.26 | | | | | |
| 5 | | 0.96 | 0.92 | 0.88 | 0.80 | 0.82 | 0.80 | 0.75 | 0.88 | 0.72 | 0.71 | 0.70 | 0.75 | 0.72 |
| | | 0.82 | 0.82 | 0.86 | 0.80 | 0.70 | 0.72 | 0.70 | 0.70 | 0.71 | 0.78 | 0.76 | 0.85 | |
| 10 | | 0.96 | 0.90 | 0.90 | 0.82 | 0.78 | 0.77 | 0.90 | 0.85 | 0.77 | 0.74 | 0.78 | 0.87 | 0.86 |
| | | 0.90 | 0.88 | 0.97 | 0.94 | 0.72 | 0.68 | 0.74 | 0.82 | 0.85 | 0.82 | 1.00 | 0.92 | |
| 15 | | 0.92 | 0.93 | 0.86 | 0.97 | 0.86 | 0.88 | 0.91 | 0.90 | 0.78 | 0.80 | 0.92 | 0.94 | 0.90 |
| | | 1.02 | 1.00 | 0.98 | 0.92 | 0.72 | 0.70 | 0.86 | 0.80 | 0.82 | 0.90 | 0.84 | 0.94 | |
| 20 | | 0.97 | 0.94 | 0.93 | 1.02 | 0.90 | 0.86 | 0.94 | 0.82 | 0.84 | 0.90 | 0.96 | 1.06 | 1.11 |
| | | 1.16 | 1.23 | 1.02 | 0.80 | 0.54 | 0.60 | 0.85 | 0.91 | 0.90 | 1.04 | 1.16 | 0.94 | |
| 25 | | 0.96 | 0.86 | 0.86 | 0.96 | 0.98 | 1.00 | 1.02 | 0.98 | 0.80 | 0.98 | 1.02 | 1.18 | 1.25 |
| | | 1.34 | 1.32 | 1.16 | 0.90 | 0.42 | 0.42 | 0.81 | 0.91 | 1.06 | 1.28 | 1.21 | 1.02 | |
| 30 | | 0.92 | 0.98 | 1.00 | 0.98 | 1.08 | 1.12 | 0.98 | 0.84 | 0.76 | 0.90 | 0.94 | 1.20 | 1.40 |
| | | 1.46 | 1.42 | 1.25 | 0.62 | 0.48 | 0.50 | 1.00 | 1.02 | 1.23 | 1.52 | 1.36 | 0.80 | |
| 35 | | 0.92 | 0.90 | 0.90 | 1.08 | 1.17 | 1.10 | 1.10 | 0.84 | 0.90 | 0.94 | 1.08 | 1.26 | 1.42 |
| | | 1.66 | 1.73 | 1.36 | 0.46 | 0.42 | 0.36 | 0.40 | 1.21 | 1.48 | 1.60 | 1.80 | 1.10 | |
| 40 | | 1.06 | 1.04 | 0.96 | 0.94 | 1.36 | 1.30 | 1.22 | 1.03 | 0.78 | 0.92 | 1.12 | 1.32 | 1.60 |
| | | 1.78 | 1.84 | 1.50 | 1.35 | 0.58 | 0.46 | 0.36 | 1.36 | 1.50 | 1.80 | 1.62 | 1.38 | |
| 45 | | 1.16 | 1.06 | 0.92 | 0.91 | 1.27 | 1.32 | 1.20 | 0.90 | 0.86 | 0.82 | 1.22 | 1.55 | 1.83 |
| | | 2.03 | 2.00 | 1.26 | 0.37 | 0.80 | 0.80 | 0.42 | 0.70 | 1.84 | 1.96 | 2.00 | 1.26 | |
| 15 | 2nd Observer | 0.94 | 0.96 | 0.94 | 0.98 | 0.94 | 0.86 | 0.90 | 0.92 | 0.84 | 0.80 | 0.88 | 0.90 | 0.98 |
| | | 1.04 | 1.08 | 1.00 | 0.88 | 0.76 | 0.76 | 0.84 | 0.76 | 0.80 | 0.90 | 0.84 | 0.90 | |
| 30 | 2nd Observer | 0.92 | 1.00 | 1.02 | 0.92 | 1.04 | 1.10 | 0.94 | 0.82 | 0.76 | 0.88 | 0.92 | 1.14 | 1.32 |
| | | 1.40 | 1.32 | 1.22 | 0.72 | 0.42 | 0.50 | 1.00 | 1.04 | 1.20 | 1.54 | 1.40 | 0.80 | |

Framing Speed: 32 frames = 7.2 milliseconds

Table 19. Film Growth Rate Data for Run Number 16

| | | Vapor Bubble Projected Diameter - Inches | | | | | | | | | | | | |
|---|---|---|---|---|---|---|---|---|---|---|---|---|---|---|
| Frame No. | Frame Station | 1<br>14 | 2<br>15 | 3<br>16 | 4<br>17 | 5<br>18 | 6<br>19 | 7<br>20 | 8<br>21 | 9<br>22 | 10<br>23 | 11<br>24 | 12<br>25 | 13<br>26 |
| wire | | | | | | | 0.46 | 0.45 | 0.45 | 0.45 | 0.45 | 0.45 | 0.46 | 0.45 |
| | | 0.45 | 0.46 | 0.45 | 0.46 | 0.46 | 0.45 | | | | | | | |
| 4 | | 1.66 | 1.52 | 1.69 | 1.76 | 1.76 | 1.82 | 1.82 | 1.86 | 1.87 | 1.72 | 1.96 | 1.76 | 1.84 |
| | | 1.94 | 2.04 | 1.40 | 1.88 | 1.78 | 1.68 | 2.06 | 2.20 | 2.26 | 1.18 | 1.84 | 1.60 | |
| 8 | | 1.96 | 2.08 | 2.18 | 2.22 | 2.44 | 2.36 | 2.24 | 2.32 | 2.20 | 2.06 | 2.04 | 1.64 | 1.48 |
| | | 1.24 | 1.00 | 1.66 | 1.84 | 2.06 | 1.65 | 1.26 | 0.96 | 0.86 | 1.16 | 1.00 | 2.12 | |
| 12 | | 2.10 | 2.20 | 2.44 | 2.46 | 2.68 | 2.83 | 2.85 | 2.62 | 2.48 | 2.30 | 1.82 | 1.20 | 0.46 |
| | | 0.52 | 0.78 | 1.22 | 1.82 | 1.82 | 1.24 | 0.78 | 0.84 | 0.84 | 0.75 | 1.10 | 2.30 | |
| 16 | | 2.32 | 2.38 | 2.44 | 2.62 | 3.00 | 2.97 | 2.88 | 2.90 | 2.70 | 2.30 | 1.20 | 0.60 | 0.80 |
| | | 0.98 | 1.18 | 1.90 | 2.00 | 2.26 | 1.42 | 1.26 | 1.22 | 1.20 | 1.14 | 0.76 | 2.30 | |
| 20 | | 2.08 | 2.52 | 2.66 | 2.60 | 2.89 | 3.00 | 2.96 | 3.06 | 3.18 | 2.82 | 1.66 | 0.66 | 0.80 |
| | | 0.69 | 0.82 | 1.62 | 2.16 | 2.52 | 2.44 | 1.95 | 1.80 | 1.40 | 1.18 | 1.12 | 0.87 | |
| 24 | | 1.00 | 2.27 | 2.62 | 3.14 | 2.90 | 2.94 | 3.26 | 3.26 | 3.26 | 2.70 | 0.80 | 0.66 | 0.84 |
| | | 0.74 | 0.54 | 1.57 | 2.41 | 2.42 | 2.47 | 2.48 | 1.80 | 1.64 | 0.86 | 0.86 | 1.00 | |
| 28 | | 0.78 | 1.29 | 3.07 | 3.12 | 3.12 | 3.19 | 3.34 | 3.25 | 3.18 | 2.26 | 0.72 | 0.58 | 0.66 |
| | | 0.63 | 0.82 | 2.02 | 2.76 | 2.92 | 2.95 | 2.93 | 2.18 | 1.60 | 0.66 | 0.98 | 1.20 | |
| 32 | | 0.72 | 0.72 | 3.02 | 3.52 | 3.48 | 3.76 | 3.78 | 3.42 | 3.10 | 1.96 | 0.84 | 0.62 | 0.72 |
| | | 0.92 | 1.24 | 2.02 | 2.86 | 3.08 | 3.22 | 3.20 | 2.55 | 1.90 | 1.16 | 0.92 | 1.26 | |
| 36 | | 0.72 | 0.84 | 1.22 | 3.46 | 4.00 | 3.96 | 3.92 | 3.64 | 2.68 | 1.64 | 0.60 | 0.88 | 0.93 |
| | | 0.80 | 1.18 | 2.34 | 2.79 | 3.20 | 3.55 | 3.40 | 2.95 | 2.38 | 1.69 | 0.90 | 0.94 | |
| 40 | | 0.79 | 0.76 | 1.38 | 2.30 | 4.40 | 4.40 | 4.14 | 4.02 | 2.56 | 0.83 | 0.60 | 0.66 | 0.72 |
| | | 0.75 | 1.16 | 2.46 | 3.02 | 3.46 | 3.60 | 3.40 | 2.95 | 1.40 | 0.80 | 1.10 | 1.28 | |
| 44 | | 1.26 | 0.84 | 1.20 | 1.86 | 4.25 | 4.74 | 4.56 | 3.62 | 2.40 | 1.22 | 0.67 | 0.92 | 0.97 |
| | | 0.78 | 1.12 | 1.85 | 3.22 | 3.56 | 3.78 | 3.30 | 3.02 | 2.30 | 1.00 | 1.02 | 1.14 | |

Framing Speed:  59 frames = 13.0 milliseconds
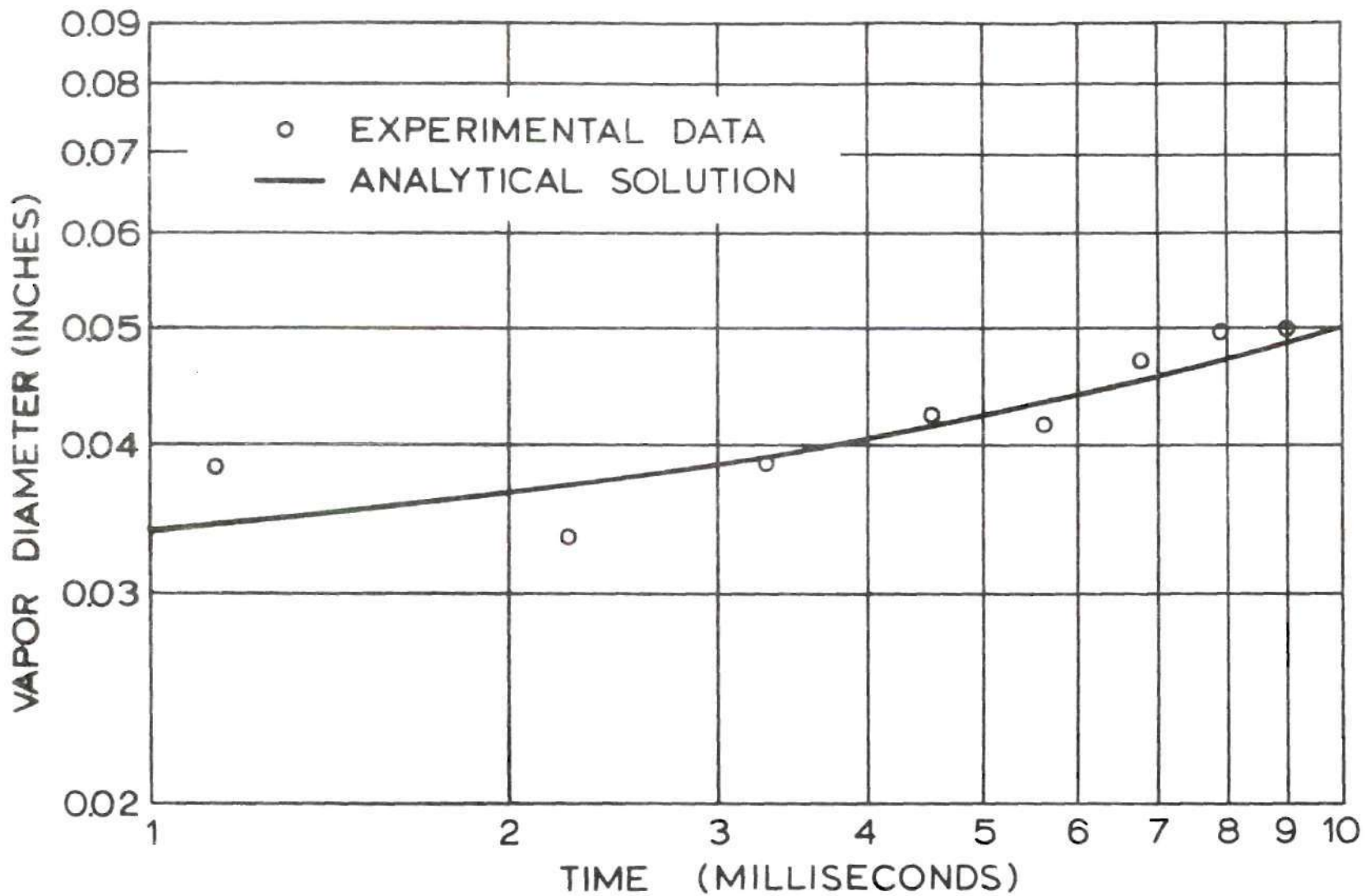
**Figure 18.** Plot of Vapor Bubble Diameter as a Function of Time for Run 1.
$$T_w - T_{sat} = 1245 - 210.7 \approx 1034°F$$

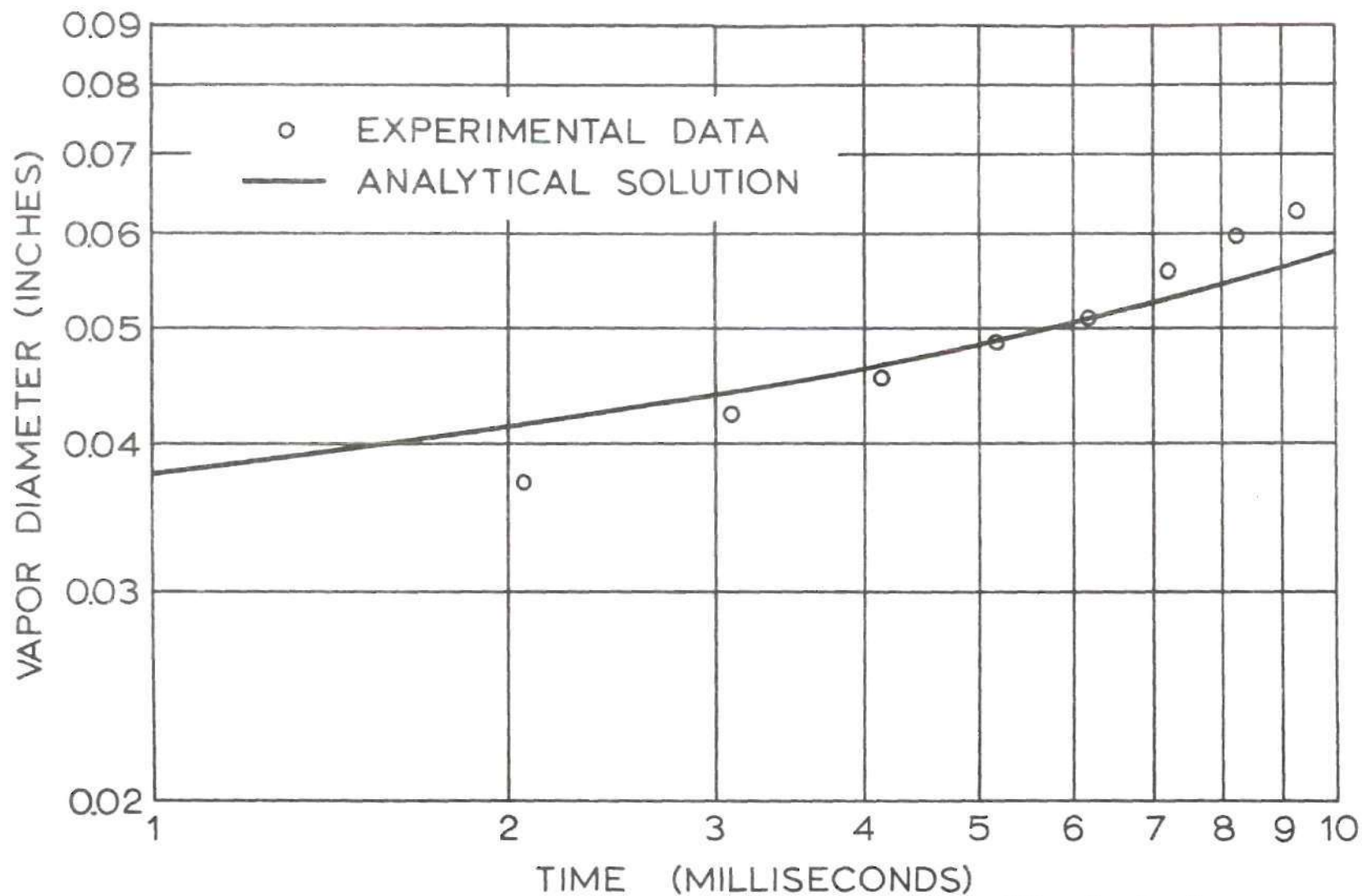Figure 20. Plot of Vapor Bubble Diameter as a Function of Time for Run 4.
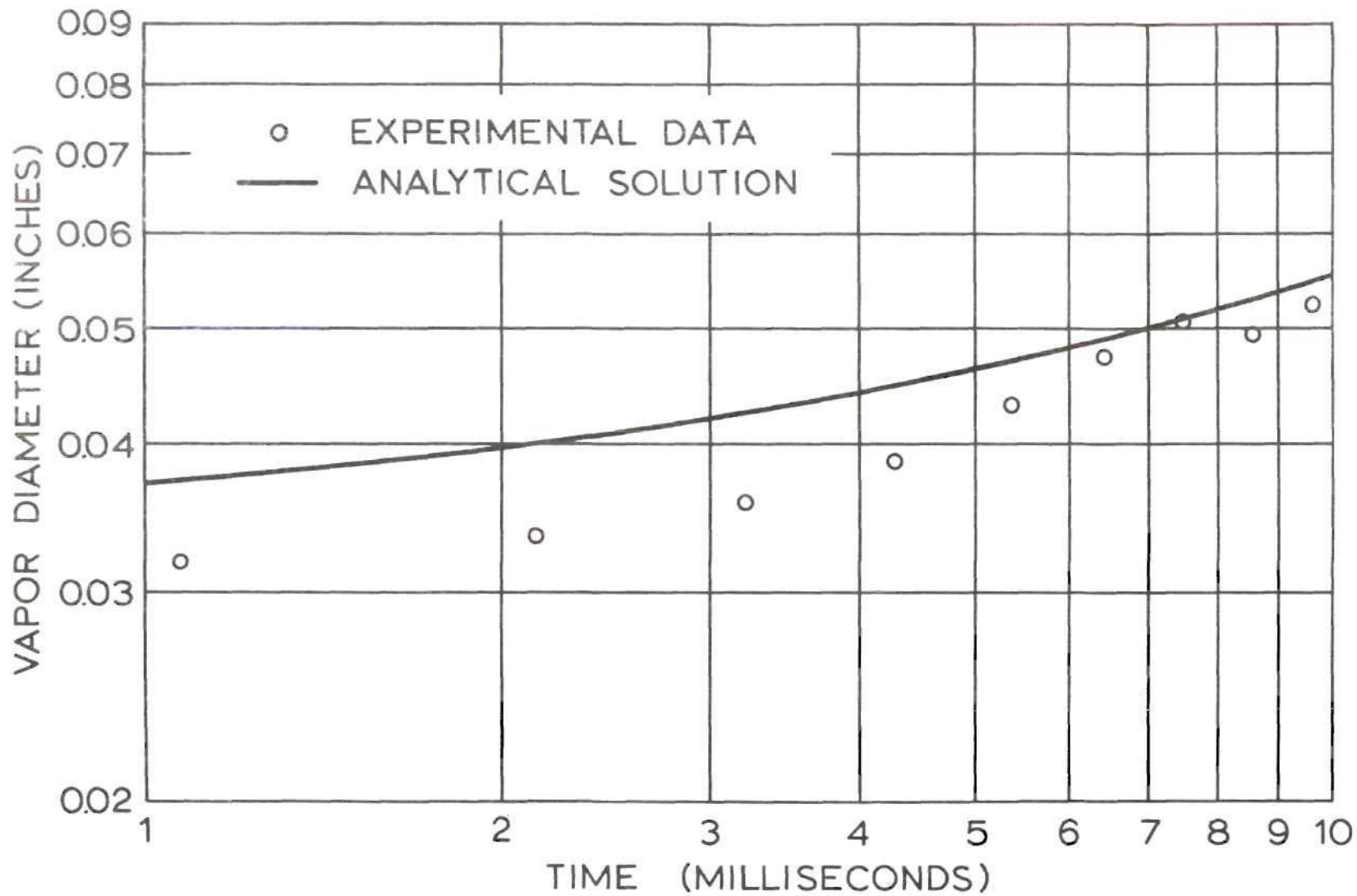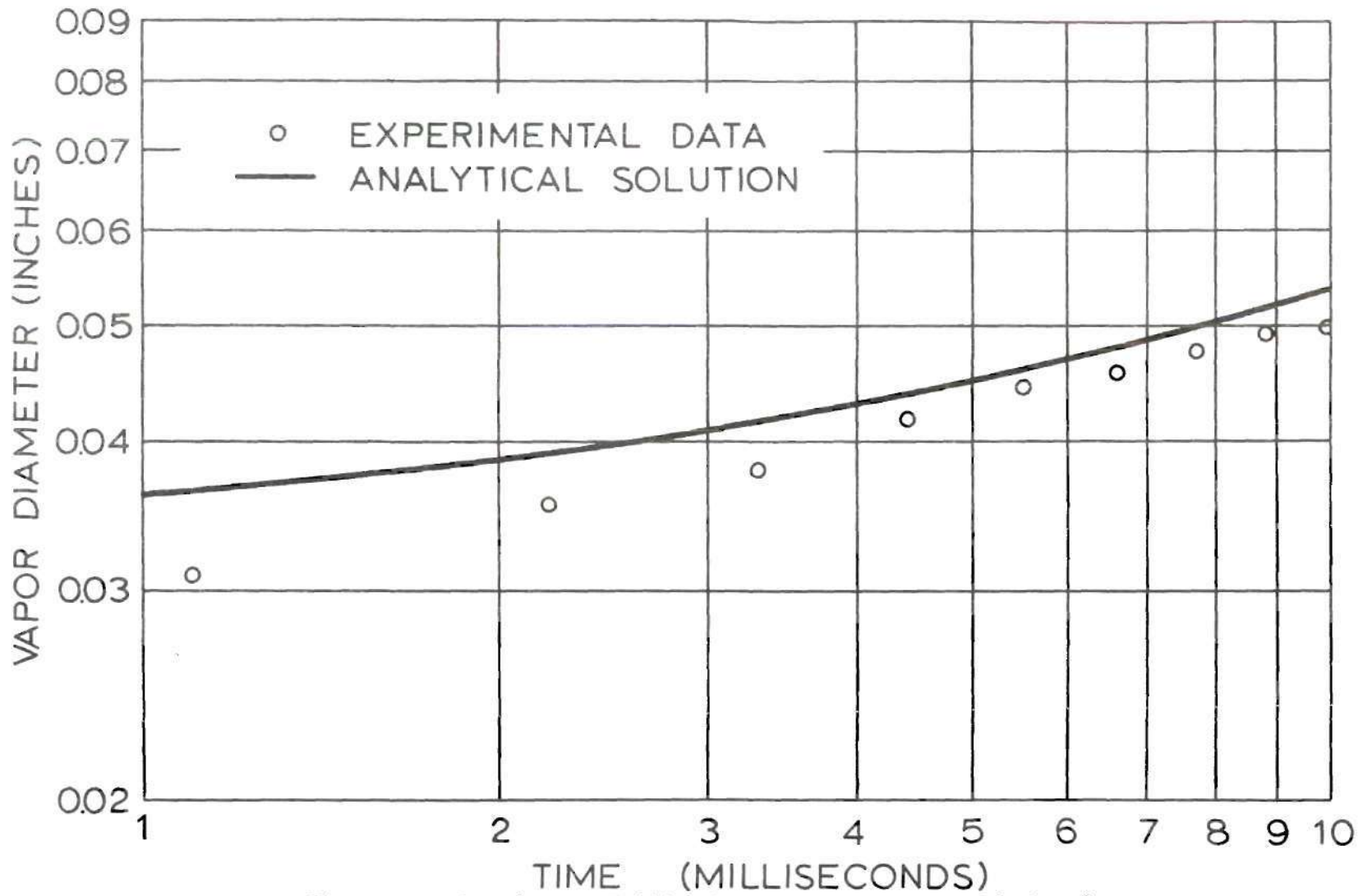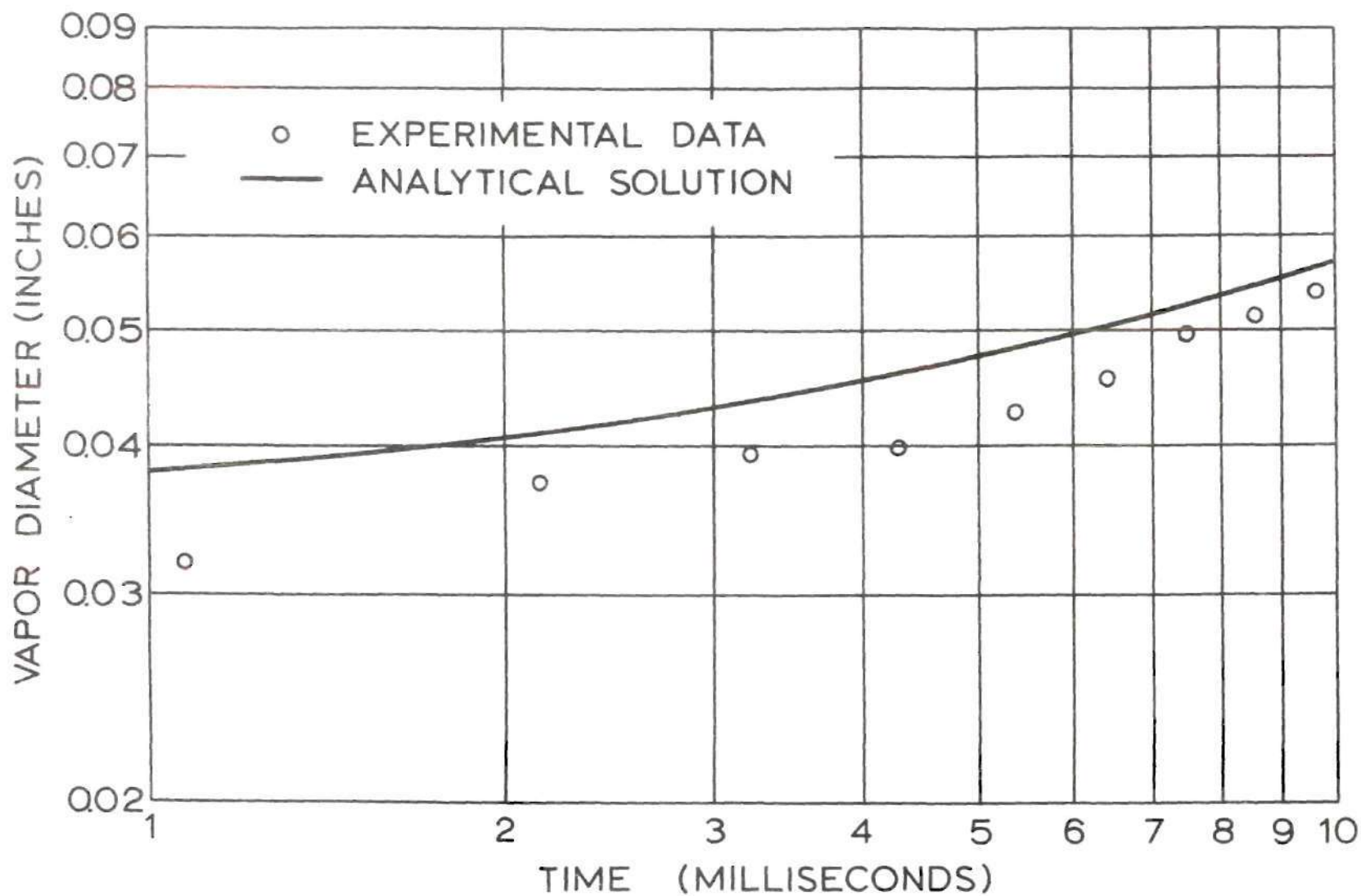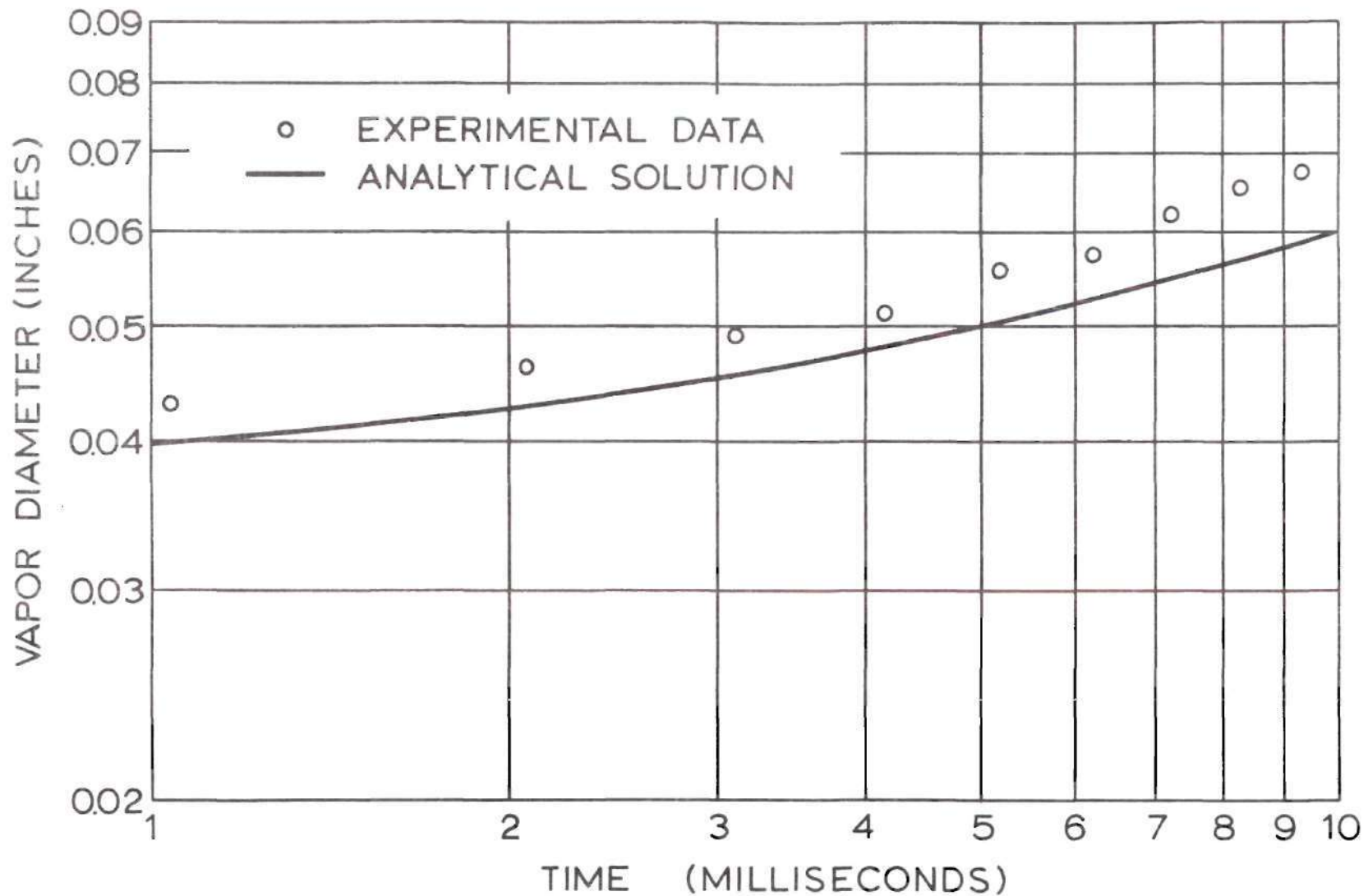
$T_w - T_{sat} = 1595 - 210.9 \approx 1384°F$

Figure 21. Plot of Vapor Bubble Diameter as a Function of Time for Run 5.
$T_w - T_{sat} = 1477 - 210.9 \approx 1266°F$

Figure 22. Plot of Vapor Bubble Diameter as a Function of Time for Run 6.

$T_w - T_{sat} = 1405 - 210.6 \approx 1194° F$

Figure 23. Plot of Vapor Bubble Diameter as a Function of Time for Run 7.
$T_w - T_{sat} = 1521 - 210.9 \approx 1310°F$

Figure 24. Plot of Vapor Bubble Diameter as a Function of Time for Run 9.

$$T_w - T_{sat} = 1680 - 210.9 \approx 1469°F$$
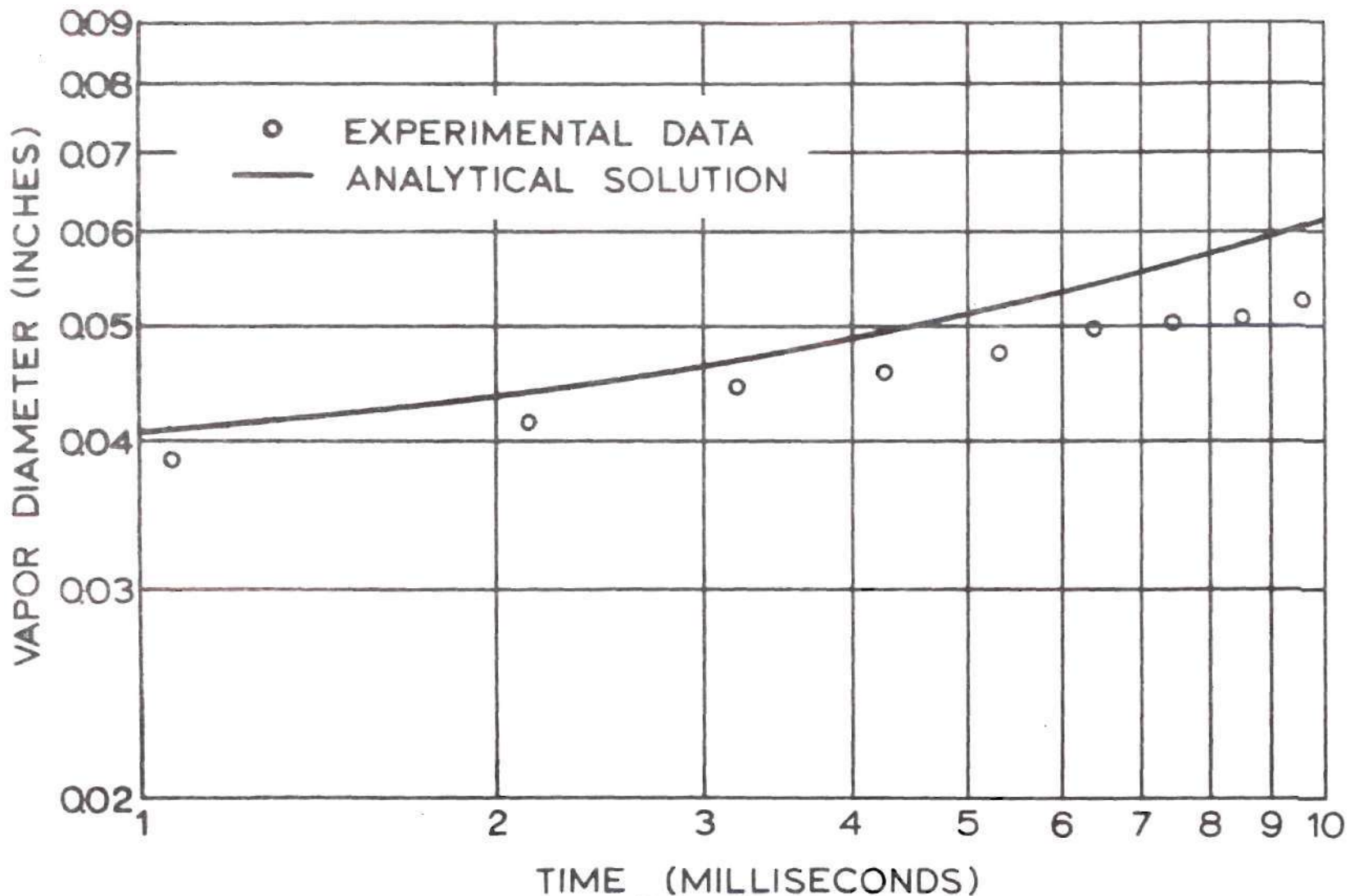
Figure 25. Plot of Vapor Bubble Diameter as a Function of Time for Run 10.

$T_w - T_{sat} = 1739 - 210.4 \approx 1529°F$
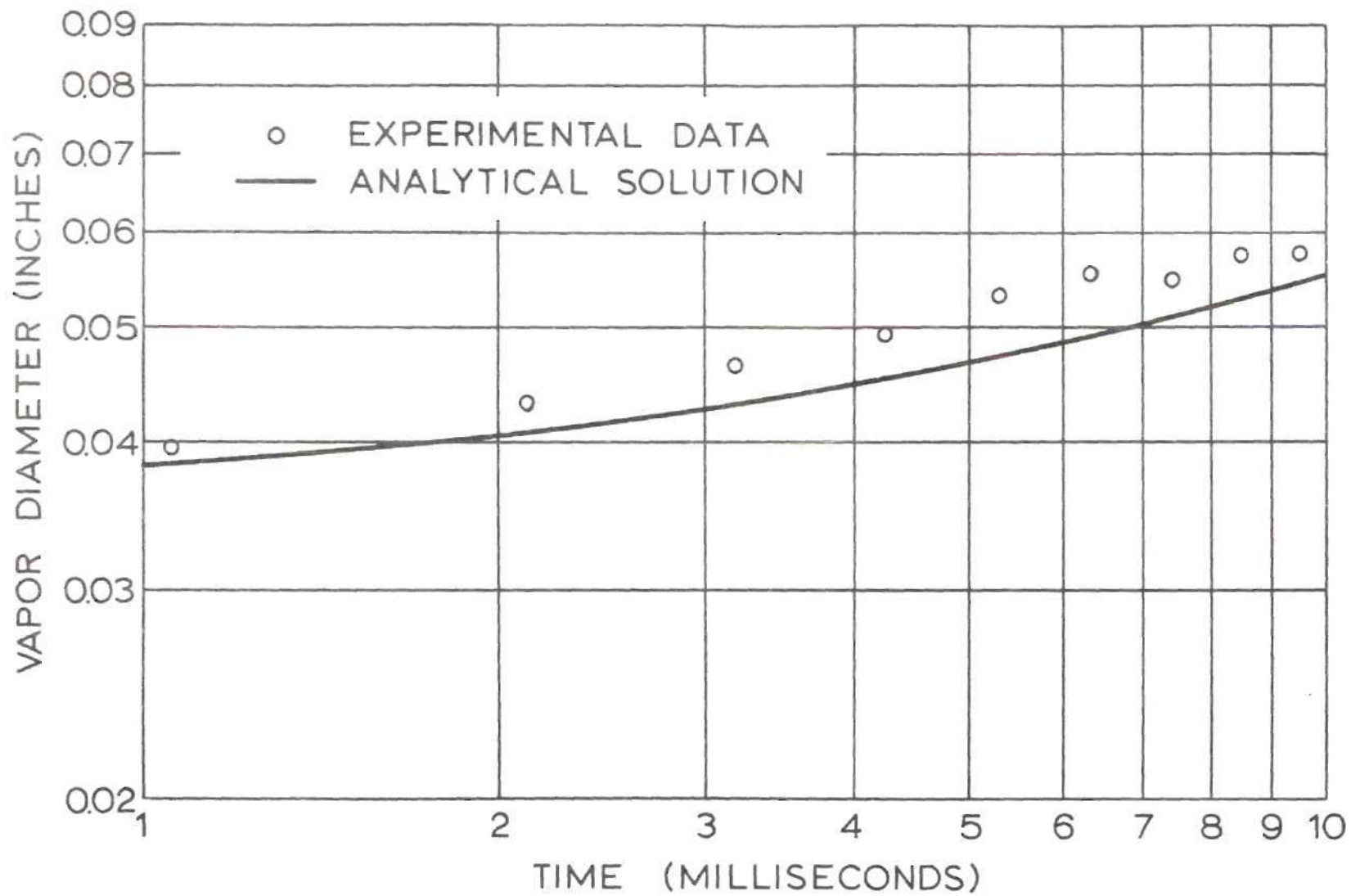
Figure 26. Plot of Vapor Bubble Diameter as a Function of Time for Run 14.

$$T_w - T_{sat} = 1303 - 210.7 \approx 1092^\circ F$$
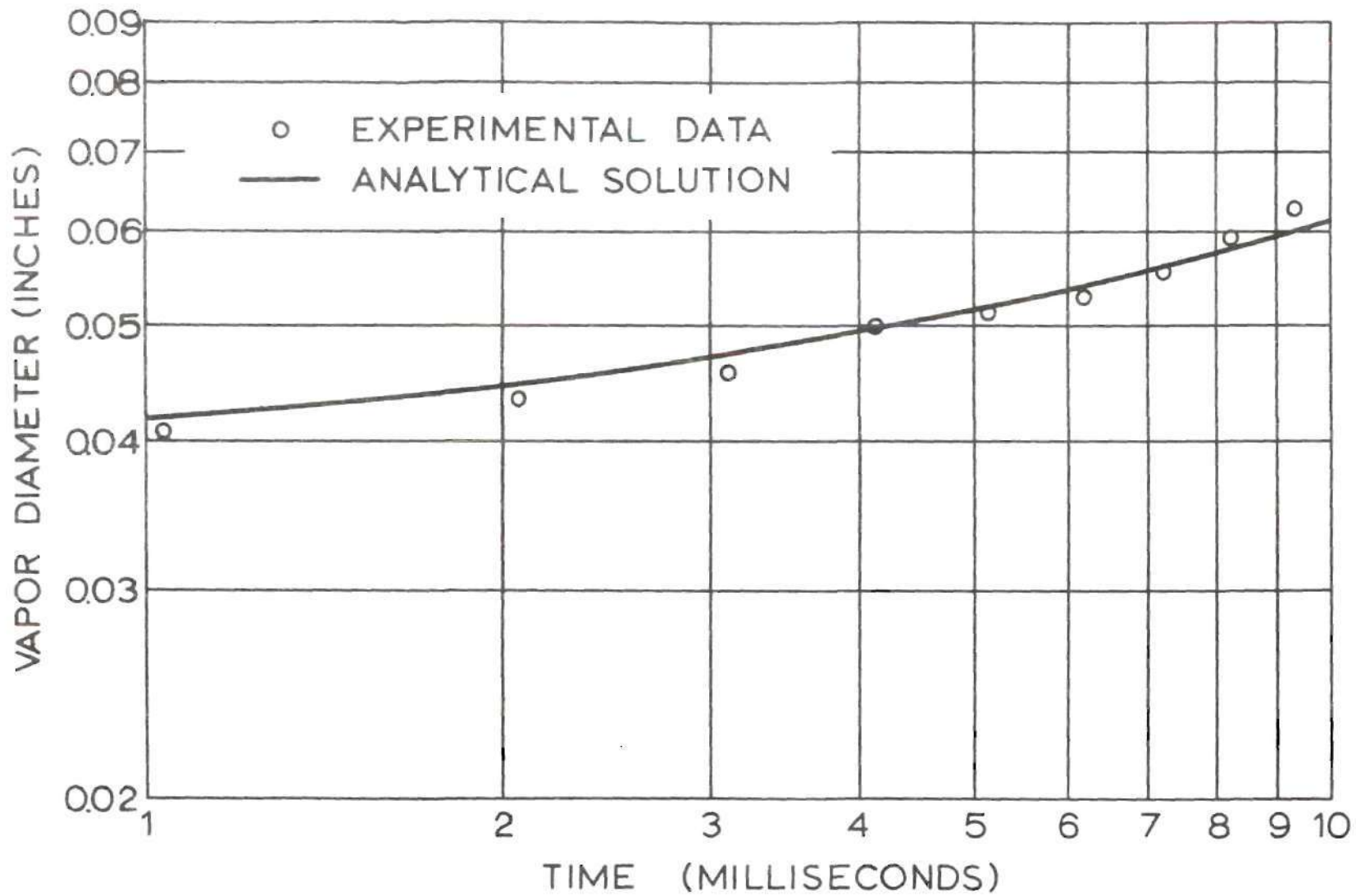
Figure 27. Plot of Vapor Bubble Diameter as a Function of Time for Run 15.
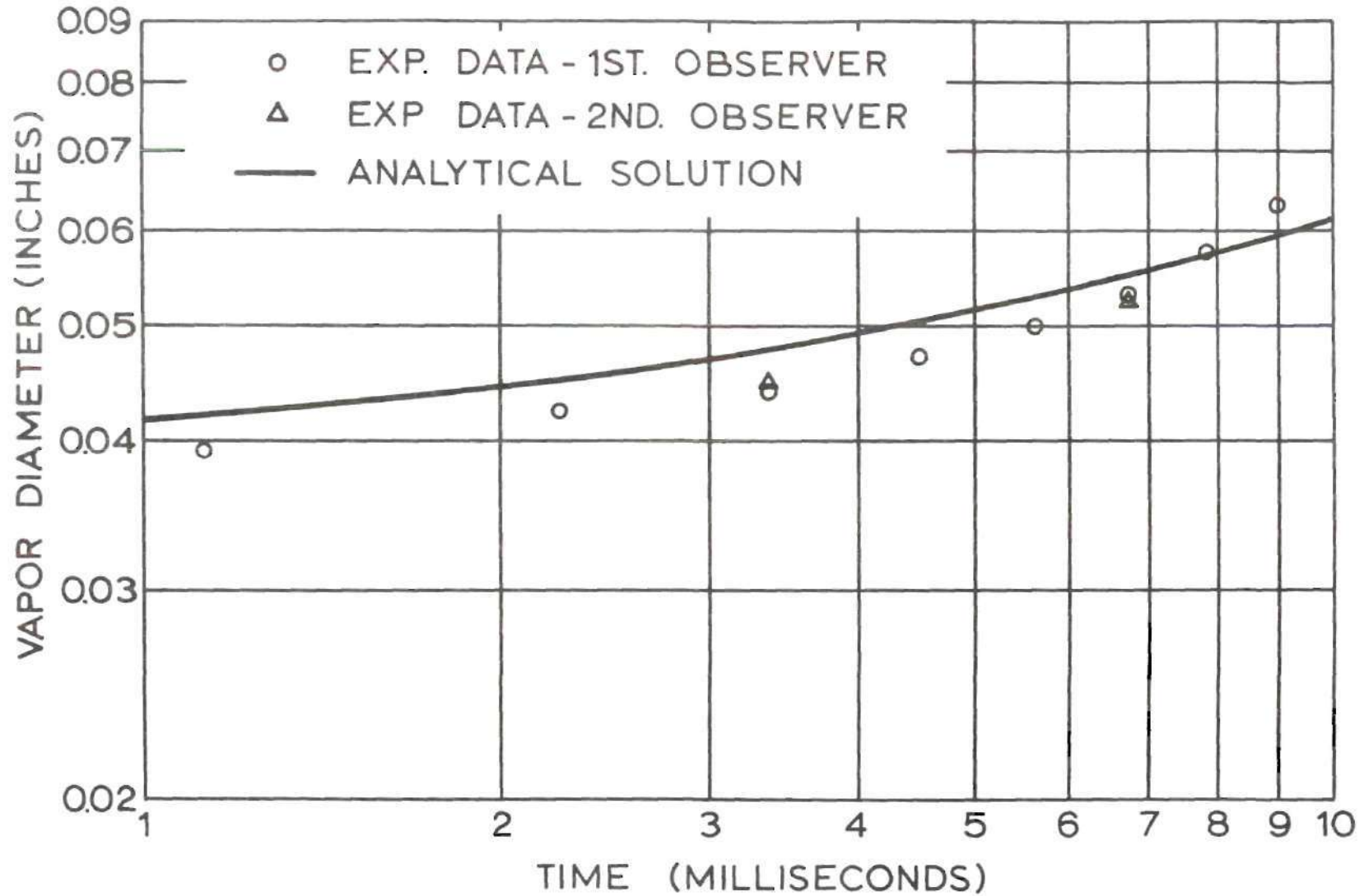$T_w - T_{sat} = 1548 - 210.7 \approx 1337°F$

Figure 28. Plot of Vapor Bubble Diameter as a Function of Time for Run 15A.
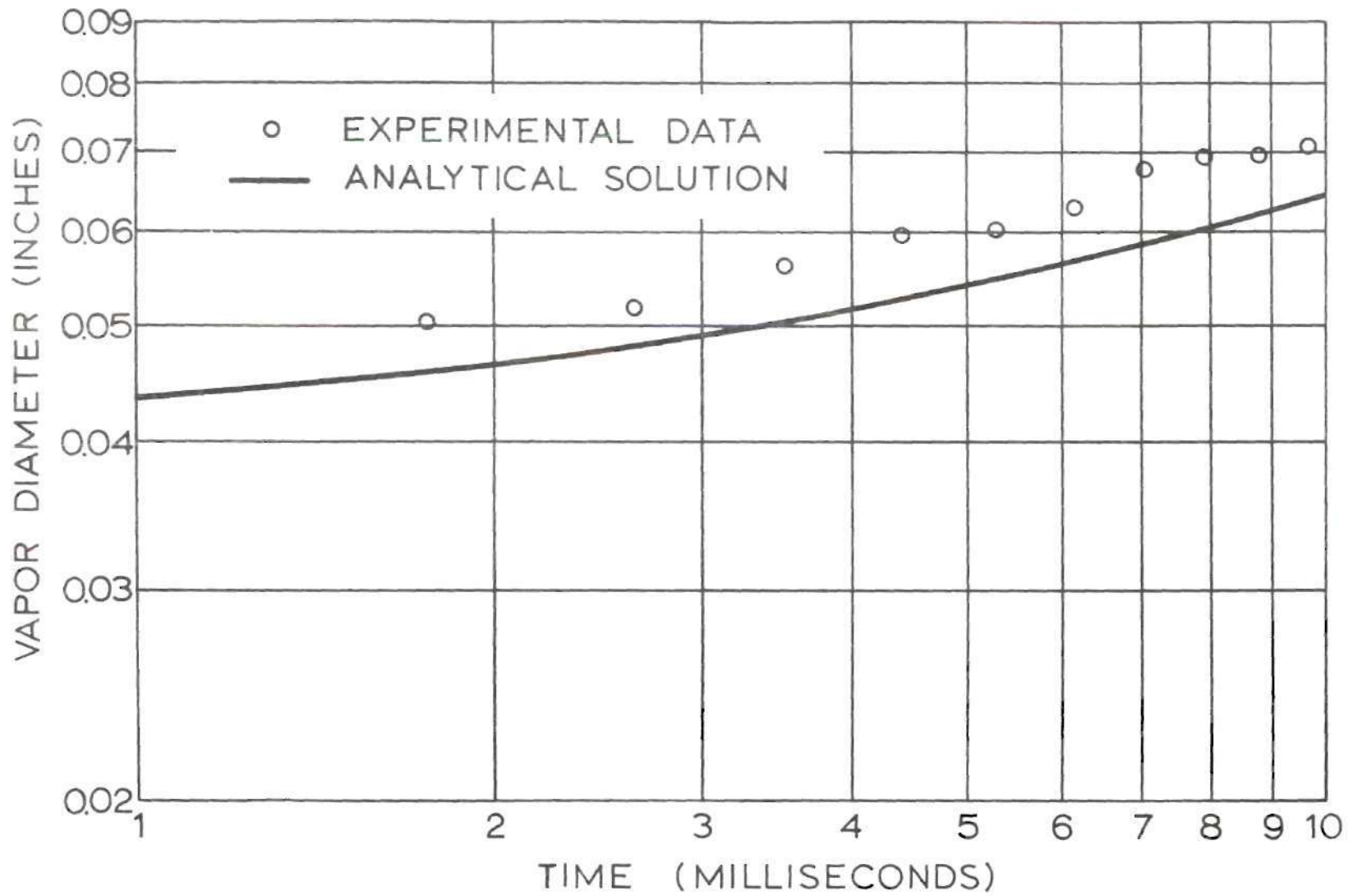$T_w - T_{sat} = 1548 - 210.7 \approx 1337°F$

Figure 29. Plot of Vapor Bubble Diameter as a Function of Time for Run 16.
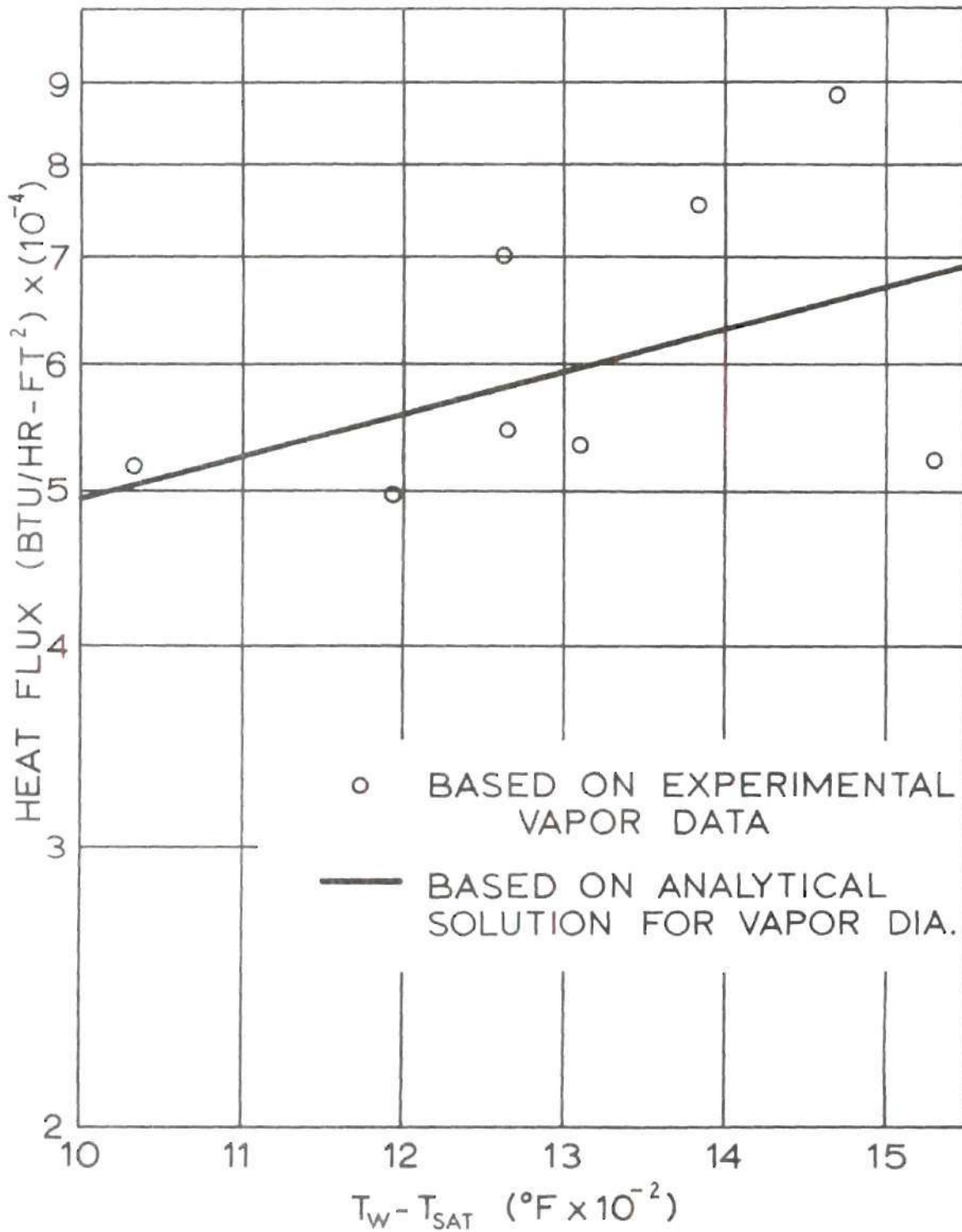$T_w - T_{sat} = 1673 - 210.7 = 1462°F$

Figure 30. Graph of Heat Flux During Transient Film Boiling of
Saturated Water from a 0.0098 Inch Diameter Platinum
Wire - Average Values for Nine Millisecond Interval.

LITERATURE CITED

1.  S. Nukuyama, "Maximum and Minimum Values of Heat Transmitted from Metal to Boiling Water under Atmospheric Pressure," Journal of the Society of Mechanical Engineers, Japan, 37, 367 (1934).

2.  N. W. Snyder in "Summary of Conference on Bubble Dynamics and Boiling Heat Transfer Held at the Jet Propulsion Laboratory, June 14 and 15, 1956," ed. by S. G. Bankoff, W. J. Colahan, Jr., and D. R. Bartz, Jet Propulsion Laboratory Memo No. 20-137, California Inst. Tech., Dec. 10, 1956.

3.  T. T. Robin, Jr., "Mass Transfer Effects in Subcooled Nucleate Boiling," Ph. D. Thesis, School of Nuclear Engineering, Georgia Institute of Technology, November, 1966.

4.  M. Jakob, Heat Transfer, Volume I, John Wiley and Sons, Inc., New York, 1949.  Chapter 29, 614-657.

5.  W. M. Rohsenow, "Heat Transfer with Boiling" in Modern Developments in Heat Transfer, ed. by W. Ibele, Academic Press, Inc., New York, 1963.  85-158.

6.  F. Kreith, Principles of Heat Transfer, International Textbook Company, Scranton, Pa., 1958.  Chapter 10, 398-438.

7.  W. H. McAdams, Heat Transmission, 3rd. ed., McGraw-Hill Book Company, Inc., New York, 1954.  Chapter 14, 368-409.

8.  L. S. Tong, Boiling Heat Transfer and Two-Phase Flow, John Wiley and Sons, Inc., New York, 1965.  Chapters 1, 2, 1-46.

9.  R. Cole, "Investigation of Transient Pool Boiling Due to Sudden Large Power Surge," NACA TN-3885, Dec., 1956.

10.  E. A. McLean, V. E. Scherrer, and C. E. Faneuff, "Film Boiling of Water by Pulse-Heating Small Wires," Journal of Applied Physics, 27, 193 (1956).

11.  M. W. Rosenthal and R. L. Miller, "An Experimental Study of Transient Boiling," ORNL-2294, Oak Ridge National Laboratory (1957).

12.  T. D. Hamill and S. G. Bankoff, "Growth of a Vapor Film at a Rapidly Heated Plane Surface," Chemical Engineering Science, 18, 355 (1963).

13.  T. D. Hamill and S. G. Bankoff, "Maximum and Minimum Rounds for the Growth of a Vapor Film at the Surface of a Rapidly Heated Plate," Chem. Engng. Sci., 19, 59 (1964).

14. H. A. Johnson, V. E. Schrock, F. B. Selph, J. H. Lienhard, and Z. R. Rosztoczy, "Transient Pool Boiling of Water at Atmospheric Pressure," International Developments in Heat Transfer, Heat Transfer Conference, Boulder Colo., American Society of Mechanical Engineers, Aug. 28 - Sept. 1, 1961. 244.

15. H. Laurie and H. A. Johnson, "Transient Pool Boiling of Water on a Vertical Surface with a Step Change in Heat Generation," Transactions of the American Society of Mechanical Engineers, Series C, Journal of Heat Transfer, 84, No. 3, 217 (1962).

16. R. W. Graham, "Experimental Observations of Transient Boiling of Subcooled Water and Alcohol on a Horizontal Surface," National Aeronautics and Space Administration Technical Note D-2507, Jan., 1965.

17. M. G. Cooper and A. J. P. Lloyd, "Transient Local Heat Flux in Nucleate Boiling," Third International Heat Transfer Conference, American Institute of Chemical Engineers, Aug. 7-12, 1966, Science Press, Inc., Ephrata, Pa.

18. W. B. Hall and W. C. Harrison, "Transient Boiling of Water at Atmospheric Pressure," 3rd Int. Heat Transfer Conf., AIChE, Aug. 7-12, 1966, Science Press, Inc., Ephrata, Pa.

19. C. C. Perry and H. R. Lissner, The Strain Gage Primer, McGraw-Hill Book Company, Inc., New York, 1955. Chapter 4, 45-48.

20. International Critical Tables of Numerical Data, Physics, Chemistry and Technology, ed. by E. W. Washburn, National Research Council, National Academy of Sciences, McGraw-Hill Book Company, Inc., New York, 1926.

21. L. A. Bromley, "Heat Transfer in Stable Film Boiling," Chemical Engineering Progress, 46, No. 5, 221-226 (1950).

22. E. Kamke, Differentialgleichungen, Losungsmethoden und Losungen, Chelsea Publishing Company, New York, 1959. 420.

23. D. F. Dyer and J. E. Sunderland, "The Transient Temperature Distribution During Sublimation Dehydration," Trans. ASME, C. J. of Heat Transfer, 89, No. 1, 109 (1967).

24. F. Kreith, Principles of Heat Transfer, 2nd. ed., International Textbook Company, Scranton, Pa., 1965. 595.

25. J. H. Keenan and F. G. Keyes, Thermodynamic Properties of Steam, John Wiley and Sons, Inc., New York, 1936.

26. W. F. Hughes and E. W. Gaylord, Basic Equations of Engineering Science, Schaum Publishing Company, New York, 1964. 20.

27. R. B. Bird, W. E. Stewart, and E. N. Lightfoot, Transport Phenomena, John Wiley and Sons, Inc., New York, 1960. 319.

28. H. S. Carslaw and J. C. Jaeger, Conduction of Heat in Solids, Oxford University Press, London, 1959. 97.

29. M. Abramowitz and I. A. Stegun, Handbook of Mathematical Functions, U. S. Government Printing Office, Washington, D. C., 1964.

OTHER REFERENCES

Akiyama, M. "Spherical Bubble Collapse in Uniformly Subcooled Liquid," Bulletin of the Japanese Society of Mechanical Engineers, 8, No. 32, 683 (1965).

Bankoff, S. G., "Asymptotic Growth of a Bubble in a Liquid with Uniform Superheat," Applied Scientific Research, Section A, 12, No. 3 (1963/1964).

Bankoff, S. G., "Bubble Dynamics at the Surface of an Exponentially Heated Plate," Industrial and Engineering Chemistry, Fundamentals, 1, No. 4, 257 (1962).

Chambre, P. L., "On the Dynamics of Phase Growth," Quarterly Journal of Mechanics and Applied Mathematics, 9, No. 2, 224 (1956).

Dergarabedian, P., "The Rate of Growth of Vapor Bubbles in Superheated Water," Journal of Applied Mechanics, 20, 537 (1953).

Dougherty, D. E. and Rubin, H. H., "The Growth and Collapse of Vapor Bubbles on a Boiling Surface," Proceedings of the Heat Transfer and Fluid Mechanics Institute, Pasadena, Stanford University Press, California, 1963. 222.

Ellion, M. E., "A Study of the Mechanism of Boiling Heat Transfer," Ph.D. Thesis, California Institute of Technology, 1953.

Florschuetz, L. W. and Chao, B. T., "On the Mechanics of Vapor Bubble Collapse," Trans. ASME, C. J. of Heat Transfer, 87, No. 2, 209 (1965).

Forster, H. K. and Zuber, N., "Growth of a Vapor Bubble in a Superheated Liquid," J. of Applied Physics, 25, 474 (1954).

Forster, K. E., "Growth of a Vapor Filled Cavity Near a Heating Surface and Some Related Questions," Physics of Fluids, 4, No. 4, 448 (1961).

Horvay, G., "Freezing into an Undercooled Melt Accompanied by Density Change," Proceedings of the Fourth National Congress of Applied Mechanics, 1315 (1962).

Levenspiel, O., "Collapse of Steam Bubbles in Water," Industrial Engineering and Chemistry, 51, 787 (1959).

Marcus, B. D., "Experiments on the Mechanism of Saturated Nucleate Pool Boiling Heat Transfer," Ph.D. Thesis, Cornell University, 1963.

Plesset, M. S. and Zwick, S. A., "A Non-Steady Heat Diffusion Problem with Spherical Symmetry," J. of Applied Physics, 23, 95 (1952).

Plesset, M. S. and Zwick, S. A., "The Growth of Vapor Bubbles in Super-heated Liquids," J. of Applied Physics, 25, 493 (1954).

Lord Rayleigh, "Pressure Developed in a Liquid During the Collapse of a Spherical Cavity," London, Edinburgh, and Dublin Philosophical Magazine and Journal of Science, 34, 94 (1917).

Savic, P. and Gosnell, J. W., "The Dynamics of the Expanding Vapor Bubble in a Boiling Liquid," Canadian Journal of Chemical Engineering, 40, No. 6, 238 (1962).

Scriven, L. E., "On the Dynamics of Phase Growth," Chem. Engng. Sci., 17, 55 (1962).

Wittke, D. D., "Collapse of Vapor Bubbles with Translatory Motion," Ph.D. Thesis, University of Illinois, 1965.

Zuber, N., "Hydrodynamic Aspects of Boiling Heat Transfer," Atomic Energy Commission Report No. AECU-4439, June, 1959.

Zwick, S. A., "Growth of Vapor Bubbles in a Rapidly Heated Liquid," Phys. Fluids, 3, No. 5, 685 (1960).

VITA

Donald Ross Pitts was born September 21, 1929 in Anniston, Alabama. He attended the public schools of Calhoun County, Alabama, and entered Auburn University in 1947. In 1951 he was awarded the Bachelor of Science degree in Mechanical Engineering, designated a distinguished military graduate, and commissioned a Second Lieutenant in the U. S. Army Reserve.

Following graduation, he entered active duty in the U. S. Army where he served for two years, the first year in the United States and the second in Korea. He attained the rank of First Lieutenant while on active duty.

After this, he worked two years as a mechanical engineer for the Goodyear Tire and Rubber Company, Akron, Ohio, and joined the Lockheed Aircraft Company, Marietta, Georgia, in 1955. He began part-time graduate study at the Georgia Institute of Technology in 1956, and was awarded the degree Master of Science in Mechanical Engineering in 1960. In 1964 he entered the Lockheed Company's graduate work-study program to pursue the doctorate in Mechanical Engineering at the Georgia Institute of Technology.

In 1952 he married Miss Bettie Jeane Nettles. They have three children, Brenda Kaye, David Wayne, and Leslie Ann.